# UC San Diego
## UC San Diego Electronic Theses and Dissertations

**Title**
Memory, dementia, and the functional role of the parietal cortex

**Permalink**
https://escholarship.org/uc/item/3xh1334q

**Author**
Seibert, Tyler Michael

**Publication Date**
2011

Peer reviewed|Thesis/dissertation

UNIVERSITY OF CALIFORNIA, SAN DIEGO


Memory, Dementia, and the Functional Role of the Parietal Cortex


A dissertation submitted in partial satisfaction of the
requirements for the degree Doctor of Philosophy


in


Bioengineering


by


Tyler Michael Seibert


Committee in charge:

> Professor Gabriel A. Silva, Chair
> Professor James B. Brewer, Co-Chair
> Professor Richard B. Buxton
> Professor Donald J. Hagler, Jr.
> Professor Marcos Intaglietta


2011

The Dissertation of Tyler Michael Seibert is approved, and it is acceptable in quality

and form for publication on microfilm and electronically:

_____

_____

_____

_____

Co-Chair

_____

Chair

University of California, San Diego

2011

DEDICATION

To Dr. Marian Diamond, for opening my eyes to the wonder of the mind
with her chalkboard, her hatbox, and her immeasurable enthusiasm.


To Dr. Warren Seibert, for providing a personal motivation
for the study of neuroscience.


To Nina, for the most precious memories in my own cortex
and a reason to hope for a beautiful future

TABLE OF CONTENTS

# LIST OF ABBREVIATIONS

MEG, magnetoencephalography

MRI, magnetic resonance imaging

fMRI, functional MRI

BOLD, blood oxygenation level dependent

dSPM, dynamic statistical parametric mapping

EEG, electroencephalography

ERP, event-related potential

PET, positron emission tomography

VPC, ventral parietal cortex

DPC, dorsal parietal cortex

AD, Alzheimer's disease

PD, Parkinson's disease

PDD, Parkinson's disease dementia

DLB, dementia with Lewy bodies

PRD, Parkinson-related dementia

MNI, Montreal Neurological Institute

RMS, root-mean-square

ICC, intraclass correlation coefficient

MMSE, mini-mental state exam

CAG, cytosine-adenine-guanine

UHDRS, Unified Huntington's Disease Rating Scale

LIST OF FIGURES

LIST OF TABLES

ACKNOWLEDGEMENTS

One name is listed on the title page, but many people contributed to this work. First, I would like to thank Dr. James Brewer for taking the time to talk to an enthusiastic undergraduate student at the Society for Neuroscience meeting in 2005. That interaction has now led to over five years of mentorship and the present dissertation. I would also like to thank all of the members of the Brewer Lab for support, friendship, and assistance with my projects. My MSTP Bioengineering classmates also deserve my appreciation—especially for a few tutoring sessions in thermodynamics, continuum mechanics and the like during our core coursework. I am additionally grateful for the staffs at the RIL and CFMRI for troubleshooting when the MRI and MEG systems gave me trouble, as well as some excellent suggestions along the way. And, of course I depended on the support and organization of the Medical Scientist Training Program, and the Departments of Bioengineering and Radiology at UCSD.

When I chose to pursue my Ph.D. studies in the Department of Bioengineering, I was seeking a strong technical background and a better understanding of the fundamentals of physics, statistics, mathematics, and of neuroimaging methods. A few people deserve credit for encouraging me to take on the challenge: Joy Liau, Gabe Silva, and Jim Brewer. Professors whose excellent courses were instrumental to the achievement of my goals were numerous, and include Tom Liu, Marcos Intaglietta, Eric Wong, Anna Leigh Rack-Gomer, Larry Frank, Rick Buxton, Eric Halgren, Andrew McCulloch, and Steve Hillyard. Others were immensely helpful with many specific problems and questions: Anders Dale, Eric Halgren, and Tom Liu. Don

Hagler deserves special mention for being my primary resource for technical advice on every project.

My family—immediate and extended—made this work possible for me. I can never thank them enough.

Chapter 1, in full, is a reprint of the material as it appears in Human Brain Mapping, 2011. Seibert, Tyler M.; Hagler, Donald J., Jr.; Brewer, James B., Wiley-Liss, 2010. The dissertation author was the primary investigator and author of this paper.

Chapter 2, in full, is a reprint of the material as it appears in NeuroImage, 2011. Seibert, Tyler M.; Gimbel, Sarah I.; Hagler, Donald J., Jr.; Brewer, James B., Elsevier, Inc, 2010. The dissertation author was the primary investigator and author of this paper.

Chapter 3, in full, is a reprint of the material as it appears in Journal of Neuroscience Methods, 2011. Seibert, Tyler M.; Brewer, James B., Elsevier, Inc, 2011. The dissertation author was the primary investigator and author of this paper.

Chapter 4, in full, has been submitted for publication of the material as it may appear in NeuroImage. Seibert, Tyler M.; Majid, Dewan-Syed A.; Aron, Adam R.; Corey-Bloom, Jody; Brewer, James B., Elsevier, Inc. The dissertation author was the primary investigator and author of this paper.

Chapter 5, in part, is currently being prepared for submission for publication of the material. Seibert, Tyler M.; Murphy, Elizabeth A.; Brewer, James B. The dissertation author was the primary investigator and author of this material.

# VITA

2005  Graduate Student Instructor, University of California, Berkeley

2005  Bachelor of Science, University of California, Berkeley

2004-2006  Research Assistant, University of California, Berkeley

2006  Research Assistant, University of California, San Diego

2008-2010  Graduate Student Instructor, Department of Bioengineering, University of California, San Diego

2010  Teaching Assistant, School of Medicine, University of California, San Diego

2011  Doctor of Philosophy, University of California, San Diego

2006-2013  Medical Scientist Training Program, School of Medicine, University of California, San Diego

ABSTRACT OF THE DISSERTATION


Memory, Dementia, and the Functional Role of the Parietal Cortex


by


Tyler Michael Seibert


Doctor of Philosophy


University of California, San Diego, 2011


Professor Gabriel A. Silva, Chair

Professor James B. Brewer, Co-Chair

Autobiographical memories are the mind's definition of self. The neural substrates of memory are therefore of tremendous scientific interest. Moreover, the impairment or loss of memory in dementia is a personal catastrophe that reverberates throughout the community and incurs enormous financial and emotional costs. The present dissertation addresses scientific and clinical interests in memory with a particular focus on an area of the brain—the parietal cortex—that is active in memory retrieval and selectively vulnerable to dementia pathology. Chapter one describes a

study using magnetoencephalography (MEG) that revealed an immediate parietal response in episodic retrieval. Chapter two discusses a repetition of the first study with another neuroimaging technique, functional magnetic resonance imaging (fMRI). The results from MEG and fMRI were combined to provide a more precise picture of the timing and localization of retrieval-related parietal activity, which onset simultaneously with a cue to retrieve and was most prominent in the intraparietal sulcus. Chapter three presents a novel method for analyzing the interregional functional correlations of the parietal cortex. This method preserves the unique anatomical features of individual subjects, allowing more accurate comparisons of functional correlations between healthy individuals and those with dementia. Chapter four describes results from application of the new analysis method to longitudinal data. Parietal and non-parietal functional correlations were contrasted in preclinical Huntington's disease and healthy adults, and the long-term stability of these correlation patterns was assessed in both populations. There proved to be little effect of preclinical Huntington's disease on functional correlations, but highly consistent group-level results over a one-year period in each population point to the potential of this technique as a quantitive clinical biomarker in dementia. Chapter five also reports results from application of the new method, in this case to resting fMRI data from patients with Parkinson's disease and Parkinson-related dementia. The strength of resting interregional fMRI correlations in demented patients was decreased relative to equivalent measurements in unimpaired elderly subjects, particularly within corticostriatal regions.

INTRODUCTION

Memory

In 1953, at the age of twenty-seven, Henry Molaison underwent an experimental brain surgery hoping to find some relief from the debilitating seizures that had prevented him from working or otherwise leading a normal life. Patient H.M., as he has since been known to decades of neuroscientists, awoke from the operation with a new neurological problem: nearly complete anterograde amnesia. The removal of Mr. Molaison's bilateral hippocampi left him unable to create new explicit memories, including those of names, faces, facts, dates, or even of events in his own life. This terrible human tragedy was pivotal in the development of our current understanding of memory circuitry in the brain and of the essential role of the hippocampus and related structures (Scoville and Milner, 2000; Squire, 2009). Nearly a half-century later, it became possible to image activation of the human hippocampus during memory tasks using functional magnetic resonance imaging, or fMRI (Brewer et al., 1998).

While focus on the hippocampus led to great strides in the neuroscience of memory, beginning in the 1970s researchers using electroencephalography (EEG) had found a robust, memory-related effect in another region of the brain—the parietal lobe. Subjects were asked to look at a series of images or words and were then tested on whether they could distinguish the items they had studied ("old") from unstudied ("new") items. During the testing phase, electric fields on the subjects' scalps were recorded. On average, there was a strong difference in neuron-generated electric field

strength measured when subjects viewed an old item relative to when they viewed a new item. This difference was particularly prominent in electrodes over the lateral parietal cortex, and the effect became known as the "left parietal old-new effect" (Friedman and Johnson, 2000; Rugg and Curran, 2007).

When functional brain imaging techniques based on regional blood flow and composition were applied to human memory in the 1990s, positron emission tomography (PET) studies confirmed activations of the left parietal lobe during memory retrieval tasks (Cabeza and Nyberg, 2000; Owen et al., 1996; Rugg et al., 1998; Tulving et al., 1994). Functional MRI experiments added further evidence (Cabeza et al., 2008; Ciaramelli et al., 2008; Vilberg and Rugg, 2008), demonstrating prominent retrieval-related activity changes in both the medial and lateral parietal cortex. More complex tasks, that required subjects to indicate whether they could remember specific details about the study event or whether they had only a general sense of familiarity for the item, suggested there was a functional division between dorsal and ventral portions of the lateral parietal cortex (Cabeza, 2008; Ciaramelli et al., 2008; Vilberg and Rugg, 2008).

There is no Henry Molaison for the parietal cortex. While lesion studies have now conclusively confirmed the importance of the hippocampus in memory, parietal lesions do not typically yield prominent memory defects (Berryhill et al., 2007; Bisiach and Luzzatti, 1978; Olson and Berryhill, 2009). Clever experimental designs and astute meta-analyses of imaging studies have led to intriguing proposed functions of the parietal cortex in memory retrieval. Some of these ideas are even supported by careful examination of patients with parietal lesions (Cabeza, 2008; Olson and

Berryhill, 2009). However, these competing hypotheses are all primarily based on the same body of imaging literature. New methodological approaches are required to differentiate these hypotheses' success in explaining the functional role of parietal activity in memory.

Dementia

One compelling motivation for seeking to understand the processes underlying memory is to inform clinical treatment of patients whose memory is disrupted. While lesions like Henry Molaison's are quite rare, another disease affecting memory has become a massive challenge in the United States and elsewhere. Dementia is approximately tied with diabetes for the 6th most common cause of death in the U.S. (Alzheimer's Association, 2010). Its prevalence increases with age and is estimated to affect 1% of Americans aged 60-64 years and 45% of those over 95 (Fratiglioni and Rocca, 2001).

Dementia also represents an enormous financial burden. Medicare costs for persons over 65 years of age are an average of three times greater than costs for persons without dementia. Total payments in 2010 for dementia patients over 65 were estimated at $172 billion, and $123 billion of those payments came from Medicare and Medicaid. For reference, it is worth noting that the entire Medicare budget for the 2010 fiscal year was $510 billion (U.S. Department of Health & Human Services, 2009). These staggering cost estimates do not include unpaid care (e.g., by family members), which totaled 12.5 billion hours in the U.S. during 2009 at a value of approximately $144 billion (Alzheimer's Association, 2010).

Unfortunately, the problem of dementia is only getting worse. While U.S. deaths from stroke, prostate cancer, breast cancer, heart disease, and HIV all decreased from 2000 to 2009, deaths from Alzheimer's disease increased by over 46% (Alzheimer's Association, 2010). From 2005 to 2009 the worldwide cost of dementia increased by 34% (Wimo et al., 2010). And the outlook for the future is not encouraging, with studies predicting the prevalence of dementia in the U.S. will more than double in the next 40 years (Alzheimer's Association, 2010).

The most common cause of dementia is Alzheimer's disease (AD), which accounts for 60-80% of dementia cases in the elderly and has a prevalence in the U.S. of 5.3 million (Alzheimer's Association, 2010). One of the hallmarks of Alzheimer's pathology is accumulation of a protein called amyloid-beta in plaques throughout the brain's cortex. Interestingly, while the most prominent cognitive changes in Alzheimer's disease are in memory, these amyloid plaques are commonly found in the medial and lateral parietal cortex—along with the medial prefrontal cortex—even in patients at the early stages of the disease (Buckner et al., 2009). These parietal and prefrontal regions are also among those affected earliest and most severely by atrophy in Alzheimer's disease (Buckner et al., 2008).

The second most common cause of neurodegenerative dementia is called dementia with Lewy bodies (DLB), named after its characteristic finding in pathology specimens. Lewy bodies are formed by accumulation of a protein called alpha-synuclein. This disease is believed to account for 15-35% of all demented patients, but it can be confused with both Alzheimer's disease and Parkinson's disease dementia. DLB has been estimated to be underdiagnosed in clinics by as much as 50%, a

problem that arises from the inherent diagnostic uncertainty in these conditions. As

with AD, a DLB diagnosis is only presumptive until it is confirmed by biopsy or

autopsy; clinical criteria and available tests are not sufficient to allow definitive

diagnosis non-invasively (Geser et al., 2005).

Parkinson's disease dementia (PDD) is a third cause of cognitive impairment

in the elderly, with 30-80% of patients with idiopathic parkinsonism eventually

developing dementia (Geser et al., 2005). PDD is distinguished from DLB by the

timing of symptom onset: if motor symptoms precede cognitive symptoms by at least

a year, the diagnosis is PDD; otherwise, the diagnosis is DLB. This arbitrary cutoff is

clearly insufficient to establish the existence of two distinct etiologies. Both conditions

are associated with alpha-synuclein Lewy bodies and may actually represent two

clinical classifications on a continuous spectrum of the manifestations of a single

disease process. In practical terms, PDD is generally easier than DLB to distinguish

from AD based on clinical history and exam. This increased confidence in clinical

diagnosis may allow use of PDD as a model of DLB in initial validation of potential

non-invasive diagnostic tools intended to distinguish DLB and AD.

Safe and accurate diagnostic tests for dementia could have a dramatic impact.

For DLB, the clinical diagnostic criteria are fairly specific, but the sensitivity of these

criteria is quite poor. In addition to frequent misdiagnosis of individual patients, this

poor sensitivity means that cohorts of AD patients in clinical trials of potential

therapies are contaminated with DLB patients unlikely to respond to an efficacious

Alzheimer's therapy. Moreover, some current treatments for AD are contraindicated in

patients with DLB (Geser et al., 2005). In summary, there is a strong clinical need for

a non-invasive diagnostic implement for distinguishing dementia associated with amyloidopathies (e.g., AD) from dementia associated with synucleinopathies (e.g., DLB, PDD), also referred to as Parkinson-related dementia (or PRD).

Parietal Cortex at Rest

Functional imaging and electrophysiology studies have highlighted the parietal lobe's involvement in memory. Examination of amyloid deposition in Alzheimer's disease and aging has revealed the selective vulnerability of the parietal lobe in memory pathology. Perhaps most surprising, clues into the functional role of the brain's parietal lobe were also uncovered by its curious activity in the rest period *between* cognitive tasks. Meta-analyses of multiple functional imaging data sets revealed that there was a group of regions, dubbed the "default network," where activity was consistently decreased whenever subjects engaged in a cognitive task. Seemingly any task led to decreased activity in the default network—from complex memory tests, to simple even-odd judgments on single-digit integers (Buckner et al., 2008; Raichle et al., 2001). The parietal lobe was repeatedly found to be among the most prominent default network regions (Buckner et al., 2008; Buckner and Vincent, 2007; Cauda et al., 2010; Franco et al., 2009; Greicius et al., 2003; Gusnard and Raichle, 2001).

Further investigation of brain activity at rest led to the discovery that regions of the default network oscillated in concert. When subjects were simply asked to lie still in the scanner, the time course of the blood oxygenation level dependent (BOLD) fMRI signal in a given default-network region was highly correlated with the signal in

the rest of the default regions (Greicius et al., 2003; Raichle and Snyder, 2007).

Interregional BOLD correlations in the default network were appealing as a potential

biomarker in disease because these highly reproducible qualitative patterns were

obtained with a simple paradigm that was feasible in both healthy and impaired

populations (Auer, 2008; Fox and Raichle, 2007; Greicius, 2008; van den Heuvel and

Hulshoff Pol, 2010; Rogers et al., 2007). Indeed, early evidence suggested resting

BOLD correlations in the default network were disrupted in Alzheimer's disease

(Allen et al., 2007; Greicius, 2008; Greicius et al., 2004; Koch et al., 2010; Sorg et al.,

2009; Supekar et al., 2008; Wang et al., 2006; Zhang et al., 2010), as well as in mild

cognitive impairment (Bai et al., 2009; Pihlajamäki et al., 2009; Sorg et al., 2007), and

even in cognitively unimpaired subjects with high amyloid burden (Hedden et al.,

2009; Sheline et al., 2010). These early results are promising and suggest that the

default-network phenomenon warrants rigorous examination to evaluate its potential

utility as a quantitative marker in scientific and clinical problems.


Overview of Dissertation

The above observations invite investigation into the functional role of the

parietal cortex in memory and disease. To this end, the present dissertation addresses

five specific aims. The first and second aims relate to adopting novel approaches to

inform current understanding and hypotheses of the parietal contribution to retrieval of

memories. The final three aims focus on the development and application of improved

methods for quantitatively analyzing the functional correlations of the parietal cortex

in health and dementia.

Chapter one introduces the hypotheses that have been recently generated for the functional role of the lateral parietal cortex in episodic memory. Episodic memory is recollection of autobiographical events (or "episodes") that can be explicitly described (Tulving, 2002), and it is therefore a subset of the explicit memory lost in patient H.M. and impaired in endless patients suffering from dementia. Most of the evidence supporting these hypotheses comes from fMRI, which has excellent spatial resolution (on the order of 3 mm for a typical whole-brain study), but depends on an evoked impulse response that is blurred over several seconds. The competing hypotheses for parietal function in memory can be dissociated based on their implications for the timing of parietal contributions, but fMRI offers very limited temporal information. Magnetoencephalography (MEG) is another non-invasive tool for measuring cortical activity *in vivo*, and it can be used to record neural activity with millisecond time resolution. The first aim of this dissertation, presented in chapter one, was to use MEG to investigate the spatiotemporal dynamics of parietal activity in episodic retrieval.

Chapter two expands on the findings from chapter one by adopting a multimodal approach. The memory retrieval task used in the MEG study was repeated using fMRI. Because the respective advantages in spatial and temporal resolution with fMRI and MEG are complementary, combining both techniques can lead to a more precise description of the parietal response in episodic retrieval. Therefore, the second aim of this dissertation was to incorporate MEG and fMRI results to refine the conclusions from the original MEG study and further characterize the spatial and temporal features of the parietal response in retrieval.

Chapter three describes how typical methods for the analysis of BOLD correlations are vulnerable to inaccuracies due to anatomic variability across subjects, a particular problem in diseases that cause structural pathology such as the atrophy commonly found in aging and dementia. Early investigations of interregional BOLD correlations depend on group-level analysis after transforming individual brains to a standardized anatomical template, or volume atlas. This process, frequently called "warping," is imperfect, and can result in inadvertently measuring correlations of neighboring cerebrospinal fluid or white matter in place of the intended cortex. The third aim of this dissertation was to develop a novel method for quantitative analysis of default-network correlations in the native space of individual brains, whether healthy or diseased.

Chapter four uses the native-space analysis method presented in chapter three to study the long-term stability of resting BOLD correlations and assess the potential usefulness of resting fMRI correlations in a clinical population in the early stages of a disease that causes dementia. As opposed to any of the other neurodegenerative dementias described above, Huntington's disease has a known genetic marker that can be detected in individuals before symptoms begin to manifest. Resting fMRI data was collected in a cohort of preclinical (asymptomatic) Huntington's patients and a cohort of age-matched healthy individuals at two time points spaced a year apart. All four data sets were analyzed using the new method in native space. The fourth aim of this dissertation was to investigate the longitudinal reliability of resting fMRI correlations and evaluate the utility of this measure as a clinical biomarker in asymptomatic Huntington's disease.

Finally, chapter five applies the native-space analysis method to Parkinson-related dementia. PRD patients, cognitively unimpaired PD patients, and age-matched elderly control subjects underwent resting fMRI scans, and resulting data were compared for population differences in resting interregional fMRI correlations. The fifth aim of this dissertation was to evaluate the utility of resting interregional correlations as a biomarker in PRD.

**References**

Allen, G, Barnard, H, McColl, R, Hester, AL, Fields, JA, Weiner, MF, et al. (2007): Reduced hippocampal functional connectivity in Alzheimer disease. Arch. Neurol, 64(10), 1482-1487.

Alzheimer's Association (2010): 2010 Alzheimer's disease facts and figures. Alzheimers Dement, 6(2), 158-194.

Auer, DP (2008): Spontaneous low-frequency blood oxygenation level-dependent fluctuations and functional connectivity analysis of the "resting" brain. Magn Reson Imaging, 26(7), 1055-1064.

Bai, F, Watson, DR, Yu, H, Shi, Y, Yuan, Y, Zhang, Z (2009): Abnormal resting-state functional connectivity of posterior cingulate cortex in amnestic type mild cognitive impairment. Brain Res, 1302, 167-174.

Berryhill, ME, Phuong, L, Picasso, L, Cabeza, R, Olson, IR (2007): Parietal lobe and episodic memory: bilateral damage causes impaired free recall of autobiographical memory. J. Neurosci, 27(52), 14415-14423.

Bisiach, E, Luzzatti, C (1978): Unilateral neglect of representational space. Cortex, 14(1), 129-133.

Brewer, JB, Zhao, Z, Desmond, JE, Glover, GH, Gabrieli, JDE (1998): Making Memories: Brain Activity that Predicts How Well Visual Experience Will Be Remembered. Science, 281(5380), 1185-1187.

Buckner, RL, Andrews-Hanna, JR, Schacter, DL (2008): The Brain's Default Network: Anatomy, Function, and Relevance to Disease. Annals of the New York Academy of Sciences, 1124(1), 1-38.

Buckner, RL, Sepulcre, J, Talukdar, T, Krienen, FM, Liu, H, Hedden, T, Andrews-Hanna, JR, Sperling, RA, Johnson, KA (2009): Cortical Hubs Revealed by Intrinsic Functional Connectivity: Mapping, Assessment of Stability, and Relation to Alzheimer's Disease. J. Neurosci., 29(6), 1860-1873.

Buckner, RL, Vincent, JL (2007): Unrest at rest: Default activity and spontaneous network correlations. NeuroImage, 37(4), 1091-1096.

Cabeza, R (2008): Role of parietal regions in episodic memory retrieval: The dual attentional processes hypothesis. Neuropsychologia, 46(7), 1813-1827.

Cabeza, R, Ciaramelli, E, Olson, IR, Moscovitch, M (2008): The parietal cortex and episodic memory: an attentional account. Nat. Rev. Neurosci, 9(8), 613-625.

Cabeza, R, Nyberg, L (2000): Imaging cognition II: An empirical review of 275 PET and fMRI studies. J Cogn Neurosci, 12(1), 1-47.

Cauda, F, Geminiani, G, D'Agata, F, Sacco, K, Duca, S, Bagshaw, AP, Cavanna, AE (2010): Functional connectivity of the posteromedial cortex. PLoS ONE, 5(9).

Ciaramelli, E, Grady, CL, Moscovitch, M (2008): Top-down and bottom-up attention to memory: a hypothesis (AtoM) on the role of the posterior parietal cortex in memory retrieval. Neuropsychologia, 46(7), 1828-51.

Fox, MD, Raichle, ME (2007): Spontaneous fluctuations in brain activity observed with functional magnetic resonance imaging. Nat. Rev. Neurosci, 8(9), 700-711.

Franco, AR, Pritchard, A, Calhoun, VD, Mayer, AR (2009): Interrater and intermethod reliability of default mode network selection. Hum Brain Mapp, 30(7), 2293-2303.

Fratiglioni, L, Rocca, WA (2001): Epidemiology of Dementia. In F. Boller & S. Cappa (Eds.), Handbook of neuropsychology: Aging and dementia (2nd ed., pp. 193-215). Amsterdam: Elsevier Health Sciences.

Friedman, D, Johnson, R (2000): Event-related potential (ERP) studies of memory encoding and retrieval: a selective review. Microsc. Res. Tech, 51(1), 6-28.

Geser, F, Wenning, GK, Poewe, W, McKeith, IG (2005): How to diagnose dementia with Lewy bodies: state of the art. Mov. Disord, 20 Suppl 12, S11-20.

Greicius, MD, Krasnow, B, Reiss, AL, Menon, V (2003): Functional connectivity in the resting brain: a network analysis of the default mode hypothesis. Proc. Natl. Acad. Sci. U.S.A, 100(1), 253-258.

Greicius, MD (2008): Resting-state functional connectivity in neuropsychiatric disorders. Curr. Opin. Neurol, 21(4), 424-430.

Greicius, MD, Srivastava, G, Reiss, AL, Menon, V (2004): Default-mode network activity distinguishes Alzheimer's disease from healthy aging: evidence from functional MRI. Proc. Natl. Acad. Sci. U.S.A, 101(13), 4637-4642.

Gusnard, DA, Raichle, ME (2001): Searching for a baseline: functional imaging and the resting human brain. Nat. Rev. Neurosci, 2(10), 685-694.

Hedden, T, Van Dijk, KRA, Becker, JA, Mehta, A, Sperling, RA, Johnson, KA, Buckner, RL (2009): Disruption of functional connectivity in clinically normal older adults harboring amyloid burden. J. Neurosci, 29(40), 12686-12694.

van den Heuvel, MP, Hulshoff Pol, HE (2010): Exploring the brain network: a review on resting-state fMRI functional connectivity. Eur Neuropsychopharmacol, 20(8), 519-534.

Koch, W, Teipel, S, Mueller, S, Benninghoff, J, Wagner, M, Bokde, ALW, et al. (2010): Diagnostic power of default mode network resting state fMRI in the detection of Alzheimer's disease. Neurobiol Aging.

Olson, IR, Berryhill, M (2009): Some surprising findings on the involvement of the parietal lobe in human memory. Neurobiol Learn Mem, 91(2), 155-65.

Owen, AM, Milner, B, Petrides, M, Evans, AC (1996): Memory for object features versus memory for object location: a positron-emission tomography study of encoding and retrieval processes. Proc. Natl. Acad. Sci. U.S.A, 93(17), 9212-9217.

Pihlajamäki, M, Jauhiainen, AM, Soininen, H (2009): Structural and functional MRI in mild cognitive impairment. Curr Alzheimer Res, 6(2), 179-185.

Raichle, ME, MacLeod, AM, Snyder, AZ, Powers, WJ, Gusnard, DA, Shulman, GL (2001): A default mode of brain function. Proc. Natl. Acad. Sci. U.S.A, 98(2), 676-682.

Raichle, ME, Snyder, AZ (2007): A default mode of brain function: a brief history of an evolving idea. Neuroimage, 37(4), 1083-1090; discussion 1097-1099.

Rogers, BP, Morgan, VL, Newton, AT, Gore, JC (2007): Assessing functional connectivity in the human brain by fMRI. Magn Reson Imaging, 25(10), 1347-1357.

Rugg, MD, Curran, T (2007): Event-related potentials and recognition memory. Trends Cogn. Sci. (Regul. Ed.), 11(6), 251-257.

Rugg, MD, Fletcher, PC, Allan, K, Frith, CD, Frackowiak, RS, Dolan, RJ (1998): Neural correlates of memory retrieval during recognition memory and cued recall. Neuroimage, 8(3), 262-273.

Scoville, WB, Milner, B (2000): Loss of recent memory after bilateral hippocampal lesions. 1957. J Neuropsychiatry Clin Neurosci, 12(1), 103-113.

Sheline, YI, Raichle, ME, Snyder, AZ, Morris, JC, Head, D, Wang, S, Mintun, MA (2010): Amyloid Plaques Disrupt Resting State Default Mode Network Connectivity in Cognitively Normal Elderly. Biological Psychiatry, 67(6), 584-587.

Sorg, C, Riedl, V, Mühlau, M, Calhoun, VD, Eichele, T, Läer, L, et al. (2007): Selective changes of resting-state networks in individuals at risk for Alzheimer's disease. Proc. Natl. Acad. Sci. U.S.A, 104(47), 18760-18765.

Sorg, C, Valentin, R, Robert, P, Alexander, K, Afra, WM (2009): Impact of Alzheimer's Disease on the Functional Connectivity of Spontaneous Brain Activity. Curr Alzheimer Res. Retrieved September 21, 2009, from http://www.ncbi.nlm.nih.gov/pubmed/19747154.

Squire, LR (2009): The legacy of patient H.M. for neuroscience. Neuron, 61(1), 6-9.

Supekar, K, Menon, V, Rubin, D, Musen, M, Greicius, MD (2008): Network analysis of intrinsic functional brain connectivity in Alzheimer's disease. PLoS Comput. Biol, 4(6), e1000100.

Tulving, E (2002): EPISODIC MEMORY: From Mind to Brain. Annu. Rev. Psychol., 53(1), 1-25.

Tulving, E, Kapur, S, Markowitsch, HJ, Craik, FI, Habib, R, Houle, S (1994): Neuroanatomical correlates of retrieval in episodic memory: auditory sentence recognition. Proc. Natl. Acad. Sci. U.S.A, 91(6), 2012-2015.

U.S. Department of Health & Human Services (2009, May 7): Fiscal Year 2010 Budget in Brief. Retrieved February 8, 2011, from http://dhhs.gov/asfr/ob/docbudget/2010budgetinbriefl.html.

Vilberg, KL, Rugg, MD (2008): Memory retrieval and the parietal cortex: a review of evidence from a dual-process perspective. Neuropsychologia, 46(7), 1787-99.

Wang, L, Zang, Y, He, Y, Liang, M, Zhang, X, Tian, L, Wu, T, Jiang, T, Li, K (2006): Changes in hippocampal connectivity in the early stages of Alzheimer's disease: evidence from resting state fMRI. Neuroimage, 31(2), 496-504.

Wimo, A, Winblad, B, Jönsson, L (2010): The worldwide societal costs of dementia: Estimates for 2009. Alzheimers Dement, 6(2), 98-103.

Zhang, H-Y, Wang, S-J, Liu, B, Ma, Z-L, Yang, M, Zhang, Z-J, Teng, G-J (2010): Resting brain connectivity: changes during the progress of Alzheimer disease. Radiology, 256(2), 598-606.

# CHAPTER 1

## Early Parietal Response in Episodic Retrieval Revealed with MEG

**Abstract**

Recent neuroimaging and lesion studies have led to competing hypotheses for potential roles of the left lateral parietal lobe in episodic memory retrieval. These hypotheses may be dissociated by whether they imply a role in pre-retrieval or post-retrieval processes. For example, one hypothesis is the left parietal cortex (particularly in more ventral subregions) forms part of an "episodic buffer" that supports the online representation of the retrieved target, a role that is, by definition, post-retrieval. An alternate view maintains parietal activity (particularly in more dorsal subregions) contributes to top-down orientation of attention to retrieval search, a pre-retrieval role. The present investigation seeks to reveal the earliest onset of lateral parietal activity in three anatomically-defined subregions of the left lateral parietal cortex in order to identify any pre-retrieval activation. Subjects performed a pair-cued recall task while neural activity was recorded with magnetoencephalography (MEG) at millisecond temporal resolution. MEG data were then mapped to each subject's cortical surface using dynamic statistical parametric mapping (dSPM). Both dorsal and ventral regions showed retrieval-related activations beginning within approximately 100 ms of the cue to retrieve and lasting up to 400 ms. We conclude that this early and transient pattern of activity in lateral parietal cortex is most consistent with a pre-retrieval role, possibly in directing attention to episodic memory retrieval.

## 1.1  Introduction

Retrieval of episodic memory is consistently associated with increases in activity of the lateral parietal cortex. Converging evidence of this association is found in studies using positron emission tomography (PET) (Tulving et al., 1994; Owen et al., 1996; Rugg et al., 1998; for review, see Cabeza and Nyberg, 2000), event-related functional MRI (fMRI) (for review, see Vilberg and Rugg, 2008a; Cabeza, 2008; Ciaramelli et al., 2008), and event-related potentials (ERPs) measured by electroencephalography (EEG) (for review, see Rugg and Curran, 2007; Friedman and Johnson, 2000). While parietal damage is not as commonly associated with memory deficits as damage to the medial temporal or prefrontal cortices, it has long been known that parietal lesions can result in deficient attention to spatial aspects of memory (Bisiach and Luzzatti, 1978), and recent studies suggest some patients with parietal lesions may have poor free recall of detailed autobiographical memories (Berryhill et al., 2007; for review, see Olson and Berryhill, 2009).

For decades electrophysiologists have described an increase in activity, most prominent in electrodes over the left parietal cortex, for items correctly labeled as previously studied ("old") relative to items correctly labeled as novel ("new") (Duarte et al., 2004; Neville et al., 1986; Wilding and Rugg, 1996; Curran, 2004; for review, see Rugg and Curran, 2007; Rugg et al., 2002). The left parietal old/new effect onsets approximately 400-450 ms after presentation of the test item, and typical average response times in recognition tests are approximately 800 ms or greater (Vilberg and Rugg, 2008a). Even allowing a few hundred milliseconds for execution of the

response, the parietal effect begins prior to response selection and therefore sufficiently early to play a role in episodic retrieval (Vilberg and Rugg, 2008a).

The magnitude of this "left parietal old/new effect" is modulated by the type of memory retrieval. For example, it is greater for recollection (memory of a studied item as well as contextual details from the study event) than for familiarity (memory of a studied item alone, without recalling the precise study event) (Vilberg and Rugg, 2008a; for review of the 'dual-process' description of recognition memory see Rugg and Yonelinas, 2003; Yonelinas, 2001). When the quality of the study experience is varied, the parietal old/new effect measured during retrieval is greater for items believed to have been deeply encoded than for those shallowly encoded (Vilberg and Rugg, 2008a). Additionally, retrieval events believed to reflect a larger retrieved load have been shown to elicit a larger left parietal old/new effect (Vilberg and Rugg, 2008a, 2008b).

Event-related fMRI studies confirmed the previous ERP findings of left parietal activation in retrieval tasks (Buckner and Wheeler, 2001; Henson et al., 1999; Kahn et al., 2004; Rugg et al., 2002; Wagner et al., 2005; Wheeler and Buckner, 2003), providing converging evidence and leading to several competing hypotheses for the still unclear role this region plays in retrieving episodic memories. One hypothesis supported by evidence from a large number of studies is that the lateral parietal cortex forms part of an "episodic buffer" acting to hold retrieved information (Baddeley, 2000; Vilberg and Rugg, 2008a; Wagner et al., 2005). Another hypothesis, also consistent with much of the current literature, is that lateral parietal cortex is involved in directing attention internally to memory (Cabeza, 2008; Ciaramelli et al.,

2008; Wagner et al., 2005). At least two other ideas have also been described: the first maintains that parietal activity does not reflect retrieval of episodic information, but rather is associated with the subjective experience of recollection (Ally et al., 2008; Olson and Berryhill, 2009); the second suggests the parietal region acts as a "mnemonic accumulator," integrating the accumulated evidence for a memory until a threshold is reached that signals recognition (Wagner et al., 2005).

With its much higher spatial resolution, studies using fMRI have produced considerable evidence suggesting the left lateral parietal cortex may be functionally dissociated with respect to episodic retrieval into dorsal and ventral subregions (Cabeza, 2008; Ciaramelli et al., 2008; Vilberg and Rugg, 2008a). As two of the leading theories for left parietal involvement in recognition memory make distinct hypotheses for the dorsal and ventral subregions, the present article will treat these subregions as having potentially distinct roles. The dorsal parietal cortex (DPC) lies in and superior to the intraparietal sulcus—corresponding most consistently to the lateral portion of Brodmann Area (BA) 7 (Cabeza, 2008; Ciaramelli et al., 2008; Vilberg and Rugg, 2008a, 2008b), but also reported as including adjacent portions of BA 19 (Ciaramelli et al., 2008) or BA 40 (Vilberg and Rugg, 2008a). The ventral parietal cortex (VPC) most consistently includes the angular gyrus (BA 39) (Cabeza, 2008; Ciaramelli et al., 2008; Vilberg and Rugg, 2008b), but also may include adjacent posterior and inferior areas, BA 40 (Cabeza, 2008; Ciaramelli et al., 2008) and BA 19 (Vilberg and Rugg, 2008b).

1.1.1   Left Dorsal Parietal Cortex (DPC)

One view maintains that DPC activity in memory tasks may reflect goal-driven, top-down direction of attention to retrieval (Cabeza, 2008; Ciaramelli et al., 2008). Familiarity judgments may require greater effort to direct attention to retrieval than recollection judgments (Ciaramelli et al., 2008), and at least two meta-analyses of left parietal fMRI activations have found the DPC to be more closely linked to familiarity than to recollection (Ciaramelli et al., 2008; Vilberg and Rugg, 2008a). Similarly, items for which subjects have lower confidence might also require greater top-down attention than items assigned high confidence judgments and therefore result in greater activation of the DPC (Cabeza, 2008; Ciaramelli et al., 2008). This assertion is supported by several studies of recognition memory where subject confidence ratings were obtained (Cabeza, 2008; Ciaramelli et al., 2008; Daselaar et al., 2006; Fleck et al., 2006; Kim and Cabeza, 2007, 2009). Finally, two meta-analyses found greater activation increases in the DPC for specific source recall relative to subjective recollection (Ciaramelli et al., 2008; Spaniol et al., 2009). As the authors point out, source recall requires retrieving specific contextual details, while subjective recollection in the "remember/know" paradigm requires only some contextual details to come to mind; thus, source recall is expected to result in greater top-down retrieval effort and greater activity in the DPC.

Another view asserts that activity in the DPC during episodic memory tasks does not contribute directly to retrieval at all, but rather reflects "processes downstream of retrieval" and depends on the salience or behavioral relevance of the presented item (Vilberg and Rugg, 2008a). The authors note DPC activity in recognition tasks may not be specific for familiarity, as DPC activity has also been

observed to accompany recollection in some studies (Henson et al., 1999; Vilberg and Rugg, 2008a). Additionally, one experiment showed the DPC recognition effect to be sensitive to the relative frequency of old and new test items, which the authors suggest would not be expected if the region contributed directly to retrieval (Herron et al., 2004).

1.1.2 Left Ventral Parietal Cortex (VPC)

There is greater agreement that the VPC plays a direct role in retrieval. One proposal for the function of the VPC is that of an episodic buffer (or part of the network supporting a buffer), whose activity serves to hold retrieved information (Baddeley, 2000; Vilberg and Rugg, 2008a; Wagner et al., 2005). Greater activations found in the VPC for recollection relative to familiarity support a VPC role in recollection (Vilberg and Rugg, 2008a). In contrast to DPC effects, VPC retrieval effects were not shown to be sensitive to the relative frequencies of old and new test items (Herron et al., 2004). Perhaps most interesting, two studies have shown VPC activity to be greater when subjects are believed to have recollected more information (Vilberg and Rugg, 2007, 2008b). Vilberg and Rugg (2008a) maintain that this dependence of VPC activity on the size of the retrieved "load" is most consistent with an episodic buffer.

The attention hypothesis assigns the VPC a role reflecting automatic, bottom-up attention that is "captured" by the retrieved output (Cabeza, 2008; Ciaramelli et al., 2008). As with the episodic buffer hypothesis, VPC activation is expected to have increased activity for recollection relative to familiarity, and that activity is expected

to vary with the size of the retrieved load. However, in the attention model, VPC activity reflects the increased attentional demands of retrieved information rather than buffering of that information (Cabeza, 2008; Ciaramelli et al., 2008). High confidence responses in recognition studies lead to greater VPC activation (Cabeza, 2008; Ciaramelli et al., 2008; Daselaar et al., 2006; Fleck et al., 2006; Kim and Cabeza, 2007, 2009), a finding that may be explained by stronger bottom-up attention paid to stronger memories (Cabeza, 2008). As recollection judgments tend to be associated with higher confidence than familiarity judgments, it follows that VPC activity is greater for recollection than familiarity (Cabeza, 2008). Additional evidence supporting the bottom-up attention to memory hypothesis comes from a meta-analysis showing greater VPC activity for deeply encoded items (Ciaramelli et al., 2008). Finally, the bottom-up attention explanation finds support in a study of patients with bilateral parietal infarcts that included VPC (Berryhill et al., 2007). The spontaneous autobiographical memories produced by these patients were poor in detail, but they were able to produce a normal amount of detail of the same memories when probed with specific questions (Berryhill et al., 2007). Interpreted in terms of the attention hypotheses, answering specific questions may rely more on top-down attention, whereas these patients' deficient spontaneous retrieval may reflect impaired bottom-up attention to the memories (Cabeza, 2008).

1.1.3   Temporal Dynamics

The respective timing of DPC and VPC activity could inform the evaluation of their proposed mechanistic roles. Some proposed roles (e.g., episodic buffer,

mnemonic accumulator, and attentional capture by retrieved information) would best explain activity that begins after retrieval has occurred, while a very early activation would be more consistent with a role in directing attention to memory. However, the temporal dynamics of left parietal subregions remain unknown. Methodological constraints have limited direct investigation of the timing of activity in the DPC and VPC: fMRI lacks sufficient temporal resolution to dissociate pre- and post-retrieval processes, and the ERP parietal old/new effect has not been localized to specific cortical subregions. However, a relatively recent method, dynamic statistical parametric mapping (dSPM), allows combination of magnetoencephalography (MEG) and structural MRI to calculate maps of estimated subregional cortical activity with millisecond temporal resolution (Dale et al., 2000).

In the present study we used MEG and dSPM to investigate the early response of left parietal cortex in episodic retrieval. Prior ERP and fMRI studies still leave at least two key points unknown. The first is whether parietal activity is present in the first 400 ms of episodic retrieval. The second is whether early parietal activity in retrieval localizes to DPC, VPC, or both. Answers to each of these questions have consequences for the hypotheses described above. For example, if retrieval-related activity in either region begins after sufficient time has passed for retrieval to occur, this finding would support roles downstream of retrieval. Alternatively, a very early pattern of activity (especially if transient) may be most consistent with orientation of attention to memory search.

To isolate whether parietal lobe subregions participate in the earliest retrieval processes, such as orientation to memory search, we examined the first 500 ms after

cue to retrieve. Healthy subjects studied pairs of drawings of common objects prior to scanning and were tested during MEG recording. A single item from one of the pairs was presented in each trial of the test phase. In the control ('classify') condition, subjects made a living/nonliving judgment on the presented item; in the retrieval ('recall-classify') condition, subjects made a living/nonliving judgment on the absent pair of the presented item, which they had to retrieve from memory. The dSPM method (Dale et al., 2000) was used to estimate relative increases in neural activity associated with retrieval in specific, anatomically-defined subregions of the left lateral parietal cortex.

## 1.2   Materials and Methods

### 1.2.1   Participants

Eleven healthy, right-handed adults (mean age: 23.7 years; 6 male) participated in this study, which was approved by the institutional review board of the University of California, San Diego. Informed consent was obtained from each subject prior to participation. Subjects received $40 for their participation.

### 1.2.2   Task

Prior to the MEG session, subjects studied 128 pairs of drawings of common objects and animals on a computer screen. Each pair was displayed for three seconds on three separate occasions, and subjects were instructed to memorize the pairs for subsequent testing.

Approximately 45 minutes after completing the study phase, subjects began the test phase while MEG signals were recorded. In all test phase trials, a single drawing from one of the studied pairs was presented for 500 ms in one of two boxes (Figure 1.1), followed by an additional 2750 ms response period. During 'classify' trials, subjects simply indicated by a finger response whether the presented stimulus was a living object. During 'recall-classify' trials, subjects indicated whether the absent *associate* of the presented stimulus was a living object, requiring recall of the paired associate. A colored box, present from 1000 ms prior to stimulus onset, designated the trial type—green for classify, red for recall-classify. A fixation cross, flanked by two black boxes, was shown for the first 250 ms of each trial. Subjects were instructed to respond as quickly and accurately as possible.

The test phase comprised 256 trials, presented in eight runs of 32 trials each. Five subjects were given 'trial list A,' and six subjects were given 'trial list B.' Each trial list was constructed by pseudorandomly choosing the order of the stimulus pairs, then, for each trial, pseudorandomly choosing which stimulus of the pair to present, which side to present it on, and which condition (classify or recall-classify) the trial would correspond to. The lists were then manually adjusted to ensure a balance between the two conditions in each run, as well as to remove any long streaks of a single condition, stimulus presentation side, or correct response (living or non-living).
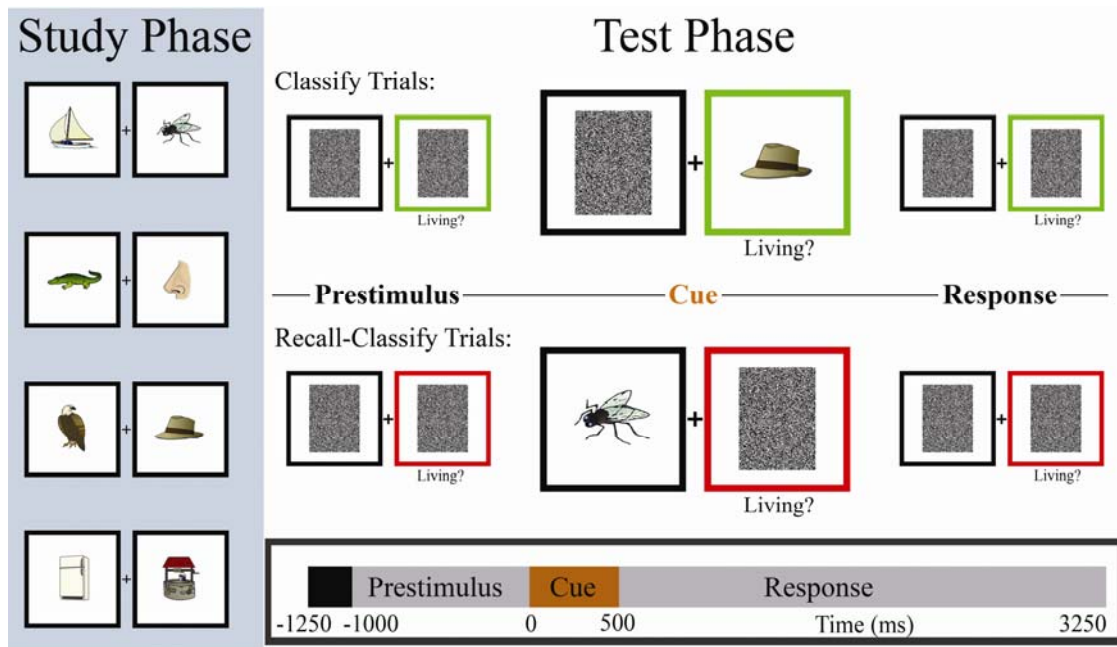
**Figure 1.1:** Pair-cued recall task. Subjects viewed each pair for 3 seconds during the study phase (repeated in random order 3 times). MEG recordings were acquired during the test phase. In classify trials subjects made a simple living/non-living judgment on the presented item. In recall-classify trials subjects retrieved the absent associate and then made a living/non-living judgment on the item in memory. In both conditions the test item was equally likely to appear on the left and right sides. The timeline at the bottom of the figure represents trial timing for the test phase. During the period of the timeline represented in black, the boxes and fixation cross were presented with both boxes in black. The cue period is enlarged only for display in the figure.

Both phases of the task were created and displayed using Presentation software (Neurobehavioral Systems, Inc., Albany, CA, USA). During MEG acquisition, stimuli were presented using a three-mirror DLP projector. Subjects indicated their responses by lifting a finger that was otherwise blocking a laser. For two subjects, a single run had to be excluded from analysis where subjects' finger movements were inadequate for response recording.

### 1.2.3  MEG Acquisition

MEG data were recorded via a 306 channel whole-head MEG system (Elekta Neuromag, Elekta, Inc., Helsinki, Finland), consisting of 204 planar gradiometers and 102 magnetometers. Two electro-oculograph (EOG) electrodes were placed, one each above and below the left eye, to monitor eye movements and blinks. To facilitate registration of the MEG sensor locations to each subject's structural MRI, three head position coils were placed, and the locations of approximately 150 fiducial landmarks were recorded with a Polhemus Fastrak digitizer (Polhemus, Colchester, VT, USA). MEG signals were sampled at 1,000 Hz, with an anti-aliasing filter of 333 Hz.

A band-pass filter was applied offline between 0.2 Hz and 33 Hz, and the data were then downsampled to 100 Hz. Individual trials containing eye blinks or other artifacts during the baseline period or time period of interest (or immediately before or after either of these periods) were excluded from analysis. No other trials were excluded. An average MEG recording (event-related field, or ERF) was calculated for each subject from all remaining trials of the same condition.

### 1.2.4  MRI Acquisition

Two high-resolution, three-dimensional, $T_1$-weighted volumes (TE: 4.9 ms, TR: 10.7 ms, TI: 1,000 ms, flip angle: 8 degrees, matrix: 256 x 256, voxel size: 1 mm x 1 mm x 1mm) were acquired for each subject on a General Electric 1.5T Signa Excite HDx using an 8-channel phased-array head coil (General Electric Healthcare, Waukesha, WI, USA). Image intensities were corrected for spatial sensitivity

inhomogeneities in the eight-channel head coil by normalizing with the ratio of a body

coil scan to a head coil scan.

1.2.5   Cortical Surface Reconstruction

A model of each subject's cortical surface was generated (Dale et al., 1999;

Fischl et al., 1999a) to serve as the source space for the locations of dipoles in the

MEG analysis. The two $T_1$-weighted MRI volumes were first corrected for spatial

distortion due to gradient nonlinearity (Jovicich et al., 2006), registered to each other,

and then averaged to improve the signal-to-noise ratio.  The FreeSurfer software

package (version 3.0.5, http://surfer.nmr.mgh.harvard.edu) was used to create a high-

resolution surface mesh for each hemisphere, representing the gray-white matter

boundary. This folded surface was subsampled to define the assumed cortical dipole

locations—approximately 2,500 dipoles per hemisphere, about 7 mm apart.  For group

analyses, individual surfaces were aligned to a spherical representation of the

FreeSurfer average subject  (Fischl et al., 1999b).

1.2.6   MEG Activity Estimates

For each condition, a time series of estimated activity at each dipole was

calculated from the gradiometer data of each subject's average MEG using the

dynamic statistical parametric mapping (dSPM) method described by Dale et al.

(2000). The dSPM method involves computing a noise-normalized, $L_2$ minimum-

norm, linear inverse to estimate the strength of each dipole's contribution to the

average MEG recording at every time point in the series. The dSPM estimate is a

measure of the MEG signal to noise ratio (SNR) at each spatial location; MEG SNR is related to neural activity, and so, in reference to MEG data, the terms activity and dSPM amplitude are used interchangeably in this paper. Forward solutions were calculated using the boundary element method (Mosher et al., 1999; de Munck, 1992; Oostendorp and van Oosterom, 1989).  A surface tesselation was created for the inner skull from the same high-resolution $T_1$-weighted MRI volume used for cortical surface reconstruction (SegLab, from Elekta). Baseline correction was performed on individual trial sensor waveforms and on the average waveforms using the period from -1090 ms to -950 ms (see Figure 1.1).

A noise covariance matrix was calculated from the same baseline period of individual trials. Three orthogonal vector components of each dipole were estimated simultaneously at every time point, thus allowing the dipole orientation to freely vary, and the corresponding vector magnitude, after normalizing by noise sensitivity, was taken as the estimated activity for that dipole. The result of the dSPM analysis was two time series (one for recall-classify, and one for classify) for each subject, representing the estimated activity at each dipole (i.e., cortical location). Because the MEG recordings were downsampled to 100 Hz, the interval between time points was 10 ms. Time series from the recall-classify and classify conditions were compared to identify activity differences attributable to episodic retrieval.

1.2.7   ROI Time Course Analysis

MEG activity was estimated at dipoles aligned to the FreeSurfer average subject, allowing anatomical ROIs to be defined using the cortical parcellation

available in FreeSurfer. Individual subject data from dipoles within the left superior parietal ROI (ROIs shown in Figure 1.2A) were combined to create an average ROI time series for each condition. This procedure was repeated for the other two ROIs: left inferior parietal and left supramarginal. Each ROI comprised approximately 160 dipoles.

A three-way repeated measures ANOVA with repeated factors of location (3 ROIs), condition, and time was performed in order to examine the data for significant ($p < 0.05$) main effects and interactions (PASW 18, SPSS Inc., Chicago, IL, USA). ROI time series data were separated into sub-periods of 100 ms (i.e., 100-190 ms, 200-290 ms, etc.), and, for the ANOVA, activity estimates from each subject were averaged across the time points in each sub-period. Five sub-periods were initially included in the analysis, corresponding to the first 500 ms after cue onset. Subject blink frequency, possibly increased at stimulus offset, and disparities in response time made exploratory analysis of the entire length of the -1000 ms to 3250 ms task impractical due to reduced power, and thus our analyses remained focused on testing for an early response in the parietal lobe.

To further explore the temporal dynamics of the activity difference between the recall-classify and classify conditions, paired *t*-tests were performed on data from individual sub-periods. Sub-periods extending from 300 ms prior to cue onset to 500 ms after cue onset were examined, and activity differences were considered significant at the $p < 0.01$ level, after applying a Bonferroni correction for multiple comparisons. For the *t*-tests, all time points from each subject's 100 Hz data were included.

A supplementary analysis was performed to assess whether a potential activity difference between the two conditions immediately prior to stimulus onset could partially account for activity differences observed after stimulus onset. Activity levels in the immediate pre-stimulus period were subtracted from the time series, and statistical comparisons were repeated. A detailed description of these methods is provided in the Supporting Information.

While the left lateral parietal cortex was the *a priori* area of interest, a *post-hoc* analysis of FreeSurfer ROIs from lateral and medial cortex of both hemispheres was also performed and is described further in the supplementary material available online (and in Section 1.7).

## 1.2.8 Individual Dipole Analysis

Left hemisphere MEG data were analyzed at each dipole on the lateral surface to visualize individual parietal dipole activity across the entirety of the lateral hemisphere. For each dipole, the average classify time series was subtracted from the recall-classify time series, giving an estimated activity difference for every time point. The activity difference at each dipole was displayed on the folded cortical surface to create an image at each time point. Together these images form a movie that shows the evolution of estimated activity on the surface of the left hemisphere in 10 ms intervals over the entire period of interest.

## 1.3 Results

### 1.3.1 Behavioral Results

On average, subjects took about half a second longer to respond in recall-classify trials than in classify trials. The mean (± standard deviation) response time was 1701 ± 228 ms for recall-classify trials and 1244 ± 181 ms for classify trials, representing a significant difference ($p < 10^{-5}$, two-tailed *t*-test).

A subject response was recorded within the specified response period in 89% of trials. Of these trials, subjects responded correctly in 96 ± 6% of classify trials and 85 ± 7% of recall-classify trials. A technical malfunction in linking one subject's recorded responses to each presented stimulus prevented exact measurement of his accuracy. Despite this, the recorded responses indicate that his performance was similar to that of other subjects.

## 1.3.2  ROI Time Course Analysis Results

A three-way repeated measures ANOVA established differences in activity between ROIs, time sub-periods, and conditions. There was a significant main effect of location, $F(2,20) = 5.0$, $p < 0.05$; of time, $F(4,40) = 4.4$, $p < 0.01$; and of condition, $F(1,10) = 4.6$, $p < 0.05$. There was also a significant interaction of time with condition, $F(4,40) = 3.1$, $p < 0.05$. Interactions of location with time and location with condition were not significant.
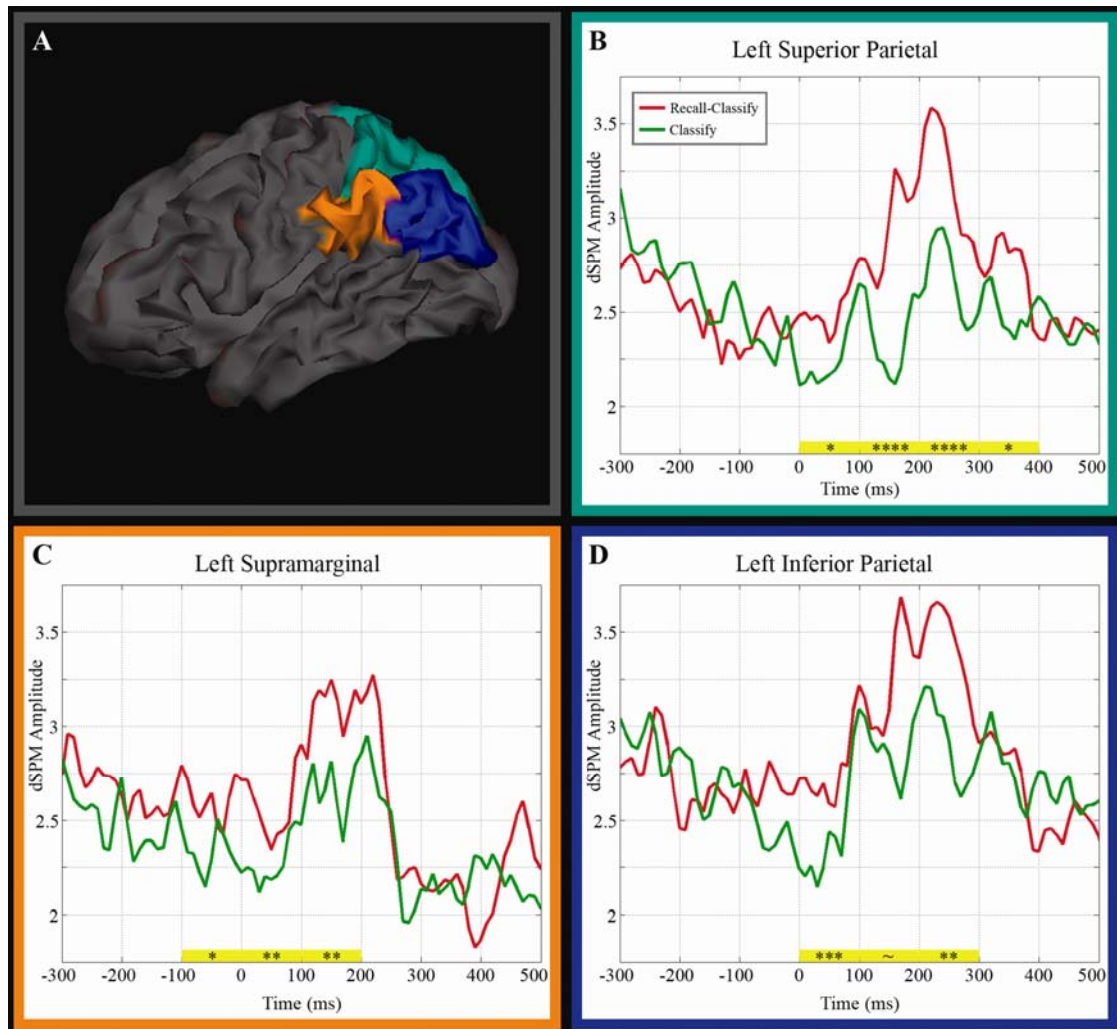
**Figure 1.2:** Three anatomical ROIs (**A**) on the left cortical surface and their estimated activity time courses  (note baseline dSPM amplitude is ~1.0) (**B-D**): Superior Parietal (green, **B**), Supramarginal (orange, **C**), Inferior Parietal (blue, **D**). Recall-classify activity was significantly greater than classify activity for 100 ms time periods indicated in yellow; *: $p < 0.01$, **: $p < 0.001$, ***: $p < 10^{-4}$, ****: $p < 10^{-7}$ (p-values from paired *t*-tests).

Time series plots show that in all three left parietal ROIs, average MEG activity in the recall-classify condition was greater than in the classify condition during the first 100 ms after stimulus onset (Figure 1.2, B-D). In the left superior parietal ROI, recall-classify activity remained greater than classify activity for

approximately 400 ms (Figure 1.2B), with a peak difference at approximately 150 ms.
Recall-classify activity was also greater than classify activity in the left supramarginal
ROI (Figure 1.2C), though the effect started earlier (100 ms prior to stimulus onset)
and was of shorter duration, resolving by 250 ms after the stimulus. Left inferior
parietal recall-classify activity (Figure 1.2D) differed from classify activity during the
first 100 ms, then temporarily approached that of the classify condition, but soon
diverged again and remains elevated above the classify time series until approximately
300 ms.

Testing 100 ms sub-periods by paired $t$-tests revealed left superior parietal
recall-classify activity was significantly greater than classify activity over 0-100 ms ($t$
= 4.4, $p < 0.001$), 100-200 ms ($t = 6.5$, $p < 10^{-7}$), and 200-300 ms ($t = 6.6$, $p < 10^{-7}$),
with a trend toward significance over 300-400 ms ($t = 3.6$, $p < 0.05$). In the left
supramarginal ROI, recall-classify activity was significantly greater over -100-0 ms ($t$
= 4.2, $p < 0.01$), 0-100 ms ($t = 4.8$, $p < 0.001$), and 100-200 ms ($t = 5.0$, $p < 10^{-4}$). In
the left inferior parietal ROI, recall-classify activity was significantly greater over 0-
100 ms ($t = 4.4$, $p < 0.001$) and 200-300 ms ($t = 4.9$, $p < 10^{-4}$), with a trend over 100-
200 ms ($t = 3.2$, $p < 0.05$). There was also a trend toward significantly greater classify
activity in the left superior parietal ROI over -200 to -100 ms ($t = -3.6$, $p < 0.05$). None
of the ROIs shows a significant activity difference over 400-500 ms. All p-values
reported for these $t$-tests were corrected for multiple comparisons using the Bonferroni
method for 24 comparisons (eight sub-periods in three ROIs).

In a supplementary analysis, all significant between-condition activity
differences in the left superior parietal and left inferior ROIs remained significant after

subtraction of immediate pre-stimulus activity. In the left supramarginal ROI,

however, no significant activity difference remained in any of the 100 ms sub-periods

after subtraction of the pre-stimulus activity. Detailed results are included in the

supplementary material.
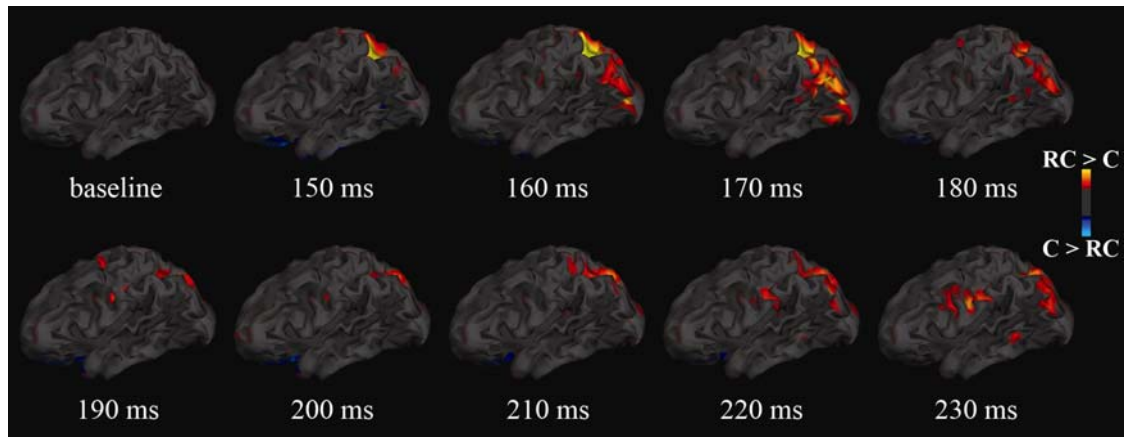


**Figure 1.3:** Early retrieval-related activity for left hemisphere. Baseline image is at -1000 ms and is representative of the other images from the baseline period. Overlay shows the activity difference between recall-classify (**RC**) and classify (**C**) conditions for baseline and from 150 to 230 ms following cue. Threshold was chosen for display purposes only; differences shown are greater than 1.0 in dSPM amplitude.

1.3.3   Individual Dipole Analysis Results

From visual inspection of the left hemisphere dSPMs, the parietal effect

appears to be the most prominent retrieval-related activity difference revealed by the

MEG recordings in this early time period (Figure 1.3). Other, smaller differences were

observed in caudal temporal and caudal frontal lobes.

## 1.4 Discussion

Our results demonstrate an early and transient activation in both dorsal and ventral regions of the left lateral parietal cortex in response to a cue to retrieve episodic memory. With an onset within 100 ms of the retrieval cue, this increase in parietal activity precedes recall of the target and therefore would not be consistent with manipulation or representation of retrieved information. Though the parietal lobe may be involved in such later processes as well, these data suggest the parietal lobe has at least an early involvement that is consistent with a role in orienting attention to retrieval.

One lateral parietal ROI (left supramarginal) had significantly greater activity in the recall-classify condition just prior to stimulus onset, and all three ROIs had recall-associated differences immediately following stimulus onset. Additionally, results from a supplementary analysis suggest post-stimulus activity differences in the left supramarginal ROI may be partially accounted for by the pre-stimulus activity difference in this region. The differences preceding stimulus onset must be dependent on the condition type generally, rather than an effort to retrieve a particular item. Recall-associated differences occurring after stimulus onset, though, may additionally depend on specific retrieval efforts. In any case, both anticipatory and reactionary parietal responses in these MEG recordings occur prior to retrieval of the target item.

These findings support a broader role for parietal lobe involvement in directing attention not only to external stimuli, but also to internal processes (e.g., Desmurget and Sirigu, 2009). MEG findings of anticipatory and reactionary responses in parietal cortex also converge with a recent fMRI study that attributes activity in left lateral

parietal cortex to processes both preceding and during an old/new recognition task (Phillips et al., 2009). The present study attempts to isolate episodic retrieval, rather than familiarity or general recognition, by using stimuli in the retrieval and control (classify) conditions that are equally familiar. This design allows for the possibility of incidental retrieval in control trials, which might have reduced measured retrieval effect. Despite this potential decrease in power, significantly greater activity was observed for trials that required episodic retrieval.

It is possible both anticipatory and reactionary effects simply reflect dissociable levels of arousal or effort in the two conditions. The recall-classify task is, overall, more difficult than the classify task because it requires retrieval of the absent associate, and subjects may therefore exhibit increased arousal or effort in the retrieval task. However, while increased general arousal might be expected to result in increased activity in the recall-classify condition throughout the duration of the trial, it is harder to explain why increased general arousal would result in the specific, transitory activity difference measured with MEG. As the effects presented here begin just before stimulus onset and last only a few hundred milliseconds, the relevant questions are whether a difficulty difference exists in the peri-stimulus onset period and, if so, whether such a difference is specifically related to episodic retrieval demands. Immediately following stimulus onset, subjects must either direct attention toward searching for episodic memory or toward searching for semantic memory. It is unknown whether subjects had more difficulty directing attention to semantic retrieval or to episodic retrieval, but the present results demonstrate that the left parietal lobe is more active when attention is directed toward search for episodic memory.

Another possible interpretation of these parietal responses is that they may represent part of a 'retrieval mode' or 'retrieval orientation,' tonic states that begin after instructions to retrieve and are maintained throughout retrieval effort (Rugg and Wilding, 2000; Tulving, 1983). Subjects were instructed to retrieve 1000 ms prior to stimulus onset, allowing time to adopt a retrieval state in anticipation of the retrieval task. There are several reasons to doubt this explanation, though. Most importantly, the retrieval mode, as defined by Tulving and colleagues, is a tonic state maintained while episodic retrieval is required (Düzel et al., 1999; see also Rugg and Wilding, 2000). The marked transience of the present parietal lobe findings argues against effects due to a sustained retrieval mode in the recall-classify condition. Further, the design of the trial would be expected to minimize such effects. There is support in the EEG literature to suggest that retrieval mode activity is poorly detected when alternating task designs are employed rather than blocks of retrieval (Herron and Wilding, 2006; Morcom and Rugg, 2002). Given that our design was a pseudorandom mixed event-related design, subjects are less likely to enter such a tonic retrieval state. Finally, prior EEG studies have not identified prominent retrieval mode effects in the left parietal lobe. Rather, these effects appear to be greatest in the right hemisphere (Düzel et al., 1999; Herron and Wilding, 2004, 2006; Morcom and Rugg, 2002; Nyberg et al., 1995; Rugg and Wilding, 2000), with some evidence for left frontal activity in retrieval orientations associated with certain types of target information (Morcom and Rugg, 2002).

Cabeza et al. (2008) and Ciaramelli et al. (2008) suggest, based on fMRI experiments, that the parietal lobe is involved in top-down attention to memory

retrieval (Cabeza, 2008; Ciaramelli et al., 2008). This hypothesis pertains specifically to the DPC. The present data lend support to this hypothesis, as the time course for our left superior parietal ROI does indeed show activation shortly after stimulus onset that could represent orientation to memory search. Regional anticipatory activity is also consistent with attention to retrieval in our task, as the subjects were instructed whether to retrieve well before stimulus onset. The transience of the activation (less than 400 ms duration) is not consistent with top-down attention to post-retrieval processes—for instance, attention to the retrieved target during classification in the recall-classify task—but the DPC activity may be involved in initiating search and retrieval.

Another hypothesis suggests DPC activity may depend on the salience or task relevance of the presented test item and that the DPC role is "downstream" of retrieval (Vilberg and Rugg, 2008a). The present data do not preclude the possibility of a later parietal activation that represents such information, but the very early DPC activation identified here, which begins over 1500 ms prior to the average behavioral response, cannot represent processes occurring only after successful completion of retrieval. Furthermore, the presented item in each condition is equally relevant to the behavioral task at hand, so the activity difference cannot easily be explained by behavioral relevance.

The early DPC activation, though likely upstream of retrieval, might nonetheless be partially driven by increased salience of the item presented under the recall-classify condition. In both conditions, the presented item had been previously studied, so they were equally 'old,' but it is difficult to determine whether salience of

the item was greater in the classify condition or in the recall-classify condition. On one hand, items presented in the classify condition were, themselves, to be classified, which might increase their salience. On the other hand, items presented in the recall-classify condition were cues that triggered a process of recall, requiring more effort and more attention. Under recall-classify conditions, this additional effort and attention is quickly directed away from the item and toward retrieval. A rapid and transient activation following the cue, such as that seen here, might therefore be consistent with such an interpretation. Activity prior to the cue cannot be explained by cue salience, but might possibly be attributed to anticipation of a more salient item.

The early VPC activity seen in MEG also suggests a pre-retrieval role for this region, though hypotheses based on fMRI focus on a post-retrieval role, including that VPC serves as a buffer for retrieved episodic memories. An episodic buffer (Baddeley, 2000; Vilberg and Rugg, 2008a; Wagner et al., 2005) whose function is to represent retrieved information would be expected to perform this function beginning once some information is retrieved, and would presumably have sustained activity as long as that retrieved information is held in mind. It is possible that a region contributing to an episodic buffer network might activate prior to actual retrieval in preparation for the coming retrieved load, but the transience of the MEG VPC effect is, again, difficult to reconcile with a role of holding retrieved information for manipulation during the task.

Current attentional hypotheses for VPC activity do not offer satisfactory interpretations of the present VPC findings. Existing attentional interpretations of VPC activity posit this region reflects the capture of bottom-up attention by the targets of retrieval (Cabeza, 2008; Ciaramelli et al., 2008). Given that cues presented during

each task were equally 'old' and that the VPC response observed using MEG preceded retrieval of the target, this hypothesis is not consistent with the current findings, unless one posits an additional, later VPC response. Another possibility, however, is that subjects, having been cued that the trial would involve retrieval, showed a differential early response in VPC elicited by the studied cue in recall-classify trials relative to those in classify trials. Nevertheless, given the timing of the response and the clearest difference between the conditions (requiring recall or not), the results of this study suggest that early VPC activity, like early DPC activity, might represent direction of attention toward memory retrieval.

## 1.5 Conclusions

We conclude that the left lateral parietal cortex is activated within 100 ms of a signal to retrieve episodic memories. In our cued-recall task, this earliest activation is also transient, persisting for only a few hundred milliseconds. While there are some differences in the timing of activity in different subregions of the lateral parietal lobe, each of our three ROIs (left superior parietal, left inferior parietal, left supramarginal) displayed an early and transient increase in estimated MEG activity when subjects were prompted to initiate retrieval. This very early response thus reflects processes prior to retrieval of the target and is most consistent with an attentional role in episodic retrieval. The finding of an early, robust, and transient activation does not preclude a later role, nor a later dissociation between subregions. Nevertheless, a comprehensive account of left lateral parietal function in episodic retrieval should include the early, transient activation revealed by MEG.

## 1.6 Acknowledgements

Chapter 1, in full, is a reprint of the material as it appears in Human Brain Mapping, 2010. Seibert, Tyler M.; Hagler, Donald J., Jr.; Brewer, James B., Wiley-Liss, 2010. The dissertation author was the primary investigator and author of this paper.

**1.7  Supplementary Materials**

<u>1.7.1  Supplementary Analysis Methods</u>

A supplementary analysis was performed to assess whether potential activity differences between the two conditions immediately prior to stimulus onset could partially account for activity differences observed after stimulus onset. The average activity level in each condition was calculated for the 100 ms prior to stimulus onset for each subject, and this average was subtracted from the corresponding activity time series. The modified activity time series were then compared by $t$-tests over 100 ms sub-periods from 0 ms to 500 ms after stimulus onset. Activity differences were considered significant at the $p < 0.01$ level, after Bonferroni correction for multiple (15) comparisons.

<u>1.7.2  Supplementary Analysis Results</u>

After subtraction of pre-stimulus activity, left superior parietal recall-classify activity remained significantly greater than classify activity over 0-100 ms ($t = 6.6$, $p < 10^{-7}$), 100-200 ms ($t = 8.32$, $p < 10^{-11}$), and 200-300 ms ($t = 9.84$, $p < 10^{-14}$). Left superior parietal recall-classify activity was also significantly greater than classify activity over 300-400 ms ($t = 5.5$, $p < 10^{-5}$); before subtraction of pre-stimulus activity, this difference showed a trend toward significance. In the left inferior parietal ROI, recall-classify activity remained significantly greater than classify activity over 0-100 ms ($t = 4.68$, $p < 0.001$) and 200-300 ms ($t = 4.84$, $p < 0.001$). In the left supramarginal ROI, no significant activity difference remained in any of the 100 ms sub-periods after subtraction of the pre-stimulus activity.

**Table 1.1:** Supplementary Table – Lateral cortex. While the left lateral parietal cortex was the *a priori* area of interest, a *post-hoc* analysis of the remaining FreeSurfer ROIs of the lateral cortex was also performed using the same methods as described for the ROI analysis in the manuscript. Several medial ROIs were also included in the analysis to rule out the possibility that the lateral parietal effects reflect crosstalk from sources in the medial temporal lobe or in primary visual cortex. Regions showing a sustained 'cluster' of significant activation are parietal and superior frontal in the left hemisphere, and dorsolateral prefrontal, parietal, and pars opercularis in the right hemisphere. P-values were corrected for multiple (294) comparisons using the Bonferroni method.
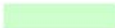
## Early Retrieval Response in Lateral and Medial Cortex

| | | time after stimulus onset ( ms) | | | | | | |
|---|---|---|---|---|---|---|---|---|
| | | -200-100 | -100-0 | 0-100 | 100-200 | 200-300 | 300-400 | 400-500 |
| Superior parietal | lh | -3.60 | 0.35 | *4.38 | §6.47 | §6.64 | 3.56 | -0.32 |
| Inferior parietal | lh | -1.71 | 2.45 | *4.35 | 3.19 | †4.92 | 0.11 | -2.54 |
| Supramarginal | lh | 1.61 | 4.20 | *4.80 | †5.00 | 2.73 | -0.65 | 0.76 |
| Superiorfrontal | lh | 2.28 | †5.49 | §6.82 | †5.44 | -1.55 | -1.90 | 2.42 |
| Rostral middle frontal | lh | 2.91 | 3.33 | 3.65 | -0.02 | 2.81 | 0.26 | 3.16 |
| Caudal middle frontal | lh | -2.20 | -0.14 | 2.02 | 2.87 | 2.92 | 1.36 | 0.38 |
| Pars orbitalis | lh | 1.02 | 0.13 | 1.47 | -1.21 | 0.58 | -0.68 | -1.72 |
| Pars opercularis | lh | -1.60 | -2.74 | -0.29 | -0.41 | 1.88 | -0.91 | -0.48 |
| Pars triangularis | lh | 2.37 | 0.97 | 2.07 | -2.76 | 0.41 | -0.88 | -1.72 |
| Precentral | lh | -2.78 | -1.08 | 2.07 | 3.13 | 1.80 | -0.41 | 1.83 |
| Postcentral | lh | -2.37 | 0.01 | 3.51 | 4.01 | 2.25 | -1.27 | 1.59 |
| Superior temporal | lh | -0.81 | 0.05 | 1.87 | 0.54 | -2.06 | †-4.93 | -3.22 |
| Middle temporal | lh | -0.61 | -0.28 | 0.73 | 0.95 | -0.11 | -0.92 | -0.37 |
| Inferior temporal | lh | 1.50 | 0.09 | -1.23 | -0.61 | 0.65 | 1.04 | 1.27 |
| Lateral occipital | lh | 0.60 | 0.97 | 0.64 | 0.85 | 3.91 | 2.85 | 4.12 |
| Parahippocampal | lh | 2.23 | 1.04 | 0.52 | -2.16 | 1.59 | 2.76 | 2.87 |
| Entorhinal | lh | 1.25 | 0.31 | -1.13 | -3.95 | 1.28 | 1.70 | 0.59 |
| Fusiform | lh | 1.60 | 1.26 | -1.19 | -1.01 | 0.95 | 2.42 | 2.96 |
| Cuneus | lh | -2.03 | 0.01 | 0.45 | -0.72 | 2.93 | 2.69 | 2.77 |
| Lingual | lh | 0.82 | -0.15 | 0.18 | 0.86 | 2.78 | 2.22 | *4.77 |
| Pericalcarine | lh | 0.30 | 0.17 | 0.35 | -0.24 | 4.02 | 2.30 | 2.89 |
| Superior parietal | rh | 3.49 | 2.86 | 0.23 | 1.29 | 0.55 | -1.49 | -1.24 |
| Inferior parietal | rh | -0.13 | 3.63 | 0.93 | 2.45 | 0.76 | -1.96 | -1.25 |
| Supramarginal | rh | 0.51 | 3.62 | 3.89 | *4.38 | §7.66 | †5.62 | 2.07 |
| Superior frontal | rh | 1.81 | 4.04 | †5.05 | †5.23 | -0.05 | -1.34 | -1.17 |
| Rostral middle frontal | rh | 0.81 | 3.81 | †5.21 | §6.82 | *4.83 | 0.97 | -0.55 |
| Caudal middle frontal | rh | †5.76 | †6.20 | †5.87 | †5.01 | 2.28 | -1.03 | 0.48 |
| Pars orbitalis | rh | †-5.40 | -1.98 | -4.04 | -1.31 | 0.30 | -1.18 | 1.44 |
| Pars opercularis | rh | 2.96 | †6.20 | 3.93 | *4.45 | 2.56 | -1.72 | -2.50 |
| Pars triangularis | rh | -2.45 | 0.29 | -0.97 | 2.98 | 1.49 | -0.76 | 0.67 |
| Precentral | rh | 2.15 | 3.44 | 2.02 | 2.89 | 3.87 | -1.31 | 1.74 |
| Postcentral | rh | 1.50 | 3.68 | 2.01 | 3.47 | 2.99 | 0.75 | 2.36 |
| Superior temporal | rh | -1.18 | 0.17 | -0.86 | 1.64 | 4.32 | -3.30 | -2.68 |
| Middle temporal | rh | -3.01 | -0.19 | -0.38 | -0.20 | 2.55 | †-5.53 | -4.03 |
| Inferior temporal | rh | -1.60 | -1.51 | -3.23 | -2.47 | -1.43 | †-6.07 | -3.05 |
| Lateral occipital | rh | -1.90 | †-5.56 | -2.66 | -2.18 | -1.88 | -2.98 | 1.60 |
| Parahippocampal | rh | †6.08 | 1.09 | -1.45 | -2.22 | -0.98 | -3.46 | -2.08 |
| Entorhinal | rh | *4.49 | 0.63 | -2.13 | -2.78 | -0.20 | -2.74 | -2.99 |
| Fusiform | rh | 1.15 | -2.21 | -3.17 | -2.58 | -1.97 | †-5.37 | -2.33 |
| Cuneus | rh | 0.16 | -3.95 | -1.98 | -1.42 | -0.20 | -0.88 | 2.93 |
| Lingual | rh | 1.31 | -1.94 | -1.07 | -1.42 | -1.48 | -2.50 | 2.13 |
| Pericalcarine | rh | -0.27 | -4.22 | -2.34 | -2.40 | -0.84 | -1.39 | 3.51 |

Data are *t* statistics from paired *t*-tests between conditions.
P-values are Bonferroni corrected for 294 comparisons (42*7).

|   |   |
|---|---|
| * | $p < 0.01$ |
| † | $p < 0.001$ |
| § | $p < 10^{-6}$ |

Recall-Classify > Classify

Classify > Recall-Classify

## 1.8 References

Ally, BA, Simons, JS, McKeever, JD, Peers, PV, Budson, AE (2008): Parietal contributions to recollection: electrophysiological evidence from aging and patients with parietal lesions. Neuropsychologia, 46(7), 1800-1812.

Baddeley, A (2000): The episodic buffer: a new component of working memory? Trends Cogn. Sci. (Regul. Ed.), 4(11), 417-423.

Berryhill, ME, Phuong, L, Picasso, L, Cabeza, R, Olson, IR (2007): Parietal lobe and episodic memory: bilateral damage causes impaired free recall of autobiographical memory. J. Neurosci, 27(52), 14415-14423.

Bisiach, E, Luzzatti, C (1978): Unilateral neglect of representational space. Cortex, 14(1), 129-133.

Buckner, RL, Wheeler, ME (2001): The cognitive neuroscience of remembering. Nat. Rev. Neurosci, 2(9), 624-634.

Cabeza, R (2008): Role of parietal regions in episodic memory retrieval: The dual attentional processes hypothesis. Neuropsychologia, 46(7), 1813-1827.

Cabeza, R, Nyberg, L (2000): Imaging cognition II: An empirical review of 275 PET and fMRI studies. J Cogn Neurosci, 12(1), 1-47.

Ciaramelli, E, Grady, CL, Moscovitch, M (2008): Top-down and bottom-up attention to memory: a hypothesis (AtoM) on the role of the posterior parietal cortex in memory retrieval. Neuropsychologia, 46(7), 1828-51.

Curran, T (2004): Effects of attention and confidence on the hypothesized ERP correlates of recollection and familiarity. Neuropsychologia, 42(8), 1088-1106.

Dale, AM, Fischl, B, Sereno, MI (1999): Cortical surface-based analysis. I. Segmentation and surface reconstruction. Neuroimage, 9(2), 179-194.

Dale, AM, Liu, AK, Fischl, B, Buckner, RL, Belliveau, JW, Lewine, JD, Halgren, E (2000): Dynamic statistical parametric mapping: combining fMRI and MEG for high-resolution imaging of cortical activity. Neuron, 26(1), 55-67.

Daselaar, SM, Fleck, MS, Cabeza, R (2006): Triple dissociation in the medial temporal lobes: recollection, familiarity, and novelty. J. Neurophysiol, 96(4), 1902-1911.

Desmurget, M, Sirigu, A (2009): A parietal-premotor network for movement intention and motor awareness. Trends Cogn. Sci. (Regul. Ed.), 13(10), 411-419.

Duarte, A, Ranganath, C, Winward, L, Hayward, D, Knight, RT (2004): Dissociable neural correlates for familiarity and recollection during the encoding and retrieval of pictures. Brain Res Cogn Brain Res, 18(3), 255-272.

Düzel, E, Cabeza, R, Picton, TW, Yonelinas, AP, Scheich, H, Heinze, HJ, Tulving, E (1999): Task-related and item-related brain processes of memory retrieval. Proc Natl Acad Sci U S A, 96(4), 1794-9.

Fischl, B, Sereno, MI, Dale, AM (1999a): Cortical surface-based analysis. II: Inflation, flattening, and a surface-based coordinate system. Neuroimage, 9(2), 195-207.

Fischl, B, Sereno, MI, Tootell, RB, Dale, AM (1999b): High-resolution intersubject averaging and a coordinate system for the cortical surface. Hum Brain Mapp, 8(4), 272-284.

Fleck, MS, Daselaar, SM, Dobbins, IG, Cabeza, R (2006): Role of prefrontal and anterior cingulate regions in decision-making processes shared by memory and nonmemory tasks. Cereb. Cortex, 16(11), 1623-1630.

Friedman, D, Johnson, R (2000): Event-related potential (ERP) studies of memory encoding and retrieval: a selective review. Microsc. Res. Tech, 51(1), 6-28.

Henson, RNA, Rugg, MD, Shallice, T, Josephs, O, Dolan, RJ (1999): Recollection and familiarity in recognition memory: an event-related functional magnetic resonance imaging study. J. Neurosci, 19(10), 3962-3972.

Herron, JE, Henson, RNA, Rugg, MD (2004): Probability effects on the neural correlates of retrieval success: an fMRI study. Neuroimage, 21(1), 302-310.

Herron, JE, Wilding, EL (2004): An electrophysiological dissociation of retrieval mode and retrieval orientation. Neuroimage, 22(4), 1554-1562.

Herron, JE, Wilding, EL (2006): Brain and behavioral indices of retrieval mode. Neuroimage, 32(2), 863-870.

Kahn, I, Davachi, L, Wagner, AD (2004): Functional-Neuroanatomic Correlates of Recollection: Implications for Models of Recognition Memory. J. Neurosci., 24(17), 4172-4180.

Kim, H, Cabeza, R (2007): Trusting our memories: dissociating the neural correlates of confidence in veridical versus illusory memories. J. Neurosci, 27(45), 12190-12197.

Kim, H, Cabeza, R (2009): Common and specific brain regions in high- versus low-confidence recognition memory. Brain Res, 1282, 103-113.

Morcom, AM, Rugg, MD (2002): Getting ready to remember: the neural correlates of task set during recognition memory. Neuroreport, 13(1), 149-152.

Mosher, JC, Leahy, RM, Lewis, PS (1999): EEG and MEG: forward solutions for inverse methods. IEEE Trans Biomed Eng, 46(3), 245-259.

de Munck, JC (1992): A linear discretization of the volume conductor boundary integral equation using analytically integrated elements. IEEE Trans Biomed Eng, 39(9), 986-990.

Neville, HJ, Kutas, M, Chesney, G, Schmidt, AL (1986): Event-related brain potentials during initial encoding and recognition memory of congruous and incongruous words. Journal of Memory and Language, 25(1), 75-92.

Nyberg, L, Tulving, E, Habib, R, Nilsson, LG, Kapur, S, Houle, S, Cabeza, R, McIntosh, AR (1995): Functional brain maps of retrieval mode and recovery of episodic information. Neuroreport, 7(1), 249-252.

Olson, IR, Berryhill, M (2009): Some surprising findings on the involvement of the parietal lobe in human memory. Neurobiol Learn Mem, 91(2), 155-65.

Oostendorp, TF, van Oosterom, A (1989): Source parameter estimation in inhomogeneous volume conductors of arbitrary shape. IEEE Trans Biomed Eng, 36(3), 382-391.

Owen, AM, Milner, B, Petrides, M, Evans, AC (1996): Memory for object features versus memory for object location: a positron-emission tomography study of encoding and retrieval processes. Proc. Natl. Acad. Sci. U.S.A, 93(17), 9212-9217.

Phillips, JS, Velanova, K, Wolk, DA, Wheeler, ME (2009): Left posterior parietal cortex participates in both task preparation and episodic retrieval. Neuroimage, 46(4), 1209-1221.

Rugg, MD, Wilding, EL (2000): Retrieval processing and episodic memory. Trends Cogn. Sci. (Regul. Ed.), 4(3), 108-115.

Rugg, MD, Curran, T (2007): Event-related potentials and recognition memory. Trends Cogn. Sci. (Regul. Ed.), 11(6), 251-257.

Rugg, MD, Fletcher, PC, Allan, K, Frith, CD, Frackowiak, RS, Dolan, RJ (1998): Neural correlates of memory retrieval during recognition memory and cued recall. Neuroimage, 8(3), 262-273.

Rugg, MD, Otten, LJ, Henson, RNA (2002): The neural basis of episodic memory: evidence from functional neuroimaging. Philos. Trans. R. Soc. Lond., B, Biol. Sci, 357(1424), 1097-1110.

Rugg, M, Yonelinas, A (2003): Human recognition memory: a cognitive neuroscience perspective. Trends Cogn. Sci. (Regul. Ed.), 7(7), 313-319.

Spaniol, J, Davidson, PSR, Kim, ASN, Han, H, Moscovitch, M, Grady, CL (2009): Event-related fMRI studies of episodic encoding and retrieval: meta-analyses using activation likelihood estimation. Neuropsychologia, 47(8-9), 1765-1779.

Tulving, E (1983): Elements of episodic memory. New York: Oxford University Press.

Tulving, E, Kapur, S, Markowitsch, HJ, Craik, FI, Habib, R, Houle, S (1994): Neuroanatomical correlates of retrieval in episodic memory: auditory sentence recognition. Proc. Natl. Acad. Sci. U.S.A, 91(6), 2012-2015.

Vilberg, KL, Rugg, MD (2007): Dissociation of the neural correlates of recognition memory according to familiarity, recollection, and amount of recollected information. Neuropsychologia, 45(10), 2216-2225.

Vilberg, KL, Rugg, MD (2008a): Memory retrieval and the parietal cortex: a review of evidence from a dual-process perspective. Neuropsychologia, 46(7), 1787-99.

Vilberg, KL, Rugg, MD (2008b): Functional significance of retrieval-related activity in lateral parietal cortex: Evidence from fMRI and ERPs. Hum Brain Mapp, 30(5), 1490-1501.

Wagner, AD, Shannon, BJ, Kahn, I, Buckner, RL (2005): Parietal lobe contributions to episodic memory retrieval. Trends in Cognitive Sciences, 9(9), 445-453.

Wheeler, ME, Buckner, RL (2003): Functional dissociation among components of remembering: Control, perceived oldness, and content. J. Neurosci, 23(9), 3869-3880.

Wilding, EL, Rugg, MD (1996): An event-related potential study of recognition memory with and without retrieval of source. Brain, 119 ( Pt 3), 889-905.

Yonelinas, AP (2001): Components of episodic memory: the contribution of recollection and familiarity. Philos. Trans. R. Soc. Lond., B, Biol. Sci, 356(1413), 1363-1374.

CHAPTER 2

## **Parietal Activity in Episodic Retrieval Measured by fMRI and MEG**

**Abstract**

Understanding the functional role of the left lateral parietal cortex in episodic retrieval requires characterization of both spatial and temporal features of activity during memory tasks. In a recent study using magnetoencephalography (MEG), we described an early parietal response in a cued-recall task. This response began within 100 milliseconds of the retrieval cue and lasted less than 400 milliseconds. Spatially, the effect reached significance in all three anatomically defined left lateral parietal subregions included in the study. Here we present a multimodal analysis of both hemodynamic and electrophysiologic responses in the same cued-recall paradigm. Functional MRI (fMRI) was used to more precisely reveal the portion of the parietal cortex with the greatest response. The MEG data set was then reanalyzed to show the early MEG time course of the region identified by fMRI. We found that the hemodynamic response is greatest within the intraparietal sulcus. Further, the MEG pattern in this region shows a strong response during the first 300 milliseconds following the cue to retrieve. Finally, when individual-dipole MEG activity is analyzed for the left cortical surface over the early 300-millisecond time window, significant recall-related activity is limited to a relatively small portion of the left hemisphere that overlaps the region identified by fMRI in the intraparietal sulcus.

## 2.1 Introduction

Recent efforts to assign a functional role for the prominent activations in left lateral parietal cortex during episodic retrieval tasks have produced competing hypotheses. One hypothesis holds that retrieved information is stored in an "episodic buffer" supported by the left parietal cortex (Baddeley, 2000; Vilberg and Rugg, 2008a; Wagner et al., 2005). Another hypothesis states that left parietal cortex participates in directing attention internally to memory search (Cabeza, 2008; Ciaramelli et al., 2008). Others have proposed that parietal cortex does not directly participate in retrieval and instead reflects the subjective experience of recollection (Ally et al., 2008).

The relatively high spatial resolution of functional magnetic resonance imaging (fMRI) has provided evidence for a further functional dissociation between left hemisphere dorsal parietal and ventral parietal cortex. In particular, ventral parietal activity has been associated with the episodic buffer. Some have questioned dorsal parietal involvement in retrieval, suggesting it may only reflect "processes downstream of retrieval" (Vilberg and Rugg, 2008a, 2008b). Under the attention to memory hypothesis, however, ventral parietal activity arises from attentional capture by retrieved information in an automatic, bottom-up process, and dorsal parietal activity supports goal-driven, top-down direction of attention to retrieval (Cabeza, 2008; Ciaramelli et al., 2008).

We recently proposed that these functional hypotheses could be distinguished by the timing of the parietal response (Seibert et al., 2010). Episodic buffer, subjective experience of recollection, and bottom-up attention all require that at least some

information has already been retrieved. Top-down attention to memory search, on the other hand, must begin prior to retrieval, and is consistent with an early parietal response. Using magnetoencephalography (MEG) in a cued-recall task, we observed a response in left posterior parietal cortex that began within 100 milliseconds (ms) of the cue and resolved in less than 400 ms. This early and transient activity increase is most consistent with an attentional role. However, the pattern of activity in the three anatomically-defined subregions probed in the study was fairly similar and did not show a dissociation of dorsal and ventral parietal cortices.

Both location and timing are required to characterize parietal activity in retrieval paradigms and improve understanding of its function. Dissociable spatial patterns within the parietal cortex have been observed with fMRI, but the hemodynamic response offers very limited information on timing. Conversely, our MEG results have revealed an early parietal response, but no clear dissociation was observed between the superior and inferior anatomical subregions probed in the study. While fMRI and MEG may measure different aspects of brain activity, both modalities provide important functional insights. The advantage of a multimodal approach is the opportunity to leverage both the spatial resolution of fMRI and the temporal resolution of MEG to investigate retrieval activity in the same region of parietal cortex.

In this manuscript, we present results from a combined analysis of a previously unpublished fMRI data set and our MEG data. We acquired BOLD functional data from subjects performing the same paradigm used in our previous MEG study (Seibert et al., 2010). We expected the hemodynamic response would reveal one or more significant activations within the left lateral posterior parietal cortex. Those regions

could then be used as masks for our MEG data to give insight into the temporal dynamics of neural activity in the functional regions of interest (ROI). We hypothesized that this multimodal analysis would confirm MEG findings of recall-associated activity in dorsal and ventral parietal subregions, while painting a more precise picture of the spatiotemporal dynamics of the left lateral parietal response in episodic retrieval.

## 2.2   Material and Methods

### 2.2.1   Participants

Sixteen healthy, right-handed adults participated in this study. Twelve subjects (mean age: $23.8 \pm 3$ years; five male) participated in the fMRI study, and eleven subjects (mean age: $23.7 \pm 3$ years; six male) participated in the MEG study. Seven subjects participated in both the fMRI and MEG studies; of these, four had fMRI first. These studies were approved by the institutional review board of the University of California, San Diego. Subjects gave informed consent prior to the experiment and received $40 for their participation.

### 2.2.2   Stimuli

Stimuli were 256 color drawings of common objects selected from Rossion and Pourtois color Snodgrass images (Rossion and Pourtois, 2004). Drawings were paired randomly into 128 pairs. Pairs were screened to remove those with obvious visual or semantic relationships.

2.2.3   Task

The behavioral task for fMRI sessions was identical to that previously

described for MEG sessions (Seibert et al., 2010). Subjects were tested on 128 pairs of

drawings of common objects and animals (which they had studied approximately 45

minutes prior to the experiment) while activity was recorded using either fMRI or

MEG. In all test phase trials, a single drawing from one of the studied pairs was

presented for 500 ms in one of two boxes (Figure 2.1), followed by an additional

2750-ms response period. During "classify" trials, subjects simply indicated by a

finger response whether the presented stimulus was a living or non-living object.

During "recall-classify" trials, subjects indicated whether the absent associate of the

presented stimulus was a living or non-living object, requiring recall of the paired

associate. A colored box, present from 1000 ms prior to stimulus onset, designated the

trial type—green for classify and red for recall-classify. A fixation cross presented

between two black boxes was shown for the first 250 ms of each trial. Subjects were

instructed to respond as quickly and accurately as possible.

The test phase comprised 256 trials, presented in eight runs of 32 trials each.

Order of presentation of stimulus pairs was pseudorandomized to create 'trial list A'

and 'trial list B,' each containing all pairs. The item presented from each pair, the side

of the screen it was presented on, and the condition associated with each pair were all

pseudorandomly determined separately for each trial list. All pairs were the same in

each list. In the MEG experiment, five subjects were given trial list A and six subjects

were given trial list B. In the fMRI experiment, six subjects were given trial list A, and

six subjects were given trial list B. Of the seven subjects who participated in both the

MEG and fMRI experiments, four were given trial list A first, and three were given trial list B first. The average interval between sessions for these subjects was 7.9 days (range: 5-11 days). During fMRI acquisition, stimuli were presented on a screen visible to the subject via a mirror, and subjects indicated their responses using an MRI compatible button box held in their right hand.
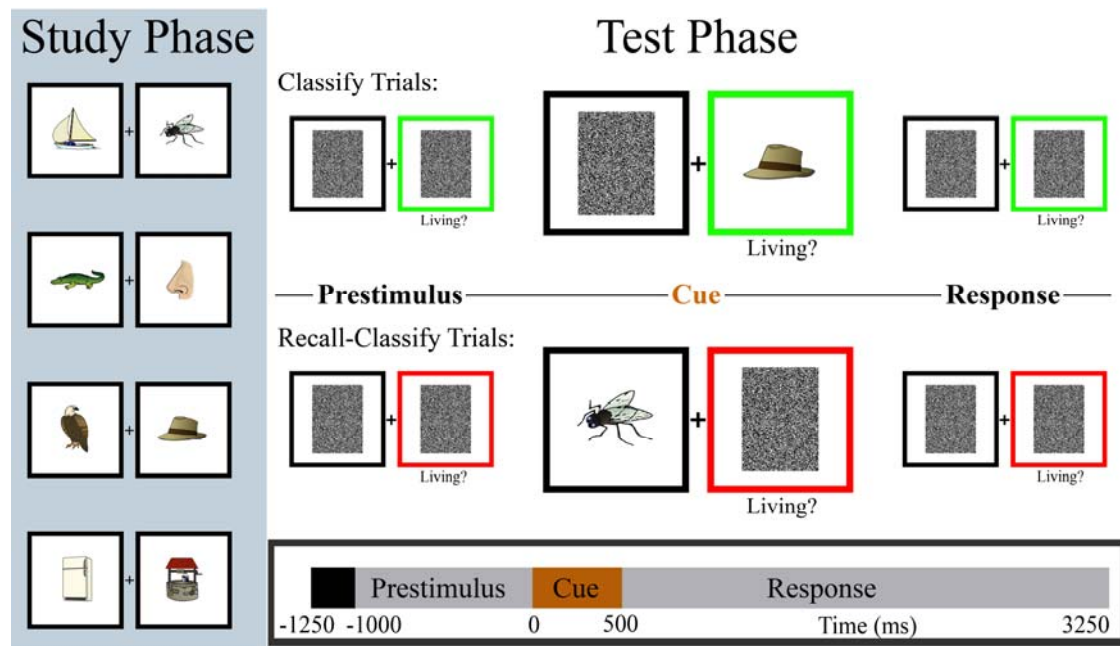


**Figure 2.1:** Pair-cued recall task. Subjects viewed each pair for 3 seconds during the study phase (repeated in random order three times). MEG or fMRI recordings were acquired during the test phase (timeline on bottom of figure). In classify trials subjects made a simple living/nonliving judgment on the presented item. In recall-classify trials subjects retrieved the absent associate and then made a living/nonliving judgment on the item in memory. In both conditions the test item was equally likely to appear on the left and right sides. A fixation cross and two black boxes were presented during the initial 250 ms of the trial. The cue period is enlarged only for display in the figure. Reproduced with permission from Seibert et al., 2010.

2.2.4   MRI Acquisition

Imaging was done with a 3T GE scanner at the Center for Functional MRI at the University of California, San Diego. Functional images were acquired using a gradient echo echo-planar, T2*-weighted pulse sequence (repetition time = 1.5 s, one shot per repetition, echo time = 30 ms, flip angle = 90°, bandwidth = 31.25 MHz). Twenty-two slices covering the entire brain were acquired perpendicular to the long axis of the hippocampus with 3.4 x 3.4 x 7 mm voxels. A T1-weighted high-resolution (1 x 1 x 1 mm), three-dimensional magnetization-prepared rapid gradient echo or fast spoiled gradient recalled anatomical dataset was also collected for each subject. An additional T1-weighted structural scan was acquired in the same slice locations as the functional images for use in confirming alignment of functional data to the high-resolution anatomical scan.

### 2.2.5   fMRI Analysis

An event-related design was used to examine parietal activity during the recall-classify and classify conditions. These were contrasted with an even-odd digit classification active baseline. Error trials (unsure, incorrect, and no-response) were excluded from the analysis. Trials were jittered with 0, 3, 6, or 9 seconds of baseline to optimize the study design (Dale, 1999).

Data from each run were reconstructed. Slices were temporally aligned and co-registered with a 3D registration algorithm. Voxels outside the brain were removed using a threshold mask of the functional data. A general linear model was constructed for multiple regression analysis using the AFNI suite of software (Cox, 1996) with six motion regressors from the registration process and regressors for recall-classify and

classify conditions correct and incorrect responses. For the recall-classify and classify conditions, a hemodynamic response was estimated, within each voxel, for the 15 seconds following trial onset using signal deconvolution .

Derived hemodynamic response time series for each condition were projected to a model of each subject's cortical surface (Dale et al., 1999; Fischl et al., 1999a) to facilitate comparison to the MEG analysis, which used surface meshes as the source space for dipole locations. The FreeSurfer software package (version 4.5.0, http://surfer.nmr.mgh.harvard.edu) was used to create a surface mesh for each hemisphere consisting of approximately 160,000 vertices per hemisphere. Anatomical regions of interest were identified through an automated parcellation of the individual surface using the Desikan-Killiany atlas (Desikan et al., 2006; Fischl et al., 2004). Three regions (corresponding to those used in the previous MEG study) were taken from the atlas as ROIs for fMRI analysis: left superior parietal, left inferior parietal, and left supramarginal.

BOLD activity was measured by averaging the expected peak parameter estimates from the hemodynamic response of each condition (corresponding to volumes acquired at 4.75, 6.25, 7.75, and 9.25 seconds following cue onset). Activity differences between conditions were assessed at the ROI and vertex levels. ROI differences were evaluated after averaging BOLD activity from all vertices within the region in each subject's native space and performing a two-tailed $t$-test across subjects for recall-classify vs. classify conditions. Vertex-wise analysis (for group-level maps) was performed after registering individual surfaces to a seventh-order icosahedron representation of the FreeSurfer average subject (Fischl et al., 1999b). To account for

variation in anatomy in the vertex-wise analysis, a conservative iterative smoothing process was applied to each subject's data before registering to the average surface, as well as to the group-level data after averaging across subjects (iterative smoothing was equivalent to a 6 mm full-width, half-maximum Gaussian kernel).

In addition to the atlas regions, a functional ROI within the left lateral parietal cortex was defined from a *t*-statistic map of BOLD activity differences between recall-classify and classify conditions. The region was defined as the cluster of supra-threshold vertices adjacent to the peak activity difference within the left lateral posterior parietal cortex, where the threshold was set by controlling the false discovery rate for the entire left hemisphere surface at 0.05 (Genovese et al., 2002). For display of the map, color thresholds were set for *t*-statistics corresponding to controlling the false discovery rate at 0.05 (minimum) and 0.01 (maximum).

2.2.6   MEG Analysis

MEG data acquisition, activity estimation using dynamic statistical parametric mapping (Dale et al., 2000), and analysis were all described previously (Seibert et al., 2010). Additionally, the functional ROI defined from the fMRI group map was resampled to a lower-resolution surface mesh used for MEG analysis (approximately 2,500 dipoles per hemisphere). Estimated individual subject MEG data from dipoles within the functional ROI were combined to create an average ROI time series for each condition. As in the previously published analysis, statistical significance of the activity difference between the two conditions was evaluated by paired, two-tailed *t*-tests across subjects for each of eight 100 ms subperiods (e.g., 100-190 ms, 200-290

ms, etc.), extending from 300 ms prior to cue onset to 500 ms after cue onset. Significance was assessed at the $p < 0.01$ level, after applying a Bonferroni correction for the eight comparisons.

A *t*-statistic map of MEG data was calculated for comparison with fMRI results and to visualize the spatial extent of significant MEG activity using a vertex-wise approach. Estimated activity for each condition was averaged across the time periods of significant MEG activity difference in the functional ROI. For each dipole (i.e., each vertex on the low-resolution surface), a *t*-test across subjects was performed to compare the average recall-classify and classify activity. This group map was then resampled to the high-resolution surface and smoothed (iterative smoothing equivalent to 6 mm full-width, half-maximum Gaussian kernel) for display consistent with the fMRI map. Color thresholds were set for *t* statistics corresponding to controlling the false discovery rate for the left hemisphere surface at 0.05 (minimum) and 0.01 (maximum).

## 2.3  Results

### 2.3.1 fMRI Behavioral Results

Mean reaction times (± standard error) from the fMRI experiment were 1743 ± 59 ms for recall-classify, and 1191 ± 46 ms for classify trials, representing a significant difference ($p < 0.001$, two-tailed *t*-test), similar to previous studies with this task (Israel et al., 2010; Seibert et al., 2010).

A subject response was recorded within the specified response period in 94% of trials. Of these trials, subjects responded correctly in 97 ± 1% of classify trials and

$90 \pm 4\%$ of recall-classify trials (mean ± standard error). Only trials with correct responses were included in signal deconvolution and comparisons of activity.

For subjects who participated in both MEG and fMRI sessions there was no significant difference in accuracy in either condition between the first and second sessions (paired *t*-tests, $p = 0.58$ and $p = 0.97$ for recall-classify and classify conditions, respectively).

### 2.3.2   Atlas ROI Analysis

MEG results from three left lateral parietal regions of the Desikan-Killiany atlas (Desikan et al., 2006) were published previously. Recall-classify activity was greater than classify activity in each of the three regions for 100 ms subperiods immediately following cue onset, with the superior parietal region showing the greatest effect. Analysis of the BOLD data shows recall-classify activity was greater than classify activity in the left superior parietal ($t = 6.1$, $p < 10^{-5}$) and left inferior parietal regions ($t = 7.7$, $p < 10^{-9}$), but not left supramarginal ($t = -1.4$, $p = 0.18$). Figures 2.4 and 2.5 (in Supplementary Materials, Section 2.7) show the MEG and fMRI time courses.

### 2.3.3   fMRI Vertex Analysis

Lateral parietal BOLD activity differences are displayed as *t*-statistics for each vertex in Figure 2.2B, alongside the three parietal atlas ROIs (Figure 2.2A). A prominent region of greater activity for the recall-classify condition was found in the intraparietal sulcus, straddling the entire boundary between the superior and inferior

parietal atlas ROIs. A smaller region of greater recall-classify activity was also

observed in the most inferior portion of the inferior parietal atlas ROI, though the peak

of this cluster was in lateral occipital cortex. *t*-statistic values for vertices outside the

parietal cortex are included in the display for context but such activations outside the *a*

*priori* ROIs are not discussed further.
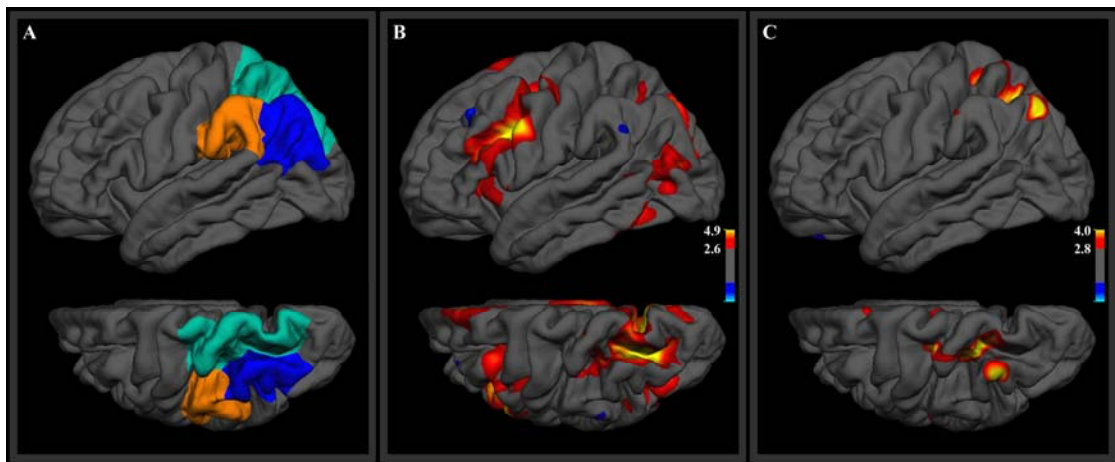


**Figure 2.2:** (A) Three anatomical ROIs in the left lateral posterior parietal cortex. (B) Group-level *t*-statistics for greater BOLD response in the recall-classify condition than in the classify condition. (C) Analogous *t*-statistics for MEG response, averaged over the period from 0-300 ms after onset of the retrieval cue. The lower image in each frame is a superior view of the left hemisphere, rotated 30 degrees to show the intraparietal sulcus. Thresholds were set for *t*-statistics corresponding to controlling the false discovery rate over the left hemisphere at 0.05 (minimum) and 0.01 (maximum).

2.3.4   Functional ROI Analysis

A functional region of interest was defined on the FreeSurfer average cortical

surface for the peak cluster of greater recall-classify activity within the left parietal

cortex (Figure 2.3A). The full, derived hemodynamic response for the functional ROI

is shown in Figure 2.3B.
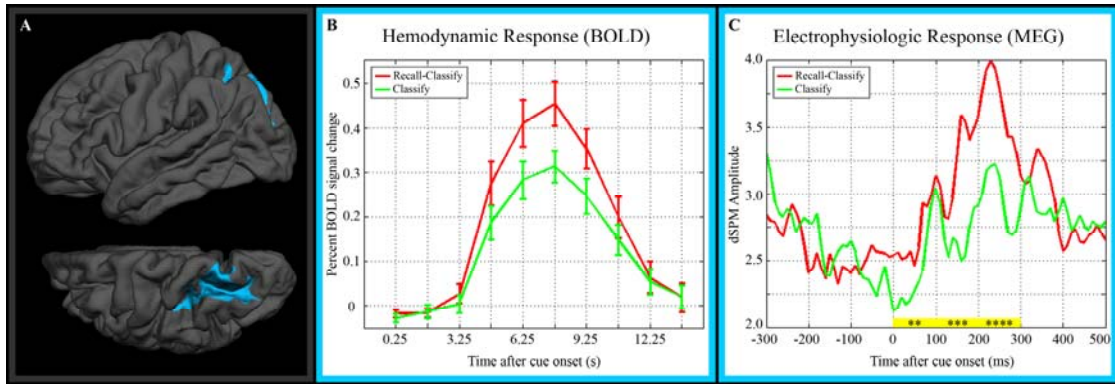
**Figure 2.3:** (A) Functional ROI defined from *t*-statistic map for greater BOLD activity in the recall-classify than in the classify condition. The lower image is a superior view of the left hemisphere, rotated 30 degrees to show the intraparietal sulcus. (B) Derived hemodynamic response functions (and standard error) for both conditions within the functional ROI. (C) Estimated MEG activity time series. "dSPM" refers to dynamic statistical parametric mapping, the MEG source localization method used. Recall-classify MEG activity was significantly greater than classify activity for the 100 ms time periods indicated in yellow (**: $p < 0.001$, ***: $p < 10^{-5}$, ****: $p < 10^{-7}$).

When this region was applied to the MEG data set, average time series for recall-classify and classify conditions appeared to diverge just prior to cue onset, with a peak difference at ~150 ms (Figure 2.3C). A temporary convergence is seen at ~100 ms, and the two conditions display similar levels of activity by ~400 ms after stimulus onset. Testing for significant activity difference in 100 ms subperiods revealed significantly greater recall-classify activity over 0-100 ms ($t = 4.4$, $p < 10^{-3}$), 100-200 ms ($t = 5.3$, $p < 10^{-5}$), and 200-300 ms ($t = 6.3$, $p < 10^{-7}$). All MEG *p*-values are corrected for multiple comparisons using the Bonferroni method for eight comparisons. An exploratory analysis of the early prestimulus period (from 1000 ms prior to cue onset to 300 ms prior to cue onset) did not suggest a MEG activity difference prior to our time period of interest.

2.3.5  MEG Vertex Analysis

MEG activity time series at each vertex were averaged over 0-300 ms, corresponding to the period of significant MEG activity difference in the functional ROI. Significant vertex-wise MEG activity differences in the lateral parietal cortex over this time window are shown in Figure 2.2C, with $t$-statistics displayed for each vertex. The spatial extent of greater recall-classify activity in this analysis is relatively limited to the intraparietal sulcus and neighboring cortex.

**2.4  Discussion**

Taking advantage of the complementary strengths of fMRI and MEG, we have described a parietal response to episodic retrieval that is centered on the intraparietal sulcus and has an early, transient time course. Vertex-wise analysis of fMRI data over the left lateral parietal cortex localized the peak region of greater recall-classify activity to the border between the superior and inferior anatomical atlas ROIs, in the intraparietal sulcus. The region identified by localization of the hemodynamic response was then used to probe the temporal dynamics of the electrophysiologic response, which exhibited greater recall-classify activity during the first 300 ms following the cue to retrieve. Vertex-wise analysis of MEG data suggested the retrieval-related electrophysiologic response over this early period was also concentrated in and near the intraparietal sulcus.

The location of the retrieval response described here supports a functional role in episodic retrieval for the intraparietal sulcus, a region that has been highlighted as part of the dorsal parietal cortex in dissociations of parietal activity in retrieval

(Cabeza et al., 2008; Ciaramelli et al., 2008; Vilberg and Rugg, 2008a). The chief

argument against an episodic retrieval role is based on a consistent observation from

fMRI studies using remember/know recognition paradigms that the intraparietal sulcus

is associated more with familiarity than with recollection (Ciaramelli et al., 2008;

Vilberg and Rugg, 2008a, 2008b). Under one view, these findings are evidence that

the intraparietal sulcus does not participate in episodic retrieval, but instead

contributes to downstream processes (Vilberg and Rugg, 2008a). Under another view,

however, it is argued that the intraparietal sulcus is more active for familiar items

because these require greater top-down attention to memory search than recollected

items (Cabeza et al., 2008; Ciaramelli et al., 2008). If the subject recognizes a test item

in the remember/know paradigm as previously studied (i.e., familiar), but some detail

from the study event does not immediately come to mind, the subject should make an

effort to retrieve such a memory. In this way, familiar items themselves represent a

cue to engage top-down attention to episodic memory search in the remember/know

task. Among the advantages of the cued-recall paradigm used in this study are that

stimuli in both conditions are equally familiar and that the conditions differ by the

presence or absence of an explicit top-down retrieval cue. Thus, the recall-related

response during this paradigm, localized to the intraparietal sulcus with both fMRI and

MEG, is difficult to reconcile with the suggestion that dorsal parietal involvement in

retrieval is limited to familiarity.

The time course of the MEG activity difference also does not support several

of the functional hypotheses associated with the left lateral parietal cortex. In

particular, the early onset and offset of increased recall-classify activity is not

consistent with processing downstream of retrieval. Other functions attributed to left parietal lobe activity similarly imply post-retrieval activity. Some retrieved information is necessary before the parietal cortex could participate in the subjective experience of recollection or in the buffering of that episodic information, but the MEG activity difference in the time courses in Figure 2.3C is clearly observed during the first 50 ms after onset of the stimulus—before completion of basic visual processing. There remains a possibility that processes associated with successful retrieval might partially contribute to the later portions of the MEG response. If, however, the intraparietal sulcus is either buffering retrieved information or utilizing retrieved information for some process occurring downstream of retrieval, the MEG response might be expected to extend closer to the behavioral response. The mean behavioral response in the retrieval condition comes more than 1400 ms after the period of significant MEG response. The early onset and the transient duration of retrieval-related MEG activity are not readily compatible with hypotheses assigning a post-retrieval role to intraparietal sulcus activity.

Both the timing and location of the present findings are consistent, however, with top-down attention to memory search. The recall-classify condition in our study encourages top-down attention to memory search by requiring retrieval of a specific paired associate and giving the instruction to retrieve prior to presentation of the cue. The intraparietal sulcus may contribute to the direction of internal attention toward episodic memory search or possibly toward a particular target in episodic memory, though the latter is less likely, given the immediate and brief MEG response. Centered in and near the intraparietal sulcus, our findings are largely localized within the dorsal

parietal cortex region proposed to be responsible for top-down attention to memory search (Cabeza et al., 2008; Ciaramelli et al., 2008).

A limitation of the present study is the relatively focused time period investigated. The present MEG data set was designed to explore the first 500 ms following cue onset (Seibert et al., 2010) and thus does not preclude the possibility of a later activity difference; however, any such activity difference would likely be distinct from that described here, as there is no significant activity difference in the 300-400 ms or 400-500 ms subperiods.

Another limitation of this study, common to all brain imaging studies comparing two conditions, is that a paired contrast does not provide proof that the process underlying the activity difference is exclusive to only one of the conditions. A graded process may participate in both the recall-classify and classify conditions but still contribute to the activity difference. Ongoing encoding and retrieval are to be expected regardless of experimental task, yet this study controls for incidental memory processes by contrasting the recall condition with a condition that does not require episodic retrieval. Thus, similar underlying processes may contribute to both conditions, but the present findings demonstrate that intraparietal sulcus activity is increased when episodic retrieval is required.

## 2.5  Conclusions

Taken together, these findings offer convergent, multimodal evidence for involvement of the intraparietal sulcus in recall and suggest that this region contributes to pre-retrieval processes, such as orienting attention to memory search. The power of

integrative analyses in evaluating functional hypotheses is demonstrated by the observation that only one of the several proposed roles for lateral parietal cortex (top-down attention to memory search) is clearly consistent with the parietal response measured in this study. By describing both the location and timing of parietal activity during recall, the present results provide a critical piece of the empirical framework necessary for understanding how the intraparietal sulcus contributes to episodic retrieval.

## 2.6  Acknowledgements

## 2.7 Supplementary Materials



**Figure 2.4:** Supplementary Figure 1 – MEG anatomical ROI time series. (A) Three anatomical ROIs in the left lateral posterior parietal cortex. (B-D) Estimated MEG activity time courses from these regions. "dSPM" refers to dynamic statistical parametric mapping, the MEG source localization method used. 100 ms time periods highlighted with yellow showed significantly greater recall-classify activity than classify activity (*: $p < 0.01$, **: $p < 0.001$, ***: $p < 10^{-4}$, ****: $p < 10^{-7}$). Adapted with permission from Seibert et al., 2010; ROIs are displayed on the higher-resolution surface used throughout the present study.
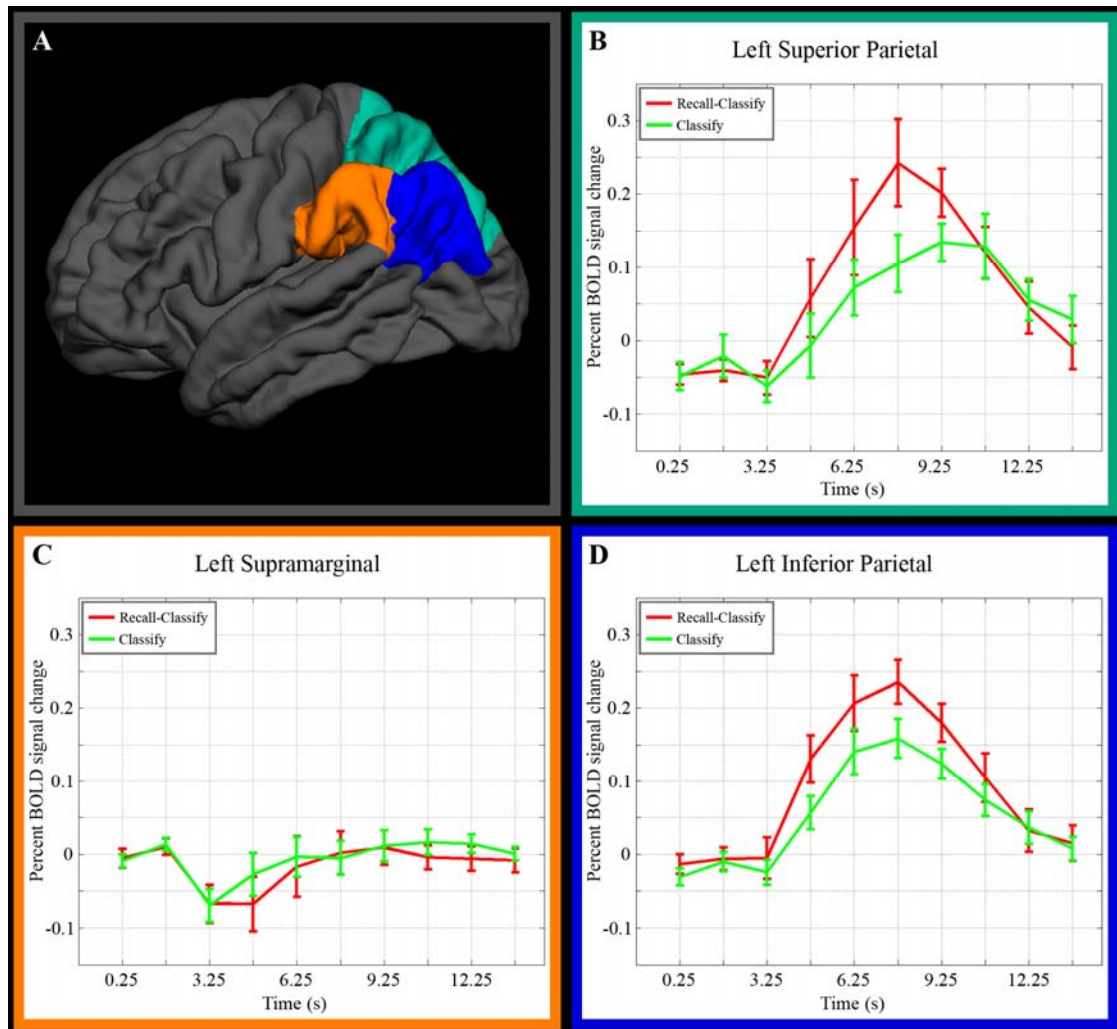
**Figure 2.5:** Supplementary Figure 2 – BOLD anatomical ROI time series. (A) Three anatomical ROIs in the left lateral posterior parietal cortex. (B-D) Derived hemodynamic response functions from these regions.

## 2.8 References

Ally, BA, Simons, JS, McKeever, JD, Peers, PV, Budson, AE (2008): Parietal contributions to recollection: electrophysiological evidence from aging and patients with parietal lesions. Neuropsychologia, 46(7), 1800-1812.

Baddeley, A (2000): The episodic buffer: a new component of working memory? Trends Cogn. Sci. (Regul. Ed.), 4(11), 417-423.

Cabeza, R (2008): Role of parietal regions in episodic memory retrieval: The dual attentional processes hypothesis. Neuropsychologia, 46(7), 1813-1827.

Cabeza, R, Ciaramelli, E, Olson, IR, Moscovitch, M (2008): The parietal cortex and episodic memory: an attentional account. Nat. Rev. Neurosci, 9(8), 613-625.

Ciaramelli, E, Grady, CL, Moscovitch, M (2008): Top-down and bottom-up attention to memory: a hypothesis (AtoM) on the role of the posterior parietal cortex in memory retrieval. Neuropsychologia, 46(7), 1828-51.

Cox, RW (1996): AFNI: software for analysis and visualization of functional magnetic resonance neuroimages. Comput. Biomed. Res, 29(3), 162-173.

Dale, AM (1999): Optimal experimental design for event-related fMRI. Hum Brain Mapp, 8(2-3), 109-114.

Dale, AM, Fischl, B, Sereno, MI (1999): Cortical surface-based analysis. I. Segmentation and surface reconstruction. Neuroimage, 9(2), 179-194.

Dale, AM, Liu, AK, Fischl, B, Buckner, RL, Belliveau, JW, Lewine, JD, Halgren, E (2000): Dynamic statistical parametric mapping: combining fMRI and MEG for high-resolution imaging of cortical activity. Neuron, 26(1), 55-67.

Desikan, RS, Ségonne, F, Fischl, B, Quinn, BT, Dickerson, BC, Blacker, D, et al. (2006): An automated labeling system for subdividing the human cerebral cortex on MRI scans into gyral based regions of interest. Neuroimage, 31(3), 968-980.

Fischl, B, van der Kouwe, A, Destrieux, C, Halgren, E, Segonne, F, Salat, DH, et al. (2004): Automatically Parcellating the Human Cerebral Cortex. Cereb. Cortex, 14(1), 11-22.

Fischl, B, Sereno, MI, Dale, AM (1999a): Cortical surface-based analysis. II: Inflation, flattening, and a surface-based coordinate system. Neuroimage, 9(2), 195-207.

Fischl, B, Sereno, MI, Tootell, RB, Dale, AM (1999b): High-resolution intersubject averaging and a coordinate system for the cortical surface. Hum Brain Mapp, 8(4), 272-284.

Genovese, CR, Lazar, NA, Nichols, T (2002): Thresholding of Statistical Maps in Functional Neuroimaging Using the False Discovery Rate. NeuroImage, 15(4), 870-878.

Israel, SL, Seibert, TM, Black, ML, Brewer, JB (2010): Going their separate ways: dissociation of hippocampal and dorsolateral prefrontal activation during episodic retrieval and post-retrieval processing. J Cogn Neurosci, 22(3), 513-525.

Rossion, B, Pourtois, G (2004): Revisiting Snodgrass and Vanderwart's object pictorial set: the role of surface detail in basic-level object recognition. Perception, 33(2), 217-236.

Seibert, TM, Hagler, DJ, Brewer, JB (2010): Early parietal response in episodic retrieval revealed with MEG. Hum Brain Mapp.

Vilberg, KL, Rugg, MD (2008a): Memory retrieval and the parietal cortex: a review of evidence from a dual-process perspective. Neuropsychologia, 46(7), 1787-99.

Vilberg, KL, Rugg, MD (2008b): Functional significance of retrieval-related activity in lateral parietal cortex: Evidence from fMRI and ERPs. Hum Brain Mapp, 30(5), 1490-1501.

Wagner, AD, Shannon, BJ, Kahn, I, Buckner, RL (2005): Parietal lobe contributions to episodic memory retrieval. Trends in Cognitive Sciences, 9(9), 445-453.

CHAPTER 3

## Default Network Correlations Analyzed on Native Surfaces

**Abstract**

Disruptions of interregional correlations in the blood oxygenation level dependent fMRI signal have been reported in multiple diseases, including Alzheimer's disease and mild cognitive impairment. "Default network" regions that overlap with areas of earliest amyloid deposition have been highlighted by these reports, and abnormal default network activity is also observed in unimpaired elderly subjects with high amyloid burden. However, one limitation of current methods for analysis of interregional correlations is that they rely on transformation of functional data to an atlas volume (e.g., Talairach-Tournoux or Montreal Neurological Institute atlases) and may not adequately account for anatomic variation between subjects, particularly in the presence of atrophy. We assessed the utility of the FreeSurfer cortical parcellation to analyze default network functional correlations on the native surfaces of individual subjects. Group-level quantitative analysis was accomplished by comparing correlations between equivalent structures in different subjects. The method was applied to resting-state fMRI data from young, healthy subjects; preliminary results were also obtained from cognitively unimpaired elderly subjects and patients with Alzheimer's disease, Parkinson's disease, Parkinson's disease dementia, and dementia with Lewy bodies.

## 3.1 Introduction

Characteristic patterns of low-frequency correlations have been repeatedly identified in the blood oxygenation level dependent (BOLD) fMRI signal when subjects are asked to simply lie still in the scanner (Biswal et al., 1995; Buckner et al., 2008; Greicius et al., 2003). The relative consistency of these patterns across studies and analysis methods, as well as the simplicity of the instructions, has led to considerable interest in their potential application as a biomarker in disease (Auer, 2008; Fox and Raichle, 2007; Greicius, 2008; van den Heuvel and Hulshoff Pol, 2010; Rogers et al., 2007). Particular attention has been paid to a collection of regions called the default network[1] and the disruption of correlations across these regions in Alzheimer's disease (Greicius et al. 2004; L Wang et al. 2006; Allen et al. 2007; Supekar et al. 2008; Koch et al. 2010; H-Y Zhang et al. 2010; for review, see Greicius 2008; Sorg et al. 2009). Disruptions in so-called functional connectivity in the default network have also been reported in conditions believed to precede onset of Alzheimer's disease, including patients with amnestic mild cognitive impairment (Bai et al., 2009; Pihlajamäki et al., 2009; Sorg et al., 2007) and cognitively unimpaired subjects with high amyloid burden (Hedden et al., 2009; Sheline et al., 2010).

Anatomical variability across subjects gives rise to two notable challenges in the analysis of spontaneous BOLD correlations within the default network. First, if analyses are to be extended beyond qualitative assessment in individual subjects, a

---

[1] A number of brain regions exhibit greater activity in functional neuroimaging studies when subjects are permitted to rest than when they are instructed to engage in a specific cognitive task. These regions have been collectively deemed the "default network" (Buckner et al., 2008; Raichle et al., 2001; Raichle and Snyder, 2007)

method of comparing results across subjects is critical. Second, the network of interest

has to be identified in each subject. In seed-correlation analyses, this is typically

accomplished by choosing an *a priori* seed region known to lie within the network

(Hedden et al., 2009; Sheline et al., 2010). For independent component analyses

(ICA), a template is used to identify the component that best matches the default

network (Greicius et al., 2004; Seeley et al., 2009).

Currently, both of these challenges are addressed by performing analyses in

atlas-volume space. Anatomical and functional images from each subject are

transformed, or warped, to match a canonical brain (e.g., Talairach-Tournoux or

Montreal Neurological Institute template). Once in a standardized, or atlas, volume,

seed regions and templates from the literature or other data sets can be applied to the

spatially transformed data to identify the default network. The process of transforming

data to an atlas volume also permits direct comparison of analysis results across

subjects and studies.

Unfortunately, atlas-space results are only valid to the extent that the warping

process is valid, a point of particular concern in conditions where participants' brains

differ considerably from the atlas due to disease. Functional correlation analyses are

subject to concerns similar to some known issues with voxel-based morphometry, a

method for structural MRI analysis which also depends heavily on accurate

registration to a template. Improper registration can lead to misleading results in both

cases because, for example, a given coordinate represents gray matter in the template

but lies in cerebrospinal fluid in a patient's warped brain. Voxel-based morphometry

gives varied results depending on the particular warping algorithm used (Senjem et al.,

2005), and even algorithms identified as "optimized," which include multiple steps to improve normalization, are still prone to errors when atrophy causes gross changes in brain structure (Ashburner and Friston, 2001; Bookstein, 2001; Senjem et al., 2005). Despite the crucial role warping plays in functional correlation analyses and the known pitfalls of common methods in the face of structural brain pathology, accuracy of individual transformations are rarely, if ever, reported or displayed.

Analysis on a subject's native surface offers potential advantages over atlas-volume methods. First, possible ambiguity about precise anatomic locations is reduced. Measuring functional correlations on native surfaces also facilitates accounting for anatomic effects of disease and age. Moreover, by preserving inter-individual anatomic variability, longitudinal patient studies can better avoid confounds due to disease-related structural changes that affect an individual patient's brain over time. Comparison of functional measures to other individual markers is also straightforward on native surfaces, in particular cross-modal imaging markers such as amyloid imaging results and regional cortical thickness. There is also a clinical appeal to obtaining and displaying functional imaging results on the brain surface of an individual patient. Prior studies have pointed to the potential of functional correlations to provide meaningful results in individual patients (Buckner and Vincent, 2007; Greicius et al., 2004; Koch et al., 2010); analyzing functional data on native surfaces may be an important step toward that aim.

We assessed the utility of the FreeSurfer (http://surfer.nmr.mgh.harvard.edu) cortical parcellation to analyze functional correlations on the native surfaces of individual subjects. Automated processes are employed to anatomically parcellate

each subject's cortical surface into distinct regions of cortex (subcortical gray matter structures are included after a similar automated volume segmentation). One cortical region, the isthmus cingulate, is proposed as a suitable native-surface seed for identification and analysis of the default network. Parcellation and segmentation regions are then used for group-level analyses by comparing interregional correlations between equivalent regions in different subjects. Additionally, registration of native sulcal and gyral patterns to an average surface allows display of group-level results after quantitative parcellation analysis on native surfaces.

Here we present results from the application of this method to BOLD data from young, healthy subjects as a proof of concept. The primary findings were reproduced in preliminary data from multiple disease populations, including Alzheimer's disease (AD), Parkinson's disease dementia (PDD), Dementia with Lewy bodies (DLB), and cognitively unimpaired elderly controls.

## 3.2 Methods

### 3.2.1 Subjects

Subject demographics are provided in Table 3.1. Patients designated 'Alzheimer's disease' had a clinical diagnosis of probable AD based on the NINCDS/ADRDA criteria (McKhann et al., 1984); diagnoses for dementia with Lewy bodies and Parkinson's disease dementia were based on the criteria established by the Movement Disorders Society Task Force (Geser et al., 2005; McKeith, 2007). Diagnosis for all patients was made by consensus of two or more neurologists in the UCSD Shiley-Marcos Alzheimer's Disease Research Center Clinical Core. Elderly

controls with no cognitive impairment had a mini mental status exam score of at least 27 and a CDR score of zero.

**Table 3.1:** Subject demographics

| Subject group | N | Age range | Field strength |
|---|---|---|---|
| Young adults | 15 | 22-28 | 3.0 Tesla |
| Elderly controls | 7 | 69-90 | 1.5 Tesla |
| Alzheimer's disease | 4 | 61-94 | 1.5 Tesla |
| Parkinson's disease dementia | 8 | 65-86 | 1.5 Tesla |
| Dementia with Lewy bodies | 7 | 61-75 | 1.5 Tesla |

3.2.2   MRI Acquisition

Functional imaging of each subject consisted of two $T_2$*-weighted sequences of approximately seven minutes each on a General Electric Signa Excite HDx using an eight-channel phased-array head coil (General Electric Healthcare, Waukesha, WI). Data for young subjects were acquired on a 3.0 Tesla system (TE: 30 ms; TR: 2124 ms; flip angle: 90°; matrix: 64 x 64; voxel size: 3.75 mm x 3.75 mm x 4 mm; 36 adjacent sagittal slices; 205 samples per series); data for elderly subjects, including patients, were acquired on a 1.5 Tesla system (TE: 45 ms; TR: 2624 ms; flip angle: 90°; matrix: 64 x 64; voxel size: 3.75 mm x 3.75 mm x 5 mm; 32 adjacent sagittal slices; 155 samples per series). The initial five samples from each functional run were excluded to allow for $T_1$-equilibration. Immediately prior to each functional series, a spin-echo volume was acquired with opposite phase-encoding polarity for field inhomogeneity correction (Holland et al., 2010). Instructions for the young subjects were to rest motionless with eyes closed. Instructions for the elderly subjects were to rest motionless with eyes open; this modification was adopted after it was suggested

that functional correlations in the default network are more robust with eyes open

(Van Dijk et al., 2009; Yan et al., 2009). In addition to the functional volumes, a high-

resolution, three-dimensional, $T_1$-weighted volume was acquired for each subject

during the same session (TE: 2.8 ms / 3.8 ms; TR: 6.5 ms / 8.5 ms; TI: 600 ms / 500

ms; flip angle: 8° / 10°; matrix: 256 x 256; voxel size:  0.9375 mm x 0.9375 mm x

1.2000 mm; values separated by '/' are for 3.0 T data / 1.5 T data). Respiratory effort

and heart rate were monitored with a pressure transducer (BioPac Systems Inc.,

Goleta, CA) and a pulse oximeter (BioPac Systems and InVivo, Orlando, FL),

respectively.


3.2.3   Structural MRI Processing

A model of each subject's cortical surface was reconstructed from the $T_1$-

weighted MRI volume (Dale et al., 1999; Fischl et al., 1999a). To ensure accuracy, the

automatically generated boundaries were overlaid on the original $T_1$-weighted volume

as thin colored lines to aid visual confirmation of the tissue boundaries on each slice—

yellow for the boundary between white and gray matter, and red for the boundary

between gray matter and cerebrospinal fluid. Where these automatically generated

lines deviated from the visually identified boundaries, manual control points were

created, and the automated algorithms were applied again. Final surfaces were visually

inspected to search for gross errors; none were found in the present data set.

The surface model was then anatomically parcellated using the Desikan-

Killiany atlas and standard FreeSurfer tools (Desikan et al., 2006; Fischl et al., 2004).

This process assigns each point (vertex) on the native surface to the most probable

anatomical label (e.g., inferior parietal, precentral, parahippocampal, etc.) based on registration to a probabilistic atlas of surface folding patterns and on the observed surface geometry at that location of the native surface (Fischl et al., 2004). Subcortical structures were similarly identified by volume segmentation (Fischl et al., 2002). Automated parcellation by this method has been shown to be comparable to manual labeling (Fischl et al., 2004). Additionally, the parcellation for each subject was visually inspected to search for gross errors; none were found in the present data set.

For direct comparison with prevailing methods, the $T_1$-weighted volume from an Alzheimer's patient exhibiting atrophy was submitted to common registration algorithms to warp the atrophied brain to the Montreal Neurological Institute (MNI) 152 T1 reference brain provided in standard software packages. Affine transformation with 12 degrees of freedom was performed using 3dWarpDrive in AFNI (http://afni.nimh.nih.gov/afni). Nonlinear transformations were performed using FNIRT in FSL (http://www.fmrib.ox.ac.uk/fsl/index.html), the "normalise" process in SPM2 (http://www.fil.ion.ucl.ac.uk/spm/), and the DARTEL process in SPM8. An older version of SPM (SPM2) was included because it appears to be among the more common packages used in the relevant literature (Buckner et al., 2009; Supekar et al., 2008; Van Dijk et al., 2009; Wang et al., 2007; Wang et al., 2010). All registration procedures followed the configurations and parameters recommended in the documentation provided with the corresponding software. Simple alignment of the original volume was also performed using manually defined markers in AFNI in order to display the original images in a similar orientation to the registered images.

### 3.2.4  fMRI Data Pre-analysis Processing

All fMRI pre-analysis processing was performed using custom software written in MATLAB (Mathworks, Natick, MA), except where noted. Functional images were first corrected for distortion due to inhomogeneity in the static magnetic field (Holland et al., 2010). Effects of respiratory fluctuations were modeled and removed from time series using RETROICOR (Glover et al., 2000). Similar removal of cardiac fluctuations did not have a meaningful impact on the results in any group, and this step was not included in final analyses for the sake of consistency across all subjects (pulse recordings were sporadically lost in approximately 20% of scans in elderly and disease subjects due to technical problems). After interpolation for slice acquisition timing, rigid body volume registration was performed using AFNI (Cox and Jesmanowicz, 1999), followed by voxel-wise regression of six head motion parameters and a cubic polynomial baseline from each functional series. Functional data were next projected onto the subject's cortical surface model using FreeSurfer, and a bandpass filter of 0.01-0.08 Hz was applied to the time series from each vertex on the surface. BOLD correlation analyses typically include a smoothing step with a Gaussian kernel to account for functional and anatomic variation across subjects, but this step is not necessary for native-surface parcellation analysis.

### 3.2.5  fMRI Correlation Analysis

We designed an fMRI correlation analysis that takes advantage of the FreeSurfer surface generation and parcellation tools and avoids transforming functional data to an atlas volume. All steps were performed using custom software

written in MATLAB, except where noted. Functional time series were averaged across surface vertices within the left isthmus cingulate region to serve as the seed time series for correlation analyses. Average time series were also calculated from each of the other 30 cortical surface parcellation regions in the Desikan-Killiany atlas not adjacent to the seed (see Figure 3.4), as well as from five volume segmentation regions from the left hemisphere (hippocampus, caudate, pallidum, putamen, and amygdala). A Pearson's correlation coefficient was calculated for the correlation between the seed time series and each region's average time series, and Fisher's $z$-transform was applied to these coefficients. The same process was repeated for right hemisphere regions, with the right isthmus cingulate region as the seed. Region time series were obtained by loading both the subject's functional data and the parcellated native surface (which contains a region code at each vertex location) in MATLAB; time series at each vertex could then be classified by the region code at the corresponding location in the parcellated surface.

Results from native-surface parcellation analysis were summarized in two ways. First, the $z$-transformed correlation coefficients from each region were averaged across subjects. Second, as it is possible that relative changes in correlation coefficient may also be informative, all 35 regions per hemisphere were ranked in order of highest to lowest coefficient for a given subject. These ranks were summarized by calculating the median rank across subjects for each region.

A power analysis was performed to give an estimate of the number of subjects needed to detect a difference between two groups. For each region, the standard deviation (across subjects) was calculated for the $z$-transformed correlation coefficient

with the isthmus cingulate seed. This standard deviation was included in Cohen's equation sample size for a population difference (Cohen, 1988; Dawson and Trapp, 2004). The expected effect size (i.e., population difference) was assumed to be 0.2; the actual value is unknown and specific to the populations studied, but available published values suggest this value is conservative for comparing unimpaired elderly with high risk for Alzheimer's disease to age-matched controls (Fleisher et al., 2009; Hedden et al., 2009; Koch et al., 2010). All calculations also assumed 80% power and an alpha value of 0.05. The final result of the power calculations was an estimated sample size for each region, corresponding to the number of subjects necessary to detect a population difference of 0.2 in the correlation coefficient.

Vertex-wise correlation analysis was performed in addition to the parcellation analysis, allowing visualization of entire hemispheres at finer resolution. Individual maps were produced by calculating the Fisher's $z$-transformed correlation coefficient for the average seed region time series and the time series of each vertex on the surface. Individual native surfaces were registered to the FreeSurfer fsaverage surface using a spherical-based algorithm in FreeSurfer (Fischl et al., 1999b). That registration was used to transform the individual maps to the fsaverage surface, also using FreeSurfer tools. Group maps were created by loading the fsaverage versions of the individual maps in MATLAB and taking the average across subjects. A surface-based smoothing process was applied using FreeSurfer for display in the figures (28 iterative steps, approximately equivalent to a 6 mm full-width half-maximum Gaussian kernel in two dimensions). Group maps were calculated from unsmoothed individual maps so that the smoothing process was only applied once. The minimum threshold for both

group and individual hemisphere maps was set as the mean coefficient across all vertices on the surface plus 0.5 times the standard deviation; the maximum threshold was set as the mean coefficient plus 1.5 times the standard deviation.

3.2.6   Comparative Analysis: Volume Atlas vs. Native Surface

To assess the degree to which warping to a volume atlas affects functional correlation results, all functional data from this study were also analyzed after nonlinear transformation to the MNI152 volume atlas. All pre-analysis processing and correlation procedures for the volume-atlas analysis were performed as in the native-surface analysis up to the point of projection of time series data to the surface. Instead of directly projecting processed functional time series to each subject's native surface, all data were transformed to volume-atlas space using standard tools in a software package cited in several resting correlation studies (SPM2). The transformation to volume-atlas space was calculated for each subject using the individual high-resolution $T_1$-weighted volumes. The time series in MNI space were then projected onto the fsaverage surface using the standard transformation provided with FreeSurfer. Subsequent bandpass filtering and correlation analysis (using the fsaverage surface parcellation) were performed as in the native-surface analysis.

Any inaccuracies in registration to the MNI volume atlas could change the definition of the seed and therefore affect correlation measures across the entire brain even if the rest of the brain was perfectly registered to MNI. To isolate the effect of whole-brain registration to a volume atlas, the time series from each subject's native-surface isthmus cingulate was used as the seed in both the native-surface and volume-

atlas analyses. Additionally, the correlation coefficient between the native-surface isthmus cingulate time series and the MNI-transformed isthmus cingulate time series was calculated for each subject to quantify the effect of MNI transformation on the seed. Note that, in order to maintain intuitive interpretation of the values, these seed-to-seed correlation coefficients were not Fisher-transformed.

MNI volume-atlas correlation coefficients for each region on the fsaverage surface were compared to the corresponding region on the native surfaces. As volume-atlas registration inaccuracies lead to a heterogeneous mix of both increases and decreases in correlation values, the magnitude of the differences was used for comparing the methods. The mean (across-subjects) difference between MNI-transformed and native-surface results was calculated for each region. Paired *t*-tests were applied to evaluate the statistical significance of any regional differences between the two methods.

Vertex-by-vertex comparison of the MNI volume-atlas results (projected on the fsaverage surface) to the native-surface results was achieved using the native-surface maps that were registered to the fsaverage surface (see section 3.2.5). Difference maps were calculated by taking the root-mean-square (RMS) average, at each vertex, of the difference between MNI-transformed and native-surface results.

## 3.3  Results

Both linear and nonlinear algorithms successfully aligned the atrophied brain to the MNI template (Figure 3.1). The nonlinear methods (FSL, SPM2, SPM8) appear to have reduced ventricular spaces and stretched the brain tissue to fill portions of the

adjacent CSF space (distortions to the skull and other tissues in the nonlinear examples

should be ignored, as the methods are optimized for registration of the brain, not

extraparenchymal tissues). None of the transformations, however, fully accounted for

the bulk atrophy in the superior brain or the enlarged sulci evident throughout the

cortex. Many MNI coordinates that lie within cortical regions in the template

correspond to cerebrospinal fluid in the transformed brains for this patient.
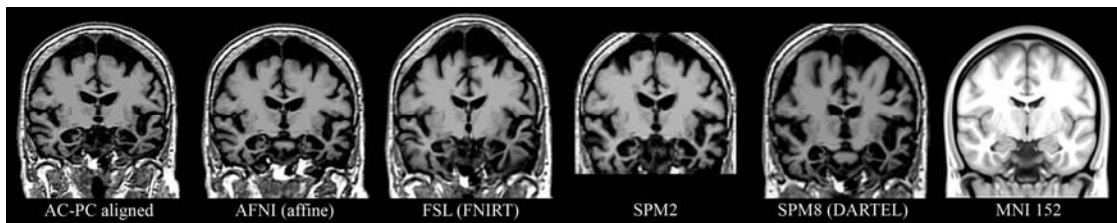


**Figure 3.1:** Warping to an atlas volume. $T_1$-weighted volume from a patient with atrophy transformed to an atlas volume using popular software packages. **AC-PC aligned:** original image, after rotation and cropping for comparison with transformed images (rotation in AFNI after manual landmark identification). **AFNI:** after affine (12 degrees of freedom) transformed with 3dWarpDrive. **FSL:** after nonlinear warping with FNIRT. **SPM2:** after nonlinear warping with "Normalise" tool. **SPM8:** after nonlinear warping with the "DARTEL" process. MNI 152: standard $T_1$ atlas volume used for all transformations presented here. None of these methods adequately accounted for the structural effects of atrophy in this patient. One consequence of the poor alignment is some cortical MNI coordinates correspond to cerebrospinal fluid in the patient's transformed brain.

**Table 3.2:** Native-surface correlation analysis in young subjects. Regions most consistently correlated with the seed region in each hemisphere. A median rank of 2 for the superior frontal region in the left hemisphere indicates that this region is among the top 2 regions most correlated with the seed in at least 50% of subjects (interquartile ranges give analogous results for the 25th and 75th percentiles). Mean $z$ and SE indicate the population mean $z$-transformed correlation coefficient and standard error, respectively. Sample size indicates the estimated sample size to detect a difference in mean $z$ of 0.2 with 80% power and alpha value set to 0.05.

### Left Hemisphere

| Region name | region ranks median | region ranks quartiles | correlation coefficients mean $z$ | correlation coefficients SE | correlation coefficients sample size |
|---|---|---|---|---|---|
| Superior Frontal | 2 | (1-2.75) | 1.06 | 0.06 | 21 |
| Inferior Parietal | 3 | (2-6.25) | 1.02 | 0.07 | 33 |
| Medial Orbitofrontal | 3 | (2-7.75) | 1.02 | 0.06 | 21 |
| Hippocampus | 6 | (5-10.5) | 0.90 | 0.05 | 16 |
| Parahippocampal | 7 | (4-13.25) | 0.89 | 0.06 | 18 |

### Right Hemisphere

| Region name | region ranks median | region ranks quartiles | correlation coefficients mean $z$ | correlation coefficients SE | correlation coefficients sample size |
|---|---|---|---|---|---|
| Superior Frontal | 4 | (2-7.75) | 0.91 | 0.06 | 22 |
| Inferior Parietal | 5 | (1.25-8.75) | 0.94 | 0.08 | 37 |
| Hippocampus | 6 | (3-10.75) | 0.89 | 0.07 | 28 |
| Parahippocampal | 7 | (4.25-18.75) | 0.80 | 0.08 | 37 |
| Medial Orbitofrontal | 8 | (2.25-13.75) | 0.87 | 0.05 | 15 |

The $T_1$-weighted volume and reconstructed cortical surface model are shown in Figure 3.2A and 3.2B, respectively, for the brain of a young subject and the atrophied brain from Figure 3.1. Anatomic features of each individual brain were preserved by the surface reconstructions. The depression of the superior aspect of the atrophied brain is reflected in the relatively flat superior aspect of the surface. Similarly, the patient's enlarged sulci are readily observable in the corresponding surface. Neither of these abnormalities prevented successful automated parcellation of the cortical surface (Figure 3.2C). The isthmus cingulate seed region is identified for each subject within the parcellation (Figure 3.2D, dark green), allowing calculation of

correlation coefficients for the rest of the cortex on the subject's native surface (Figure

3.2D, 3.2E).
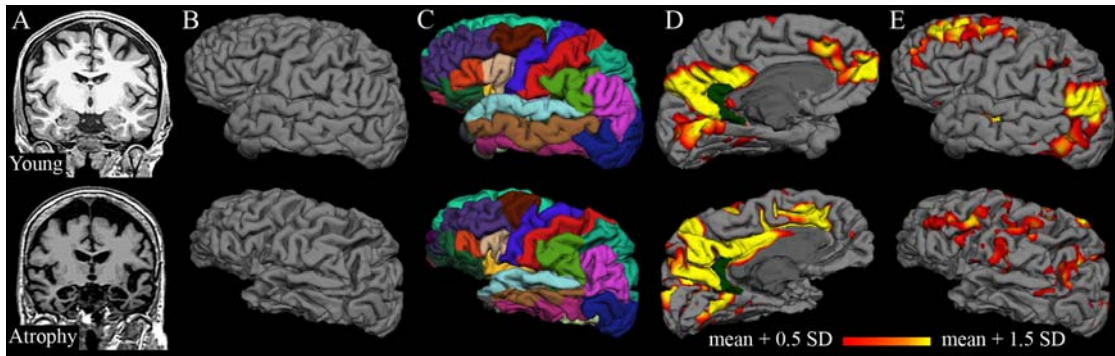


**Figure 3.2: Analysis on native surfaces.** The top row shows structural and functional analysis for a young subject; the bottom row shows corresponding images from a patient with atrophy (see Figure 1). **A:** Original $T_1$-weighted volumes after AC-PC alignment. **B:** Cortical surface models generated from $T_1$-weighted volumes; anatomical features from individual subjects, including effects of atrophy, are preserved. **C:** Automated anatomical parcellation of cortical surface for each subject. **D-E:** Individual correlation maps consisting of coefficients (z-transformed) from correlation of each surface vertex with the average time series of the isthmus cingulate seed (dark green). The isthmus cingulate region was defined on the native surface for each subject during the automated anatomical parcellation. Thresholds (for display only) were determined separately for each subject from the mean and standard deviation of correlation coefficients for the vertices on the individual surface.

Cortical surface models reconstructed from five individual young subjects are

shown in Figure 3.3A (all subjects are included in supplementary material). As

expected, substantial variability in anatomy is observed between individuals; brain

size, gyral patterns, and structural landmarks are all unique for each surface. The

inferior parietal region identified by the FreeSurfer parcellation is also shown for each

subject.

Functional correlation maps are displayed on the native surfaces for the same

five individual young subjects in Figure 3.3B. Many individual subject maps resemble

the well-known default network pattern typically reported in group averages. As with

the anatomy, though, the functional maps demonstrate considerable variability from

one individual to another.

**Table 3.3:** Native-surface correlation analysis in elderly subjects and patients. Regions most consistently correlated with the seed region in each hemisphere. A median rank of 2 for the superior frontal region in the left hemisphere indicates that this region is among the top 2 regions most correlated with the seed in at least 50% of subjects (interquartile ranges give analogous results for the $25^{th}$ and $75^{th}$ percentiles). Mean $z$ and SE indicate the population mean $z$-transformed correlation coefficient and standard error, respectively. Sample size indicates the estimated sample size to detect a difference in mean $z$ of 0.2 with 80% power and alpha value set to 0.05.

**Left Hemisphere**

| Region name | region ranks | | correlation coefficients | | |
|---|---|---|---|---|---|
| | median | quartiles | mean z | SE | sample size |
| Inferior Parietal | 2 | (1-4) | 0.84 | 0.05 | 36 |
| Superior Frontal | 4 | (2-5) | 0.77 | 0.05 | 30 |
| Caudal Middle Frontal | 6 | (4-14) | 0.67 | 0.05 | 38 |
| Hippocampus | 10 | (6-19) | 0.57 | 0.04 | 24 |
| Caudate | 10.5 | (7-17) | 0.59 | 0.04 | 27 |

**Right Hemisphere**

| Region name | region ranks | | correlation coefficients | | |
|---|---|---|---|---|---|
| | median | quartiles | mean z | SE | sample size |
| Inferior Parietal | 3 | (1-5) | 0.84 | 0.05 | 28 |
| Superior Frontal | 3 | (2-8) | 0.79 | 0.05 | 31 |
| Pericalcarine | 8.5 | (4-14) | 0.66 | 0.05 | 29 |
| Caudal Middle Frontal | 9 | (6-15) | 0.64 | 0.05 | 38 |
| Middle Temporal | 9 | (6-19) | 0.60 | 0.05 | 40 |
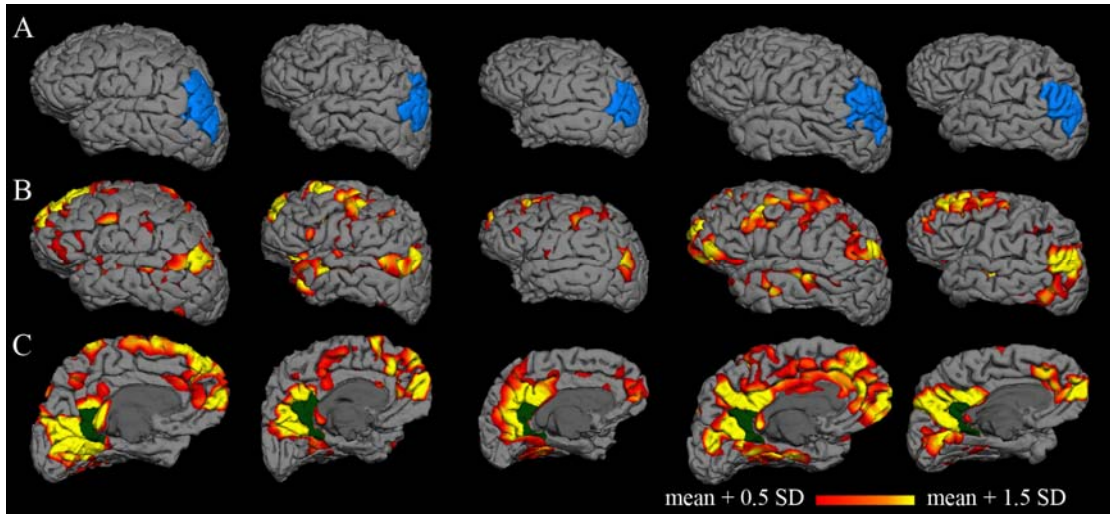
**Figure 3.3:** Individual correlation maps. Columns represent individual subjects. A: Cortical surface models with a single parcellation region (inferior parietal) highlighted in blue. The substantial anatomic variability across subjects is captured by the individual surfaces. **B-C:** Individual correlation maps for five young subjects, consisting of coefficients (z-transformed) from correlation of each vertex on the surface with the average time series of the isthmus cingulate seed (dark green). The isthmus cingulate region was defined on the native surface for each subject during the automated anatomical parcellation. Individual correlation maps for all fifteen young subjects are included in the supplementary material.

Native-surface regions most consistently correlated with the seed region in each hemisphere are shown in Table 3.2. All of the top five regions in each hemisphere are among those frequently included in the default network (dorsolateral prefrontal, medial prefrontal, inferior parietal, and medial temporal). Both the mean correlation coefficient and median rank measures identify default network regions as the most strongly correlated with the isthmus cingulate seed.

Group-average functional correlation maps for the young subjects are displayed in Figure 3.4. While interindividual variability is lost in the group average, the pattern at the group level confirms that typical default network patterns are identified using the isthmus cingulate seed.
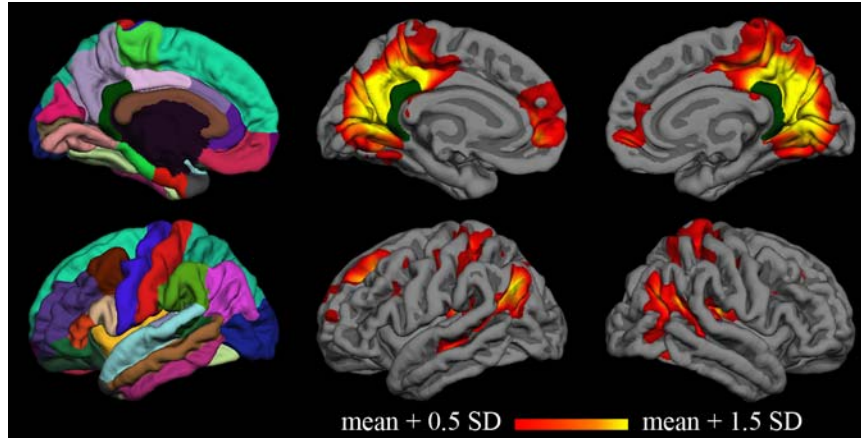
**Figure 3.4:** Group correlation map for young subjects. Vertex-wise average correlation map across fifteen young subjects after surface-based registration to the FreeSurfer "fsaverage" subject. The Desikan-Killiany cortical parcellation atlas is shown in the first column, and the isthmus cingulate seed is shown in dark green on all medial surfaces.

Power analysis estimated the sample size required for a difference in population mean for the regions in Table 3.2. Sample sizes for the regions in Table 3.2 had a median of 21.5 subjects. Among these regions, the right inferior parietal and right parahippocampal regions had the greatest estimated sample sizes at 37 subjects each. Right medial orbitofrontal had the smallest estimated sample size at 15 subjects.
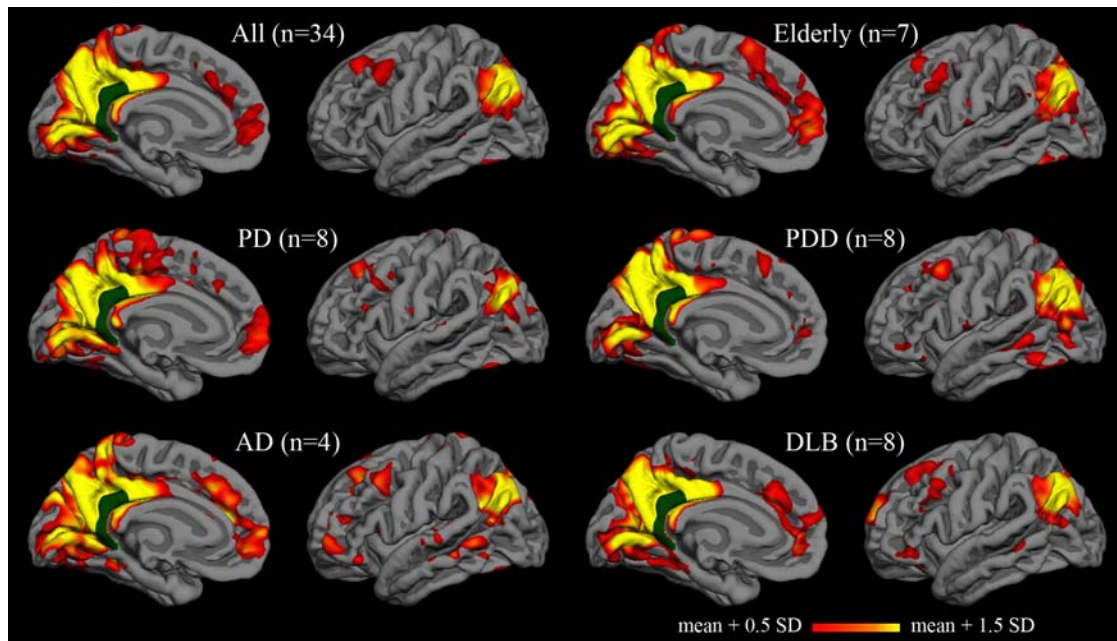
**Figure 3.5:** Group correlation maps for elderly subjects and patients. Vertex-wise average correlation maps after surface-based registration to the FreeSurfer "fsaverage" subject. The isthmus cingulate seed is shown in dark green. The upper left map is the average across all thirty-four elderly subjects and patients; the other five maps are averages within elderly and disease subgroups.

Functional correlation maps were calculated for five additional populations (Figure 3.5). The qualitative patterns in these group-average maps were similar for cognitively unimpaired elderly, Parkinson's disease, Parkinson's disease dementia, Alzheimer's disease, and dementia with Lewy bodies. Characteristic features of the default network are observed in each group. Sample sizes from each group are insufficient for intergroup comparisons, but pooled analysis across groups demonstrates that some of the same regions remain most consistently correlated with the isthmus cingulate seed in native-space analysis (Table 3.3). As with the young subjects, the top two most consistently correlated regions in both hemispheres were inferior parietal and superior frontal.
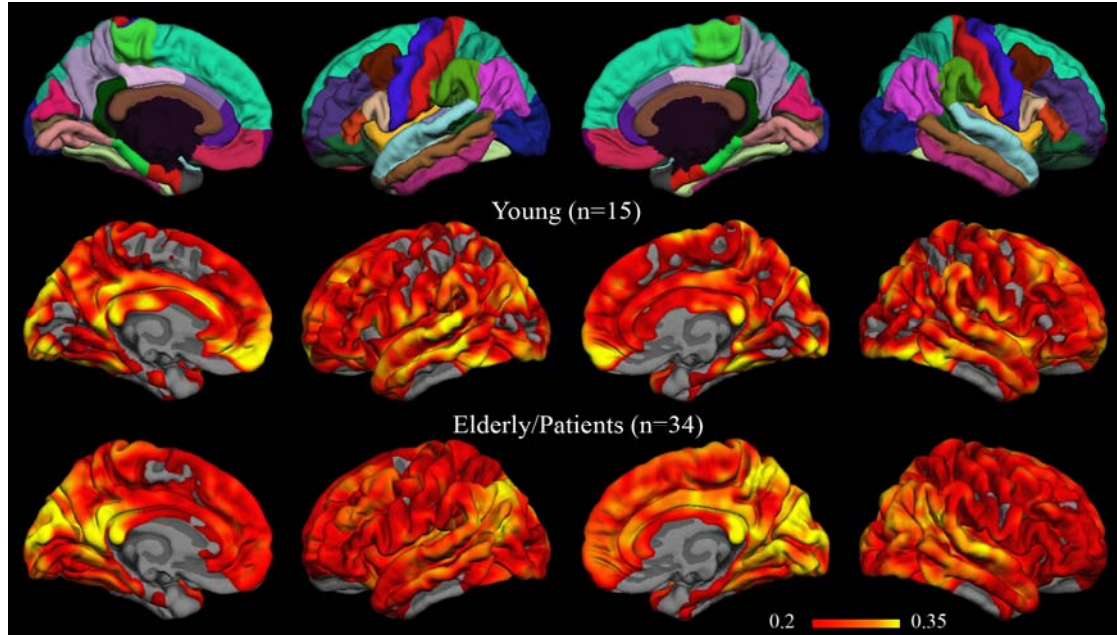
**Figure 3.6:** Group RMS difference maps for volume-atlas versus native-surface correlation results. The overlays in the bottom two rows show the root-mean-square difference between correlation results obtained after nonlinear transformation to the MNI152 volume-atlas and results obtained from analysis on each subject's native surface. The minimum threshold for the RMS difference (0.2) matches the magnitude of estimated population difference used in power analyses (see Table 3.2 and Table 3.3). For reference, the fsaverage parcellation is included in the top row.

The effect of defining a seed in volume-atlas space rather than defining a seed on the native surface was quantified by calculating the correlation coefficient between the two average time series for each subject. For young subjects, the median correlation coefficient (and interquartile range) between the MNI isthmus cingulate and native-surface isthmus cingulate was 0.84 (0.81-0.86) for the left hemisphere and 0.87 (0.85-0.87) for the right hemisphere. The minimum coefficient among the young subjects was 0.63, and the maximum was 0.93. For healthy and impaired elderly subjects, the median correlation coefficient was 0.77 (0.65-0.85) for the left isthmus

cingulate and 0.79 (0.66-0.85) for the right. The minimum coefficient among the elderly and patients was -0.09, and the maximum was 0.95.

Registration to an atlas volume also led to significant effects on correlation results throughout the rest of the cortex, even when the same (native-surface) seed time series was used for both methods. Correlation coefficients for MNI-transformed regions on the fsaverage surface differed from their native-surface homologues by a mean magnitude of $0.14 \pm 0.06$ (standard deviation) in young subjects. Paired $t$-tests for a non-zero magnitude difference between MNI and native regions gave $p$-values less than 0.005 for all regions in both hemispheres in the young subjects, and the median $p$-value was less than $10^{-4}$. In the elderly (including patients) group, the mean magnitude of the difference was $0.16 \pm 0.04$, which was significantly greater than in the young subjects ($t$-test, $p < 0.05$). Paired $t$-tests between MNI and native regions gave $p$-values less than $10^{-5}$ for all regions in both hemispheres in the elderly and patients group, and the median $p$-value was less than $10^{-7}$.

Vertex-wise group-level maps showing the root-mean-square difference between correlation coefficients obtained with MNI-transformed time series versus native-surface coefficients are displayed in Figure 3.6. The maps have a threshold RMS difference of 0.2, corresponding to the magnitude of the estimated population difference used in the power analysis above. Root-mean-square differences greater than 0.2 are widespread throughout both hemispheres in both young and elderly/diseased subjects. Among regions with the greatest RMS differences (greater than 0.35) are some associated with the default network, including the isthmus cingulate, inferior parietal, and medial prefrontal cortices.

### 3.4 Discussion

Spontaneous BOLD correlation studies may afford opportunities to increase our understanding of how regions of the brain interact and to develop clinical tools for diagnosis or measurement of disease progression. Already, intriguing results have been reported in various diseases, including mild cognitive impairment and Alzheimer's disease. Analysis in native space may improve accuracy, allow more rigorous investigation into resting-state correlation phenomena, and otherwise facilitate transition to clinical utility.

Reliance on warping to atlas space has the potential to critically influence results of functional correlation analyses. Despite the critical importance of accurate localization and known issues with warping, very few studies report on the accuracy of transformations, and transformed images are rarely included in published manuscripts. Many methods for warping to atlas volumes exist, and these usually have many user-selected parameters that affect the transformation but are not typically reported in methods descriptions. In the case of patients with atrophy or other structural abnormalities, these issues become more apparent and have been described previously (Ashburner and Friston, 2001; Bookstein, 2001; Senjem et al., 2005).

Figure 3.1 gives a striking example of the pitfalls of warping an atrophied brain to a normal template. Four methods from three standard software packages, using the recommended parameters, produced warped volumes that have obvious inconsistencies with the MNI template. Analysis of this subject with current methods might yield decreased correlations relative to controls, for example, in regions corresponding to the hippocampus or dorsal cortex. Following typical practices,

statistical results would be overlaid on the atlas brain to show the effect. However, decreased correlations in this hypothetical example might be explained by the fact that relatively large portions of the MNI cortex correspond to cerebrospinal fluid in the patient's warped brain, and therefore in the patient's warped functional data.

Analysis on native surfaces avoids warping individual brains to atlas volumes and the accompanying issues. Figure 3.2 demonstrates how the model of the individual cortical surface can still readily capture the features of the severely atrophied brain from the previous example. Remaining within the individual anatomy rather than attempting to distort it through spatial normalization, reduces the risk of mistakenly analyzing correlations outside the gray matter, or outside the brain altogether. Images of other brains, especially those without atrophy, may transform more accurately to the template. Use of other warping algorithms, other warping parameters, or other templates may improve the registration of this, and other, imaged brain volumes. However, at a minimum, the accuracy of the transformations for brains with structural pathology must be assessed and reported alongside functional analyses that depend on that transformation. Moreover, it is possible even studies using young, healthy subjects with no pathology could benefit from analysis on individual surfaces.

The effects of warping to a volume atlas on seed definition and on interregional correlations are quantified in this manuscript by direct comparison of native-surface results to results obtained after warping to the MNI152 volume atlas. In one such comparison, MNI transformation was shown to affect the isthmus cingulate seed time series, yielding MNI seed time series that were often poorly correlated with the seed defined on the subject's native surface. 25% of the healthy and impaired

elderly subjects had MNI-to-native isthmus cingulate correlation coefficients less than 0.66, and two subjects had coefficients less than 0.10. The weak correlation between the MNI and native time courses in this region suggests defining the seed on the native surface may impact resting correlation analyses independent of other methodological considerations. Moreover, a region-by-region comparison of volume-atlas and native-surface results revealed significant differences in every region tested, even when controlling for potential differences in the seed time series. This was true both in the young and elderly/patient groups. Finally, group maps of vertex-wise root-mean-square differences between the two methods also showed that MNI transformation led to sizeable effects throughout the cortex in both groups. Of concern is the observation that these group-level effects were as large as population differences reported in the literature, and regions highly correlated with the seed (in this case, default network regions) may be particularly vulnerable to modulation during transformation to an atlas volume. As the accuracy of registration to a volume atlas is logically dependent on the severity of structural pathology, studies of disease populations require special attention to these possible confounds.

Quantitative, native-surface parcellation analysis of spontaneous fMRI in young subjects highlights known default network regions when the isthmus cingulate is used as a seed (Table 3.2). Because the seed is defined on the native surface, individual vertex-wise maps can also be calculated to show both the similarities across subjects and the unique features of each subject's data. Inter-individual variability in both anatomy and functional correlations is preserved in this method, and composite statistics still allow comparisons between groups and between sessions.

Association with other individual markers is one of the primary advantages of analysis in native space. Native-surface cortical analysis is especially convenient for comparison to cortical thickness, as many morphometry studies already use FreeSurfer to measure cortical thickness in the same parcellation regions used in the present study for functional analysis (Desikan et al., 2010; Du et al., 2007; Liu et al., 2010; Rimol et al., 2010). A potential confound in all functional MRI studies of populations with atrophy, including those using the present method, is that decreased tissue volume might lead to a decrease in BOLD signal-to-noise ratio. Therefore, while a decrease in functional correlations with atrophy is expected due to effects on neural communication, it is difficult to distinguish this neural effect from the signal-to-noise effect. While this limitation is not entirely addressed by analysis on native surfaces, the availability of regional cortical thickness and volume measurements allows local atrophy effects to be accounted for in each subject. This may be additionally advantageous in longitudinal studies of patients with neurodegenerative disorders where atrophy may give structural changes over the course of the experiment.

The power analysis for the native-surface parcellation analysis suggests that a moderate difference in correlation coefficient (with the isthmus cingulate seed) can be detected in any of the regions in Table 3.2 with practical sample sizes for neuroimaging studies and clinical trials (Jack et al., 2010). Sample sizes range from 16 to 42 subjects, depending on the region; this is consistent with another report of regional differences in variability of correlation strength (Chang and Glover, 2010). The actual sample size necessary to detect a change is highly dependent on the effect size between the populations (sample size is proportional to the square of the effect

size). Both the intersubject variance and the effect size will be unique to each disease

studied, so caution should be exercised when extrapolating the values presented in

Table 3.2 to other populations. Further research is warranted to estimate population-

specific sample sizes; these power analyses will provide additional quantitative

information to guide inference and practical application of correlation measurements

in those diseases. The value of the power analysis presented here is to demonstrate that

the range of expected sample sizes suggests studies of diseases with moderate

differences in BOLD correlations are feasible using the native-surface method.

In addition to the benefits of quantitative native-surface analysis of individual

subject data, it is also valuable to display surface-based, group-level results.

Integrating and interpreting large numbers of individual maps can be difficult, and

space constraints will prevent many authors from including maps for each individual

in publications. Comparison to other published group maps, particularly those of

cortical thickness in aging and dementia (Dickerson et al., 2009; Salat et al., 2004),

might also be useful. Registration of individual surface models to a surface average

(e.g., the "fsaverage" subject in FreeSurfer) requires transformation to an atlas space,

which raises some of the same concerns described for volume transformations, but

evidence suggests that surface registration may be substantially more accurate (Fischl

et al., 1999b). Importantly, since cortex is being registered to cortex, the risk of

mapping an atlas coordinate to white matter or cerebrospinal fluid is greatly decreased.

Results from the patient and elderly subjects demonstrate that default network

regions are highlighted in native-surface analysis in multiple populations and with

relatively small sample sizes. The robustness of default network correlations to the

effects of age, atrophy, and dementia (of at least two different presumed etiologies) is also evident. However, the group maps also serve as an illustration of the degree to which inter-individual differences can be hidden by group averages. The Alzheimer's disease group map in Figure 3.5, for example, was generated from only four subjects. This map shows many of the characteristics of typical default network maps and is not remarkably different from the maps of the other groups. At least one of the four subjects, though, has a functional correlation map (Figure 3.2C, 3.2D) divergent from the typical default pattern. Investigation into the cognitive and pathological correlates of inter-individual differences in functional correlation patterns may prove enlightening, and native-surface analyses would be a powerful approach for such investigation.

Limitations of analysis on native surfaces include the computational cost of reconstructing and parcellating each subject's surface, which can take approximately 24 hours processing time per node. Visual confirmation of automated pial and white matter boundaries in the $T_1$-weighted volume is also recommended. In our opinion, however, checking the anatomical boundary definition is simpler than an equivalent check on a warping algorithm's match of each gyrus in each slice in the volume. We also find it easier to correct small errors in the boundaries for the surface than to optimize nonlinear registration parameters for individual subjects. Analysis with this method requires a high-resolution $T_1$-weighted volume for each subject, which may be viewed as a limitation to authors not routinely including this acquisition in their scanning protocols.

The parcellation atlas itself poses a limitation to the size and shape of the regions tested with the native-space parcellation analysis. Some applications may require more flexibility in region definitions, smaller regions, or specific subdivisions within some of the atlas regions. For others, there may be reason to question the implied assumption of relative functional homogeneity within the anatomically-defined regions. Exploratory studies may require functionally-defined regions or a vertex-wise analysis, which makes transformation to the atlas surface necessary for inter-subject comparisons. Investigators may also consider another atlas available in FreeSurfer for native surfaces that subdivides the regions shown in Figure 3.4 into gyral and sulcal cortex (Destrieux et al., 2010). Many other atlases exist, and custom atlases can be created within FreeSurfer or elsewhere; these additional atlases typically rely on registration to the average surface, though, and are not automatically produced in the reconstruction process within FreeSurfer. The primary advantages of the Desikan-Killiany atlas parcellation are its common use for cortical thickness studies and its definition based on landmarks that can be consistently identified in individual subjects' anatomy.

An alternative to native-surface analysis is analysis within the native volumes of individual subjects. To avoid manual ROI selection, the seed region could be defined by a coordinate in the atlas volume and reverse-transformed to each subject by applying the inverse of the transformation matrix from the warping algorithm. Accuracy of seed placement in this case, however, is subject to the same limitations of the transformation matrix as analysis in atlas space. Seed location should be verified for each subject, most likely by visual inspection. A spherical region centered on a

reverse-transformed atlas coordinate may increase the chances of including the desired cortex, but if the spheres are much larger than the thickness of the cortex, it is very likely voxels containing primarily white matter or cerebrospinal fluid will be included in the seed. Common diameters for spheres range from 8 mm to 12 mm or larger (Fox et al., 2005; Fox et al., 2006; Hedden et al., 2009; Vincent et al., 2006), compared to cortical thickness which is around 2 mm (Du et al., 2007; Liu et al., 2010).

Even if the reverse-transformed seed is sufficiently accurate, the native-surface functional correlation maps generated with it cannot be quantitatively compared across individuals unless additional regions are defined. One approach is to create more regions of interest from other reverse-transformed atlas volume coordinates, but each of these regions will be subject to the same limitations as the seed. Another approach is to use the reverse-transformed seed to perform seed-correlation analysis in the native brain. However, inter-subject comparisons of the native results in this voxel-wise approach still requires warping the functional data to an atlas volume, and it is unlikely that any advantage is gained by applying that transformation to final statistics rather than to the raw data. An analogous challenge faces independent component analysis (ICA) in native space: even if a suitable template is defined for each subject to identify the component of interest, warping the native-space components to atlas space is necessary for comparison across subjects or groups.

Future development of this method could focus on broadening the scope of its applications. Parcellation regions other than the isthmus cingulate might be used as seeds for other cortical networks that are associated with neurological or psychiatric diseases (Ebisch et al., 2010; Greicius, 2008; Seeley et al., 2009). Additional methods

of analyzing functional correlations might also be adapted to native surfaces. Currently, methods such as ICA could be readily applied within the average surface space; however, ICA components are difficult to compare quantitatively across subjects without transforming to atlas space. One idea for native-space ICA is to use one or more of the anatomical parcellation regions highlighted in this study as a template for identifying the default network components. Independent components could then be compared across subjects within analogous parcellation regions. A similar approach could be taken to define templates for other resting-state network components. Regardless of analysis method, investigation of these resting-state functional patterns in disease can benefit from leveraging the underlying anatomy and pathology of individual subjects.

## 3.5   Acknowledgements

Chapter 3, in full, is a reprint of the material as it appears in Journal of Neuroscience Methods, 2011. Seibert, Tyler M.; Brewer, James B., Elsevier, Inc, 2011. The dissertation author was the primary investigator and author of this paper.

## 3.6   Supplementary Materials
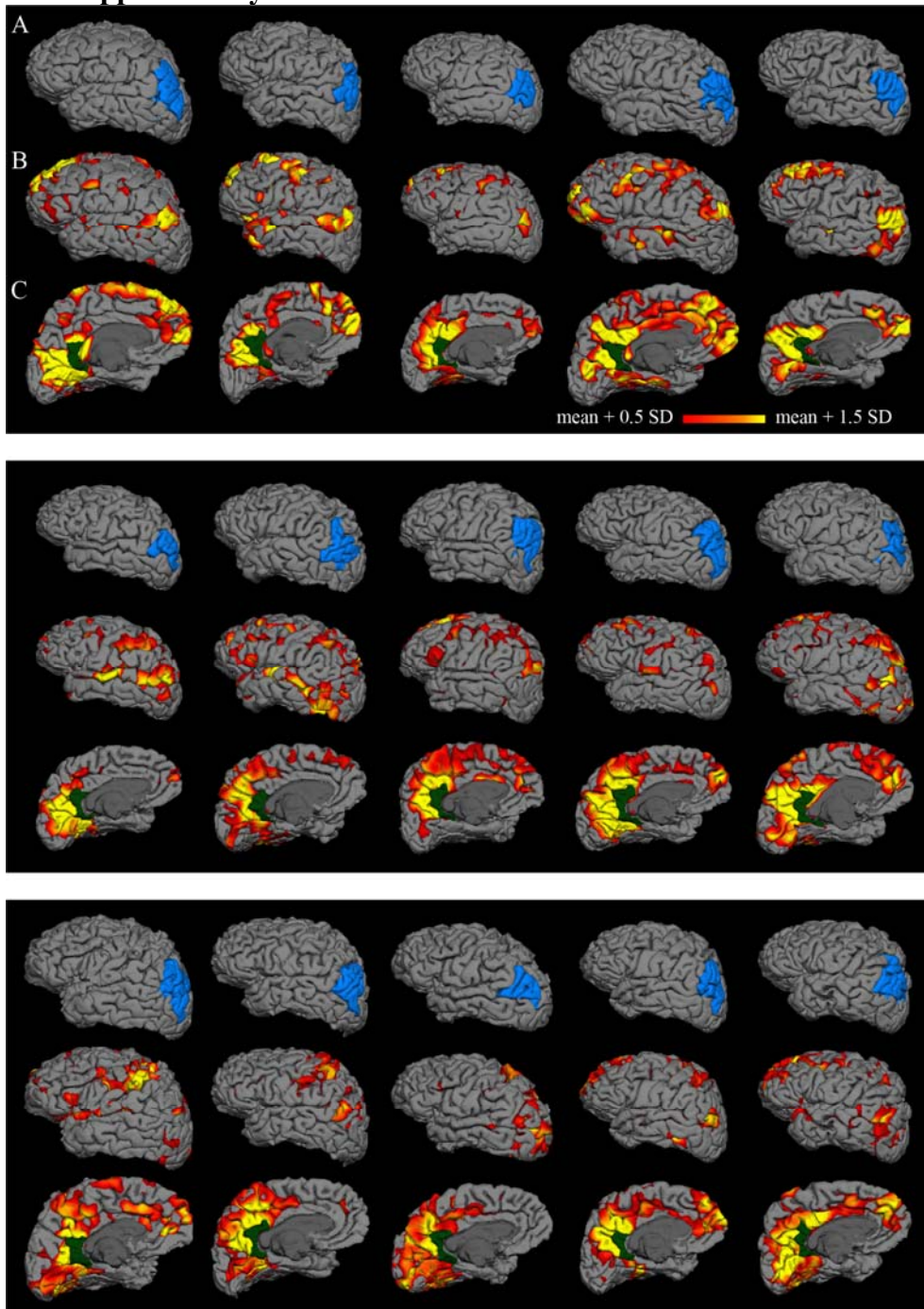


**Figure 3.7:** Supplementary Figure – Individual correlation maps for all young subjects. Columns within each block represent individual subjects. **A:** Cortical surface models with a single parcellation region (inferior parietal) highlighted in blue. **B-C:** Individual correlation maps consisting of coefficients (z-transformed) from correlation of each vertex on the surface with the average time series of the isthmus cingulate seed (dark green).

## 3.7 References

Allen, G, Barnard, H, McColl, R, Hester, AL, Fields, JA, Weiner, MF, et al. (2007): Reduced hippocampal functional connectivity in Alzheimer disease. Arch. Neurol, 64(10), 1482-1487.

Ashburner, J, Friston, KJ (2001): Why Voxel-Based Morphometry Should Be Used. NeuroImage, 14(6), 1238-1243.

Auer, DP (2008): Spontaneous low-frequency blood oxygenation level-dependent fluctuations and functional connectivity analysis of the "resting" brain. Magn Reson Imaging, 26(7), 1055-1064.

Bai, F, Watson, DR, Yu, H, Shi, Y, Yuan, Y, Zhang, Z (2009): Abnormal resting-state functional connectivity of posterior cingulate cortex in amnestic type mild cognitive impairment. Brain Res, 1302, 167-174.

Biswal, B, Yetkin, FZ, Haughton, VM, Hyde, JS (1995): Functional connectivity in the motor cortex of resting human brain using echo-planar MRI. Magn Reson Med, 34(4), 537-541.

Bookstein, FL (2001): "Voxel-Based Morphometry" Should Not Be Used with Imperfectly Registered Images. NeuroImage, 14(6), 1454-1462.

Buckner, RL, Andrews-Hanna, JR, Schacter, DL (2008): The Brain's Default Network: Anatomy, Function, and Relevance to Disease. Annals of the New York Academy of Sciences, 1124(1), 1-38.

Buckner, RL, Sepulcre, J, Talukdar, T, Krienen, FM, Liu, H, Hedden, T, Andrews-Hanna, JR, Sperling, RA, Johnson, KA (2009): Cortical Hubs Revealed by Intrinsic Functional Connectivity: Mapping, Assessment of Stability, and Relation to Alzheimer's Disease. J. Neurosci., 29(6), 1860-1873.

Buckner, RL, Vincent, JL (2007): Unrest at rest: Default activity and spontaneous network correlations. NeuroImage, 37(4), 1091-1096.

Chang, C, Glover, GH (2010): Time-frequency dynamics of resting-state brain connectivity measured with fMRI. Neuroimage, 50(1), 81-98.

Cohen, J (1988): Statistical power analysis for the behavioral sciences (Second.). Psychology Press.

Cox, RW, Jesmanowicz, A (1999): Real-time 3D image registration for functional MRI. Magn Reson Med, 42(6), 1014-1018.

Dale, AM, Fischl, B, Sereno, MI (1999): Cortical surface-based analysis. I. Segmentation and surface reconstruction. Neuroimage, 9(2), 179-194.

Dawson, B, Trapp, RG (2004): Basic & clinical biostatistics (Fourth.). Lange Medical Books/McGraw-Hill.

Desikan, RS, Ségonne, F, Fischl, B, Quinn, BT, Dickerson, BC, Blacker, D, et al. (2006): An automated labeling system for subdividing the human cerebral cortex on MRI scans into gyral based regions of interest. Neuroimage, 31(3), 968-980.

Desikan, RS, Sabuncu, MR, Schmansky, NJ, Reuter, M, Cabral, HJ, Hess, CP, et al. (2010): Selective Disruption of the Cerebral Neocortex in Alzheimer's Disease. PLoS ONE, 5(9), e12853.

Destrieux, C, Fischl, B, Dale, AM, Halgren, E (2010): Automatic parcellation of human cortical gyri and sulci using standard anatomical nomenclature. Neuroimage, 53(1), 1-15.

Dickerson, BC, Bakkour, A, Salat, DH, Feczko, E, Pacheco, J, Greve, DN, et al. (2009): The cortical signature of Alzheimer's disease: regionally specific cortical thinning relates to symptom severity in very mild to mild AD dementia and is detectable in asymptomatic amyloid-positive individuals. Cereb. Cortex, 19(3), 497-510.

Du, A-T, Schuff, N, Kramer, JH, Rosen, HJ, Gorno-Tempini, ML, Rankin, K, Miller, BL, Weiner, MW (2007): Different regional patterns of cortical thinning in Alzheimer's disease and frontotemporal dementia. Brain, 130(4), 1159 -1166.

Ebisch, SJH, Gallese, V, Willems, RM, Mantini, D, Groen, WB, Romani, GL, Buitelaar, JK, Bekkering, H (2010): Altered intrinsic functional connectivity of anterior and posterior insula regions in high-functioning participants with autism spectrum disorder. Hum Brain Mapp.

Fischl, B, van der Kouwe, A, Destrieux, C, Halgren, E, Segonne, F, Salat, DH, et al. (2004): Automatically Parcellating the Human Cerebral Cortex. Cereb. Cortex, 14(1), 11-22.

Fischl, B, Salat, DH, Busa, E, Albert, M, Dieterich, M, Haselgrove, C, et al. (2002): Whole brain segmentation: automated labeling of neuroanatomical structures in the human brain. Neuron, 33(3), 341-355.

Fischl, B, Sereno, MI, Dale, AM (1999a): Cortical surface-based analysis. II: Inflation, flattening, and a surface-based coordinate system. Neuroimage, 9(2), 195-207.

Fischl, B, Sereno, MI, Tootell, RB, Dale, AM (1999b): High-resolution intersubject averaging and a coordinate system for the cortical surface. Hum Brain Mapp, 8(4), 272-284.

Fleisher, AS, Sherzai, A, Taylor, C, Langbaum, JBS, Chen, K, Buxton, RB (2009): Resting-state BOLD networks versus task-associated functional MRI for distinguishing Alzheimer's disease risk groups. Neuroimage, 47(4), 1678-1690.

Fox, MD, Raichle, ME (2007): Spontaneous fluctuations in brain activity observed with functional magnetic resonance imaging. Nat Rev Neurosci, 8(9), 700-11.

Fox, MD, Snyder, AZ, Vincent, JL, Corbetta, M, Van Essen, DC, Raichle, ME (2005): The human brain is intrinsically organized into dynamic, anticorrelated functional networks. Proc Natl Acad Sci U S A, 102(27), 9673-8.

Fox, MD, Corbetta, M, Snyder, AZ, Vincent, JL, Raichle, ME (2006): Spontaneous neuronal activity distinguishes human dorsal and ventral attention systems. Proceedings of the National Academy of Sciences, 103(26), 10046 -10051.

Geser, F, Wenning, GK, Poewe, W, McKeith, IG (2005): How to diagnose dementia with Lewy bodies: state of the art. Mov. Disord, 20 Suppl 12, S11-20.

Glover, GH, Li, TQ, Ress, D (2000): Image-based method for retrospective correction of physiological motion effects in fMRI: RETROICOR. Magn Reson Med, 44(1), 162-167.

Greicius, MD, Krasnow, B, Reiss, AL, Menon, V (2003): Functional connectivity in the resting brain: a network analysis of the default mode hypothesis. Proc. Natl. Acad. Sci. U.S.A, 100(1), 253-258.

Greicius, MD (2008): Resting-state functional connectivity in neuropsychiatric disorders. Curr. Opin. Neurol, 21(4), 424-430.

Greicius, MD, Srivastava, G, Reiss, AL, Menon, V (2004): Default-mode network activity distinguishes Alzheimer's disease from healthy aging: evidence from functional MRI. Proc. Natl. Acad. Sci. U.S.A, 101(13), 4637-4642.

Hedden, T, Van Dijk, KRA, Becker, JA, Mehta, A, Sperling, RA, Johnson, KA, Buckner, RL (2009): Disruption of functional connectivity in clinically normal older adults harboring amyloid burden. J. Neurosci, 29(40), 12686-12694.

van den Heuvel, MP, Hulshoff Pol, HE (2010): Exploring the brain network: A review on resting-state fMRI functional connectivity. European Neuropsychopharmacology, 20(8), 519-534.

Holland, D, Kuperman, JM, Dale, AM (2010): Efficient correction of inhomogeneous static magnetic field-induced distortion in Echo Planar Imaging. NeuroImage, 50(1), 175-183.

Jack, CR, Bernstein, MA, Borowski, BJ, Gunter, JL, Fox, NC, Thompson, PM, et al. (2010): Update on the magnetic resonance imaging core of the Alzheimer's disease neuroimaging initiative. Alzheimers Dement, 6(3), 212-220.

Koch, W, Teipel, S, Mueller, S, Benninghoff, J, Wagner, M, Bokde, ALW, et al. (2010): Diagnostic power of default mode network resting state fMRI in the detection of Alzheimer's disease. Neurobiol Aging.

Liu, Y, Paajanen, T, Zhang, Y, Westman, E, Wahlund, L-O, Simmons, A, et al. (2010): Analysis of regional MRI volumes and thicknesses as predictors of conversion from mild cognitive impairment to Alzheimer's disease. Neurobiology of Aging, 31(8), 1375-1385.

McKeith, IG (2007): Dementia with Lewy bodies and Parkinson's disease with dementia: where two worlds collide. Practical Neurology, 7(6), 374-382.

McKhann, G, Drachman, D, Folstein, M, Katzman, R, Price, D, Stadlan, EM (1984): Clinical diagnosis of Alzheimer's disease: report of the NINCDS-ADRDA Work Group under the auspices of Department of Health and Human Services Task Force on Alzheimer's Disease. Neurology, 34(7), 939-944.

Pihlajamäki, M, Jauhiainen, AM, Soininen, H (2009): Structural and functional MRI in mild cognitive impairment. Curr Alzheimer Res, 6(2), 179-185.

Raichle, ME, MacLeod, AM, Snyder, AZ, Powers, WJ, Gusnard, DA, Shulman, GL (2001): A default mode of brain function. Proc. Natl. Acad. Sci. U.S.A, 98(2), 676-682.

Raichle, ME, Snyder, AZ (2007): A default mode of brain function: a brief history of an evolving idea. Neuroimage, 37(4), 1083-1090; discussion 1097-1099.

Rimol, LM, Hartberg, CB, Nesvåg, R, Fennema-Notestine, C, Hagler Jr., DJ, Pung, CJ, et al. (2010): Cortical Thickness and Subcortical Volumes in Schizophrenia and Bipolar Disorder. Biological Psychiatry, 68(1), 41-50.

Rogers, BP, Morgan, VL, Newton, AT, Gore, JC (2007): Assessing functional connectivity in the human brain by fMRI. Magn Reson Imaging, 25(10), 1347-1357.

Salat, DH, Buckner, RL, Snyder, AZ, Greve, DN, Desikan, RS, Busa, E, Morris, JC, Dale, AM, Fischl, B (2004): Thinning of the cerebral cortex in aging. Cereb. Cortex, 14(7), 721-730.

Seeley, WW, Crawford, RK, Zhou, J, Miller, BL, Greicius, MD (2009): Neurodegenerative diseases target large-scale human brain networks. Neuron, 62(1), 42-52.

Senjem, ML, Gunter, JL, Shiung, MM, Petersen, RC, Jack, J (2005): Comparison of different methodological implementations of voxel-based morphometry in neurodegenerative disease. NeuroImage, 26(2), 600-608.

Sheline, YI, Raichle, ME, Snyder, AZ, Morris, JC, Head, D, Wang, S, Mintun, MA (2010): Amyloid Plaques Disrupt Resting State Default Mode Network Connectivity in Cognitively Normal Elderly. Biological Psychiatry, 67(6), 584-587.

Sorg, C, Riedl, V, Mühlau, M, Calhoun, VD, Eichele, T, Läer, L, et al. (2007): Selective changes of resting-state networks in individuals at risk for Alzheimer's disease. Proc. Natl. Acad. Sci. U.S.A, 104(47), 18760-18765.

Supekar, K, Menon, V, Rubin, D, Musen, M, Greicius, MD (2008): Network analysis of intrinsic functional brain connectivity in Alzheimer's disease. PLoS Comput. Biol, 4(6), e1000100.

Van Dijk, KRA, Hedden, T, Venkataraman, A, Evans, KC, Lazar, SW, Buckner, RL (2009): Intrinsic Functional Connectivity As a Tool For Human Connectomics: Theory, Properties, and Optimization. J. Neurophysiol.

Vincent, JL, Snyder, AZ, Fox, MD, Shannon, BJ, Andrews, JR, Raichle, ME, Buckner, RL (2006): Coherent Spontaneous Activity Identifies a Hippocampal-Parietal Memory Network. J Neurophysiol, 96(6), 3517-3531.

Wang, K, Liang, M, Wang, L, Tian, L, Zhang, X, Li, K, Jiang, T (2007): Altered functional connectivity in early Alzheimer's disease: a resting-state fMRI study. Hum Brain Mapp, 28(10), 967-978.

Wang, L, Negreira, A, LaViolette, P, Bakkour, A, Sperling, RA, Dickerson, BC (2010): Intrinsic interhemispheric hippocampal functional connectivity predicts individual differences in memory performance ability. Hippocampus, 20(3), 345-351.

Wang, L, Zang, Y, He, Y, Liang, M, Zhang, X, Tian, L, Wu, T, Jiang, T, Li, K (2006): Changes in hippocampal connectivity in the early stages of Alzheimer's disease: evidence from resting state fMRI. Neuroimage, 31(2), 496-504.

Yan, C, Liu, D, He, Y, Zou, Q, Zhu, C, Zuo, X, Long, X, Zang, Y (2009):
Spontaneous brain activity in the default mode network is sensitive to different
resting-state conditions with limited cognitive load. PLoS ONE, 4(5), e5743.

Zhang, H-Y, Wang, S-J, Liu, B, Ma, Z-L, Yang, M, Zhang, Z-J, Teng, G-J (2010):
Resting brain connectivity: changes during the progress of Alzheimer disease.
Radiology, 256(2), 598-606.

CHAPTER 4

**Stability of resting fMRI interregional correlations analyzed in subject-native space: a one-year longitudinal study in healthy adults and premanifest Huntington's disease**

**Abstract**

The pattern of interregional functional MRI correlations at rest is being actively considered as a potential noninvasive biomarker in multiple diseases. Before such methods can be used in clinical studies it is important to establish their usefulness in three ways. First, the long-term stability of resting correlation patterns should be characterized, but there have been very few such studies. Second, analysis of resting correlations should account for the unique neuroanatomy of each subject by taking measurements in native space and avoiding transformation of functional data to a standard volume space (e.g., Talairach-Tournox or Montreal Neurological Institute atlases). Transformation to a standard volume space has been shown to variably influence the measurement of functional correlations, and this is a particular concern in diseases which may cause structural changes in the brain. Third, comparisons within the patient population of interest and comparisons between patients and age-matched controls, should demonstrate sensitivity to any disease-related disruption of resting functional correlations. Here we examine the test-retest reliability of resting fMRI correlations over a period of one year in a group of healthy adults and in a group

of gene-positive, asymptomatic individuals with Huntington's disease. A recently-developed method is used to measure functional correlations in the native space of individual subjects. The utility of resting functional correlations as a biomarker in premanifest Huntington's disease is also investigated. Results in control and premanifest Huntington's populations were both highly consistent at the group level over one year. We thus show that when resting fMRI analysis is performed in native space (to avoid confounds in registration between subjects and groups) it has good long-term reliability at the group level. No significant effect of premanifest Huntington's disease on prespecified interregional fMRI correlations was observed relative to the control group, either at baseline or with regards to the longitudinal change. Within the premanifest Huntington's group, though, there was evidence that decreased striatal functional correlations might be associated with disease severity, as gauged by estimated years to symptom onset or by striatal volume.

**Keywords:** test-retest; reliability; default network; fMRI; functional connectivity

**Abbreviations:** BOLD, blood oxygenation level dependent; fMRI, functional magnetic resonance imaging; HD, Huntington's disease; pre-HD, preclinical Huntington's disease; MNI, Montreal Neurological Institute; ICC, intraclass correlation coefficient; MMSE = mini-mental state exam; CAG = cytosine-adenine-guanine; UHDRS = Unified Huntington's Disease Rating Scale.

## 4.1 Introduction

There is currently great interest in measuring interregional correlations of the resting blood oxygenation level dependent (BOLD) fMRI signal as a biomarker in disease. This approach could have advantages over structural MRI as it might reveal changes in physiological function before widespread and substantial cell loss occurs (Bohanna et al., 2008). Resting fMRI has a strong clinical appeal because it affords the ability to study multiple networks of the entire brain at once and without confounding effects of cognitive ability to perform a given behavioral task (Auer, 2008; Fox and Raichle, 2007; Greicius, 2008; van den Heuvel and Hulshoff Pol, 2010; Rogers et al., 2007). Already, variations in resting functional correlations (often termed "functional connectivity") have been reported in a wide range of neurological and psychiatric disorders, including Alzheimer's disease (Greicius et al., 2004; Sorg et al., 2009), mild cognitive impairment (Bai et al., 2009; Pihlajamäki et al., 2009; Sorg et al., 2007), amyotrophic lateral sclerosis (Mohammadi et al., 2011b), schizophrenia (Jafri et al., 2008; Repovs et al., 2011), depression (Greicius, 2008), writer's cramp (Mohammadi et al., 2011a), and Parkinson's disease (Helmich et al., 2010; Wu et al., 2009). In the case of amyloid-associated pathology, there is evidence that resting functional correlations may be sensitive to neurological changes prior to onset of clinical symptoms (Hedden et al., 2009; Sheline et al., 2010). Taken together, these many reports motivate resting fMRI as a tool for investigating the disease process across time (i.e. in longitudinal biomarker studies) with the eventual aim of evaluating neuroprotection or treatment.

It is important, however, to first evaluate the test-retest reliability of resting

fMRI. Reliability may be a particular concern in resting fMRI because whereas task-

based studies attempt to tightly control brain behavior, resting fMRI uses an

unconstrained paradigm that allows the potential for markedly different states of

mental activity from one scan session to the next. Existing studies of reliability in

resting fMRI have used data transformed to a standard volume (Chen et al., 2008;

Damoiseaux et al., 2006; Meindl et al., 2010; Shehzad et al., 2009; Thomason et al.,

2011; Van Dijk et al., 2009; Zuo et al., 2010), and to our knowledge, only one data set

has been examined with longitudinal measurements in adults (mean age 20.5 years)

for a period longer than 16 days (5-16 months) (Shehzad et al., 2009). Thus, further

investigation of the long-term reliability of resting functional correlations is needed.

For resting fMRI to be a useful biomarker in neurological disease it may also

be necessary to use an analysis method that takes into account the fact that patient or

gene-positive groups may already have changes in gray and white matter—for

example, to regions adjacent to cerebrospinal fluid, such as the periventricular basal

ganglia regions. When such changes occur, it is possible that resting correlations can

be mistakenly measured from voxels in white matter or cerebrospinal fluid. We

recently showed that transforming functional data to a standard volume (e.g.,

Talairach or MNI152) can introduce large, widespread effects on resting fMRI

correlations due to imperfect registration of native anatomy to the volume atlas

(Seibert and Brewer, 2011). This was true even in young, healthy subjects, but is a

particular concern in disease. We proposed an alternative method that addresses these

issues by analyzing resting BOLD correlations on models of the native cortical surface

created for each subject's brain (Seibert and Brewer, 2011). Here we again apply this native-space method.

Finally, the utility of resting fMRI to biomarker development also requires establishing that longitudinal inter-regional correlations can indeed detect differences between a disease group and a healthy one. Huntington's disease (HD) is a genetic neurodegenerative disorder that causes deficits in both motor and cognitive function. Though HD affects a number of brain regions, including cerebral cortex, the most prominent neuropathologic changes occur in the striatum, made up of the caudate and putamen (Eidelberg and Surmeier, 2011; Rosas et al., 2008). Strikingly, atrophy in the caudate and putamen has been identified using neuroimaging more than a decade prior to the estimated onset of manifest symptoms, i.e. during the premanifest stage of HD (pre-HD) (Aylward et al., 1996, 2004, 2011; Paulsen et al., 2010; Stoffers et al., 2010; Tabrizi et al., 2009). In this study, we compare gene-positive premanifest HD participants with a group of healthy controls matched for age and IQ.

Diagnosis of Huntington's disease is aided by the presence of genetic markers, and these genetic markers permit identification of high-risk individuals prior to onset of clinical symptoms. An imaging biomarker is highly desirable in premanifest Huntington's disease (pre-HD) to track progression, inform prognosis, and measure the effects of potential therapies. We have previously shown that MRI can detect structural changes (atrophy) over one year in pre-HD (Majid et al., 2011). A functional MRI technique might complement structural MRI and suggest physiological relevance of structural changes; additionally, functional imaging may have the potential to detect acute effects of therapies before major structural pathology occurs (Rosas et al., 2004).

Differences between pre-HD and age-matched control populations have already been demonstrated using task-based fMRI (Klöppel et al., 2009; Paulsen et al., 2004; Reading et al., 2004; Wolf et al., 2008; Zimbelman et al., 2007), but disease-related changes in functional activation have yet to be identified longitudinally in pre-HD, and resting fMRI correlations have not been evaluated in pre-HD.

Thus, the present study had two main objectives. First, we aimed to investigate the long-term stability (over one year) of resting fMRI correlations in 22 healthy adults and also 34 adults with pre-HD. Second, we aimed to ascertain whether a detectable difference exists in the resting interregional functional correlations between pre-HD subjects and age-matched controls (cross-sectionally and longitudinally). Importantly, to avoid artifactual effects from transformation to a standard volume, functional correlations in this study are calculated on each subject's native cortical surface and within native-space subcortical structures.

## 4.2   Methods

### 4.2.1   Subjects

Thirty-seven pre-HD ($\geq$ 38 CAG repeats) and 22 healthy age-matched control participants underwent resting state scans at two visits, with a one-year interval between visits. Consent was provided in accordance with an Institutional Review Board at the University of California, San Diego. A movement disorder specialist evaluated the pre-HD participants using the United Huntington's Disease Rating Scale (UHDRS) (Huntington Study Group, 1996), as described previously (Majid et al., 2011). With this scale, participants were assigned a 'motor score' (range: 0-124) and

were rated as to the clinician's confidence that the presenting motor abnormalities

represent symptoms of HD (range: 0-4). A confidence rating of 0 represents a normal

evaluation with no motor abnormalities, a rating of 1 represents < 50% confidence of

an HD diagnosis, and a rating of 4 represents a definitive HD diagnosis. All

participants rated below 2 at visit 1, confirming pre-HD status. At follow-up, two

initially pre-HD participants rated 4, indicating conversion to manifest HD. These two

were removed from the analysis. An additional pre-HD participant was removed

because of considerable signal dropout due to dental implants. This left a pre-HD

group of 34 individuals.

Global cognitive ability was measured using the mini-mental state exam

(MMSE) (Folstein et al., 1975) at both timepoints. Furthermore, the length of the

CAG repeat expansion was used to calculate estimated years-to-onset (YTO) using

both the Aylward and Langbehn methods (Aylward et al., 1996; Langbehn et al.,

2004).

4.2.2   MRI acquisition

A General Electric (GE; Milwaukee, WI) 3T Signa HDx scanner was used to

acquire 182 functional T2*-weighted ecoplanar images (EPI) (axial acquisition, 4mm

slice thickness, 32 slices per volume, TR = 2s, TE = 30ms, flip angle = 90°, field of

view = 220mm). Before the resting state scan, participants were instructed to close

their eyes, relax, and try not to fall asleep during the procedure. Additionally, a

matched-bandwidth high-resolution fast spin echo (FSE) scan (axial acquisition, 4mm

slice thickness, 32 slices per volume, TR = 5s, TE = 103.224ms, flip angle = 90°, field

of view = 220mm, matrix = 128x128) was acquired for each subject for registration

purposes. Structural $T_1$-weighted imaging data were obtained on a GE 1.5T Excite

HDx scanner. Image acquisition included a GE "PURE" calibration sequence and a

high-resolution three-dimensional $T_1$-weighted IRSPGR sequence (axial acquisition,

1.2mm slice thickness, TR = 6.496ms, TE = 2.798ms, TI = 600ms, flip angle = 12°,

bandwidth = 244.141 Hz/pixel, field of view = 240mm, matrix = 256x192).

## 4.2.3   Structural MRI processing

A model of each subject's cortical surface was reconstructed from the $T_1$-

weighted MRI volume at visit 1 (Dale et al., 1999; Fischl et al., 1999a). The surface

was then anatomically parcellated using the Desikan-Killiany atlas (Desikan et al.,

2006; Fischl et al., 2004). Subcortical structures were similarly identified by volume

segmentation (Fischl et al., 2002). Results from each of these automated steps were

inspected for accuracy, and manual corrections were applied as necessary according to

procedures described previously, ensuring accurate native surfaces and identification

of tissue boundaries (Seibert and Brewer, 2011).

## 4.2.4   fMRI data pre-analysis processing

Functional volumes were first corrected for static field inhomogeneity using

field maps acquired in each functional session (Smith et al., 2004). After interpolation

for slice acquisition timing, rigid-body volume registration was performed using AFNI

(Cox and Jesmanowicz, 1999), followed by voxel-wise regression of six head motion parameters, the average signal from white matter voxels, and a cubic polynomial baseline. White matter voxels were identified with a subject-specific white matter mask, eroded away from tissue boundaries (gray matter and cerebrospinal fluid) to avoid partial volume effects. Functional data were next projected onto the subject's cortical surface model, and a bandpass filter of 0.01-0.08 Hz was applied to the time series from each vertex on the surface. To avoid differences that might arise from any variation in surface reconstruction, functional data from both visits were projected to the visit 1 surface. This was achieved by first registering each functional volume to a matched-bandwidth, spin-echo $T_2$-weighted volume acquired during the same session. The $T_1$-weighted volume from visit 1 was registered to the spin-echo $T_2$-weighted volume from each visit, and these registrations were used for surface projection.

4.2.5   fMRI interregional correlation analysis

Procedures for fMRI correlation analysis on native surfaces are described in detail elsewhere (Seibert and Brewer, 2011); these procedures take advantage of the FreeSurfer surface generation and parcellation tools and avoid transforming functional data to an atlas volume. Briefly, a single region from the automated parcellation of each individual surface is used as the seed time series for each hemisphere. The functional time series from the seed region is then correlated with the average time series from 33 cortical surface parcellation regions and five volume segmentation regions (hippocampus, caudate, pallidum, putamen, amygdala) in the Desikan-Killiany atlas, excluding regions adjacent to the seed. Fisher's $z$-transform was applied to these

native-surface correlation coefficients. Potential differences in native-space results were evaluated with *t*-tests corrected for multiple comparisons. In addition, power analysis estimated the number of subjects needed to detect a difference between two groups, following steps described previously (assuming population difference of 0.2 in *z*-tranformed correlation coefficient, alpha value of 0.05, and 80% power) (Seibert and Brewer, 2011; Cohen, 1988; Dawson and Trapp, 2004).

Vertex-wise correlation analysis (surface equivalent to voxel-wise analysis) was also performed after spherical-based surface registration to the FreeSurfer fsaverage surface (Fischl et al., 1999b; Seibert and Brewer, 2011). The minimum and maximum thresholds were set based on the group map for control subjects' first visit; the minimum threshold was one standard deviation above the map mean, and the maximum threshold was two standard deviations above the map mean. To account for possible variation in functional anatomy, individual maps were subjected to a surface-based smoothing process (approximately equivalent to a 6 mm Gaussian kernel in two dimensions) prior to performing vertex-wise group statistics. All group summary maps were similarly smoothed for display. Tissue mislabeling can frequently arise during transformation to a volume atlas such as Talairach or MNI152, introducing large effects on functional correlations; surface-based registration reduces these errors (Fischl et al., 1999a, 1999b; Seibert and Brewer, 2011).

The main analyses were performed with two seed regions. The isthmus cingulate region has been shown to be a reliable seed for study of the default network (Seibert and Brewer, 2011). Additionally, the putamen was chosen as a seed for investigating intrastriatal and corticostriatal correlations in light of known striatal

involvement in Huntington's pathology and MRI evidence that the putamen may be the most prominently affected structure in early Huntington's disease (Harris et al., 1992). In a supplementary analysis, group maps were also created with the caudate as a seed for qualitative comparison of correlation patterns arising from caudate or putamen seeds.

4.2.6  Stability of fMRI intrerregional correlations

Long-term stability of group-level interregional correlation results (from visit 1 to visit 2, approximately one year later) was investigated in both the native-surface parcellation regions and the vertex-wise group-surface maps. Consistency of the overall pattern of correlations with the seed was evaluated by calculating the Pearson's correlation coefficient across native-surface regions for group-mean results from visit 1 and visit 2. Paired $t$-tests across subjects were then applied to the visit 1 and visit 2 results of each native-surface region to identify any regions that changed significantly over time. Maps of longitudinal consistency were then created with paired $t$-tests for every vertex on the group surface. All $t$-test results were assessed for statistical significance after controlling the false discovery rate at less than 0.05 to correct for multiple comparisons (Genovese et al., 2002).

Subject-level stability from visit 1 to visit 2 was also evaluated with the Pearson's correlation coefficient across native-surface regions for each subject. Additionally, the relative intrasubject and intersubject variance was compared by calculating intraclass correlation coefficients (ICC) for each native-surface region. Intraclass correlation coefficients were obtained using the following formula:

$$ICC = \frac{BMS - EMS}{BMS + (k-1)EMS},$$

where $k$ is the number of observations; $BMS$ is the between-subjects mean-square

error; and $EMS$ is the within-subjects mean-square error (mean-square errors

computed with a repeated-measures, mixed-effects ANOVA) (Shrout and Fleiss,

1979). ICC values can have magnitude between 0 and 1, and large ICC values reflect

low within-subjects variance (across sessions) and high between-subjects variance.

ICC values were tested for significance against a zero-value null hypothesis based on

an $F$ distribution, where

$$F_0 = \frac{BMS}{EMS},$$

and the degrees of freedom are ($n$-1) and ($n$-1)($k$-1), where $n$ is the number of subjects

(Shrout and Fleiss, 1979).

## 4.2.7   Effect of pre-HD on interregional correlations

Subjects with pre-HD were compared to healthy controls to test for a potential

population difference attributable to early pathology. Two-sample $t$-tests were applied

to pre-HD and control data from each native-surface parcellation region. Vertex-wise

comparisons were also made, using two-sample $t$-tests at each vertex on the group

surface. The $t$-tests made no assumption of equal variance between groups and were

assessed for statistical significance after controlling the false discovery rate at less

than 0.05 to correct for multiple comparisons (Genovese et al., 2002). These tests were

performed on both visit 1 and visit 2 data.

The potential for differential longitudinal change in interregional correlations between pre-HD and control groups was also investigated. Subject difference values were computed for each native-surface region, and two sample *t*-tests evaluated whether pre-HD subjects experienced a greater change from visit 1 to visit 2 than control subjects. Analogous vertex-wise two-sample *t*-tests were also performed on the longitudinal differences for subjects in the two groups.

Indicators of disease severity were also compared to interregional correlations. Langbehn and Aylward estimates of years to onset were tested for association with strength of functional correlations, as were FreeSurfer-based structural volume measures for the putamen and caudate (see below). The three regions most strongly correlated with each seed in the control group were included in these comparisons. Associations were evaluated by calculating the Pearson's correlation coefficient across subjects. We note that all the subjects studied here all had T1 scans, and we have reported on cross-section, between group (voxel based and whole-brain based) and longitudinal analyses (whole-brain based) of those data (Majid et al., 2011; Stoffers et al., 2010). Further analysis of T1 images also used FreeSurfer-based subcortical segmentation of caudate and putamen and also found significant cross-sectional and longitudinal group differences (Majid et al. under review).

## 4.3  Results

### 4.3.1  Participant characteristics

At visit 1, control and pre-HD groups were similar in age and MMSE scores ($p = 0.906$ and $p = 0.180$, respectively) (Table 4.1). For MMSE, ANOVA [group x visit]

revealed no between-group difference ($F < 1$), but did show a main effect of time

($F(1,56) = 6.872$, $p = 0.011$), with scores decreasing in both groups as time

progressed. There was no interaction ($F(1,54) = 1.112$, $p = 0.296$). UHDRS motor

scores were significantly elevated in pre-HD compared to controls ($t(54) = 3.664$, $p =$

.001), consistent with subtle motor signs that were insufficient to meet diagnostic

criteria for manifest HD. Follow-up UHDRS motor scores were significantly elevated

in the pre-HD group after the one-year duration, indicating a slightly worsening

condition ($t(33) = 3.123$, $p = 0.004$). Follow-up UHDRS motor scores were not

obtained in controls.

**Table 4.1:** Participant characteristics. Regions are ordered by strength of correlation with the seed region. Mean $z(r)$ and SE indicate the population mean $z$-transformed correlation coefficient and standard error, respectively. Sample size indicates the estimated sample size to detect a difference in mean $z(r)$ of 0.2 with 80% power and alpha value of 0.05.

| | Controls (N=22) | | Pre-HD (N=34) | |
|---|---|---|---|---|
| | Baseline | Follow-up | Baseline | Follow-up |
| Age at start (yrs, mean± SD) | 40.1 ± 12.2 | | 40.5 ± 10.4 | |
| Sex (F/M) | 15/7 | | 20/14 | |
| Between-scan interval (yrs, mean ± SD} | 1.0 ± 0.1 | | 1.1 ± 0.1 | |
| MMSE (mean ± SD) * | 28.8 ± 1.4 | 28.4 ± 1.7 | 29.2 ± 1.0 | 28.4 ± 1.6 |
| Number of CAG repeats (mean ± SD) [range] | N/A | | 42.4 ± 2.5 [38-48] | |
| Estimated years-to-onset, Aylward method (yrs, mean ± SD) | N/A | | 6.2 ± 7.4 | |
| Estimated years-to-onset, Langbehn method (yrs, mean ± SD) | N/A | | 14.3 ± 7.2 | |
| UHDRS motor score (mean ± SD) ** | 0.1 ± 0.3 | N/A | 1.5 ± 1.7 | 3.6 ± 4.4 |

SD = standard deviation; MMSE = mini-mental state exam; CAG = cytosine-adenine-guanine; UHDRS = Unified Huntington's Disease Rating Scale; Pre-HD = preclinical Huntington's disease; N/A = not applicable.
[a] ANOVA revealed main effect of time ($p = 0.011$) but no effect of group.
[b] Significantly different between groups at baseline ($p = 0.001$) and between timepoints in pre-HD group ($p = 0.004$). UHDRS was not obtained for controls at follow-up.

4.3.2   fMRI interregional correlation analysis

      Native-surface regions most consistently correlated with the isthmus cingulate

are shown in Table 4.2; among these are several areas frequently associated with the

default network (dorsolateral prefrontal, medial prefrontal, inferior parietal, and

medial temporal). This observation is common to both hemispheres, both visits, and

both populations. The putamen seed also yielded results that were replicated across

data sets (Table 4.3). Areas associated with motor function such as the caudate,

supplementary motor area, pre-supplementary motor area, and ventral pre-motor

cortex are among those most strongly correlated with the putamen seed. Group maps

are displayed in Figure 4.1 (isthmus cingulate seed) and Figure 4.2 (putamen seed).

Isthmus cingulate maps are thresholded from 0.18 to 0.32, corresponding to one to two

standard deviations above the group mean (across both hemispheres) for the control

group at visit 1. Putamen maps are thresholded from 0.09 to 0.16, using analogous

summary statistics. For qualitative comparison with the putamen maps, group maps

were also calculated with the caudate as seed (Figure 4.6 in Supplementary Materials).

**Table 4.2:** Native-surface correlation analysis with isthmus cingulate seed. Regions are ordered by strength of correlation with the seed region in visit 1. Mean $z(r)$ and SE indicate the population mean $z$-transformed correlation coefficient and standard error.

## CONTROL

### LEFT HEMISPHERE

| Region name | Visit 1 rank | Visit 1 mean $z(r)$ (SE) | Visit 2 rank | Visit 2 mean $z(r)$ (SE) |
|---|---|---|---|---|
| Medial Orbitofrontal | 1 | 0.52 (0.06) | 3 | 0.33 (0.05) |
| Rostral Anterior Cingulate | 2 | 0.46 (0.05) | 6 | 0.24* (0.05) |
| Frontal Pole | 3 | 0.43 (0.05) | 4 | 0.28 (0.06) |
| Inferior Parietal | 4 | 0.41 (0.06) | 1 | 0.43 (0.05) |
| Superior Frontal | 5 | 0.32 (0.04) | 7 | 0.21 (0.07) |
| Cuneus | 6 | 0.31 (0.06) | 2 | 0.36 (0.06) |
| Hippocampus | 7 | 0.30 (0.05) | 5 | 0.27 (0.07) |

### RIGHT HEMISPHERE

| Region name | Visit 1 rank | Visit 1 mean $z(r)$ (SE) | Visit 2 rank | Visit 2 mean $z(r)$ (SE) |
|---|---|---|---|---|
| Medial Orbitofrontal | 1 | 0.44 (0.06) | 3 | 0.32 (0.06) |
| Rostral Anterior Cingulate | 2 | 0.39 (0.06) | 9 | 0.18 (0.07) |
| Inferior Parietal | 3 | 0.37 (0.04) | 1 | 0.49 (0.05) |
| Cuneus | 4 | 0.37 (0.06) | 2 | 0.39 (0.06) |
| Superior Frontal | 5 | 0.31 (0.04) | 10 | 0.17 (0.06) |
| Frontal Pole | 6 | 0.30 (0.04) | 4 | 0.29 (0.06) |
| Parahippocampal | 7 | 0.29 (0.05) | 5 | 0.24 (0.05) |

## PRE-HD

### LEFT HEMISPHERE

| Region name | Visit 1 rank | Visit 1 mean $z(r)$ (SE) | Visit 2 rank | Visit 2 mean $z(r)$ (SE) |
|---|---|---|---|---|
| Medial Orbitofrontal | 1 | 0.43 (0.04) | 1 | 0.42 (0.04) |
| Inferior Parietal | 2 | 0.36 (0.05) | 2 | 0.31 (0.04) |
| Rostral Anterior Cingulate | 3 | 0.36 (0.04) | 4 | 0.22† (0.04) |
| Frontal Pole | 4 | 0.30 (0.05) | 3 | 0.31 (0.05) |
| Superior Frontal | 5 | 0.21 (0.04) | 5 | 0.22 (0.04) |
| Parahippocampal | 6 | 0.21 (0.04) | 7 | 0.18 (0.04) |
| Hippocampus | 7 | 0.20 (0.05) | 9 | 0.14 (0.04) |

### RIGHT HEMISPHERE

| Region name | Visit 1 rank | Visit 1 mean $z(r)$ (SE) | Visit 2 rank | Visit 2 mean $z(r)$ (SE) |
|---|---|---|---|---|
| Inferior Parietal | 1 | 0.39 (0.04) | 1 | 0.38 (0.04) |
| Medial Orbitofrontal | 2 | 0.38 (0.04) | 2 | 0.27 (0.04) |
| Rostral Anterior Cingulate | 3 | 0.30 (0.04) | 7 | 0.22 (0.04) |
| Superior Frontal | 4 | 0.29 (0.04) | 4 | 0.25 (0.04) |
| Caudal Middle Frontal | 5 | 0.24 (0.05) | 5 | 0.24 (0.03) |
| Parahippocampal | 6 | 0.22 (0.04) | 11 | 0.16 (0.04) |
| Hippocampus | 7 | 0.21 (0.04) | 9 | 0.19 (0.04) |

* significant (FDR < 0.05)
† trend (FDR < 0.10)

**Table 4.3:** Native-surface correlation analysis with putamen seed. Regions are ordered by strength of correlation with the seed region in visit 1. Mean $z(r)$ and SE indicate the population mean $z$-transformed correlation coefficient and standard error.

## CONTROL

### LEFT HEMISPHERE

| Region name | rank | Visit 1 mean $z(r)$ (SE) | rank | Visit 2 mean $z(r)$ (SE) |
|---|---|---|---|---|
| Caudate | 1 | 0.53 (0.06) | 1 | 0.54 (0.05) |
| Superior Frontal | 2 | 0.33 (0.03) | 5 | 0.23 (0.05) |
| Pars Triangularis | 3 | 0.29 (0.04) | 3 | 0.27 (0.04) |
| Pars Opercularis | 4 | 0.28 (0.05) | 2 | 0.30 (0.04) |
| Precentral | 5 | 0.23 (0.07) | 8 | 0.20 (0.05) |
| Amygdala | 6 | 0.19 (0.04) | 14 | 0.09 (0.06) |
| Caudal Anterior Cingulate | 7 | 0.19 (0.05) | 7 | 0.20 (0.05) |

### RIGHT HEMISPHERE

| Region name | rank | Visit 1 mean $z(r)$ (SE) | rank | Visit 2 mean $z(r)$ (SE) |
|---|---|---|---|---|
| Caudate | 1 | 0.44 (0.05) | 1 | 0.48 (0.05) |
| Pars Opercularis | 2 | 0.31 (0.05) | 2 | 0.32 (0.04) |
| Superior Frontal | 3 | 0.26 (0.05) | 7 | 0.17 (0.06) |
| Caudal Anterior Cingulate | 4 | 0.25 (0.06) | 3 | 0.32 (0.07) |
| Pars Triangularis | 5 | 0.24 (0.04) | 4 | 0.27 (0.05) |
| Posterior Cingulate | 6 | 0.22 (0.05) | 8 | 0.17 (0.05) |
| Precentral | 7 | 0.19 (0.08) | 10 | 0.13 (0.06) |

## PRE-HD

### LEFT HEMISPHERE

| Region name | rank | Visit 1 mean $z(r)$ (SE) | rank | Visit 2 mean $z(r)$ (SE) |
|---|---|---|---|---|
| Caudate | 1 | 0.48 (0.05) | 1 | 0.54 (0.04) |
| Pars Opercularis | 2 | 0.32 (0.04) | 3 | 0.25 (0.04) |
| Pars Triangularis | 3 | 0.23 (0.05) | 2 | 0.26 (0.03) |
| Superior Frontal | 4 | 0.22 (0.04) | 5 | 0.19 (0.04) |
| Caudal Anterior Cingulate | 5 | 0.19 (0.03) | 4 | 0.19 (0.04) |
| Amygdala | 6 | 0.15 (0.04) | 11 | 0.12 (0.04) |
| Rostral Middle Frontal | 7 | 0.15 (0.04) | 10 | 0.13 (0.04) |

### RIGHT HEMISPHERE

| Region name | rank | Visit 1 mean $z(r)$ (SE) | rank | Visit 2 mean $z(r)$ (SE) |
|---|---|---|---|---|
| Caudate | 1 | 0.44 (0.04) | 1 | 0.46 (0.05) |
| Pars Opercularis | 2 | 0.34 (0.04) | 3 | 0.23 (0.04) |
| Pars Triangularis | 3 | 0.27 (0.04) | 2 | 0.25 (0.03) |
| Caudal Anterior Cingulate | 4 | 0.22 (0.03) | 4 | 0.22 (0.04) |
| Posterior Cingulate | 5 | 0.20 (0.04) | 6 | 0.17 (0.04) |
| Superior Frontal | 6 | 0.16 (0.04) | 7 | 0.14 (0.05) |
| Rostral Middle Frontal | 7 | 0.14 (0.04) | 8 | 0.14 (0.04) |

**Figure 4.1:** Group correlation maps with isthmus cingulate seed. Fisher's *z*-transformed correlation coefficients for the correlation of each vertex on the surface with the average time series of the isthmus cingulate seed. The minimum and maximum thresholds for the functional overlay represent one and two standard deviations, respectively, above the mean coefficient from the first-visit group map for control subjects (i.e., Figure 4.1B). The top row (A) shows the Desikan-Killiany cortical parcellation atlas.
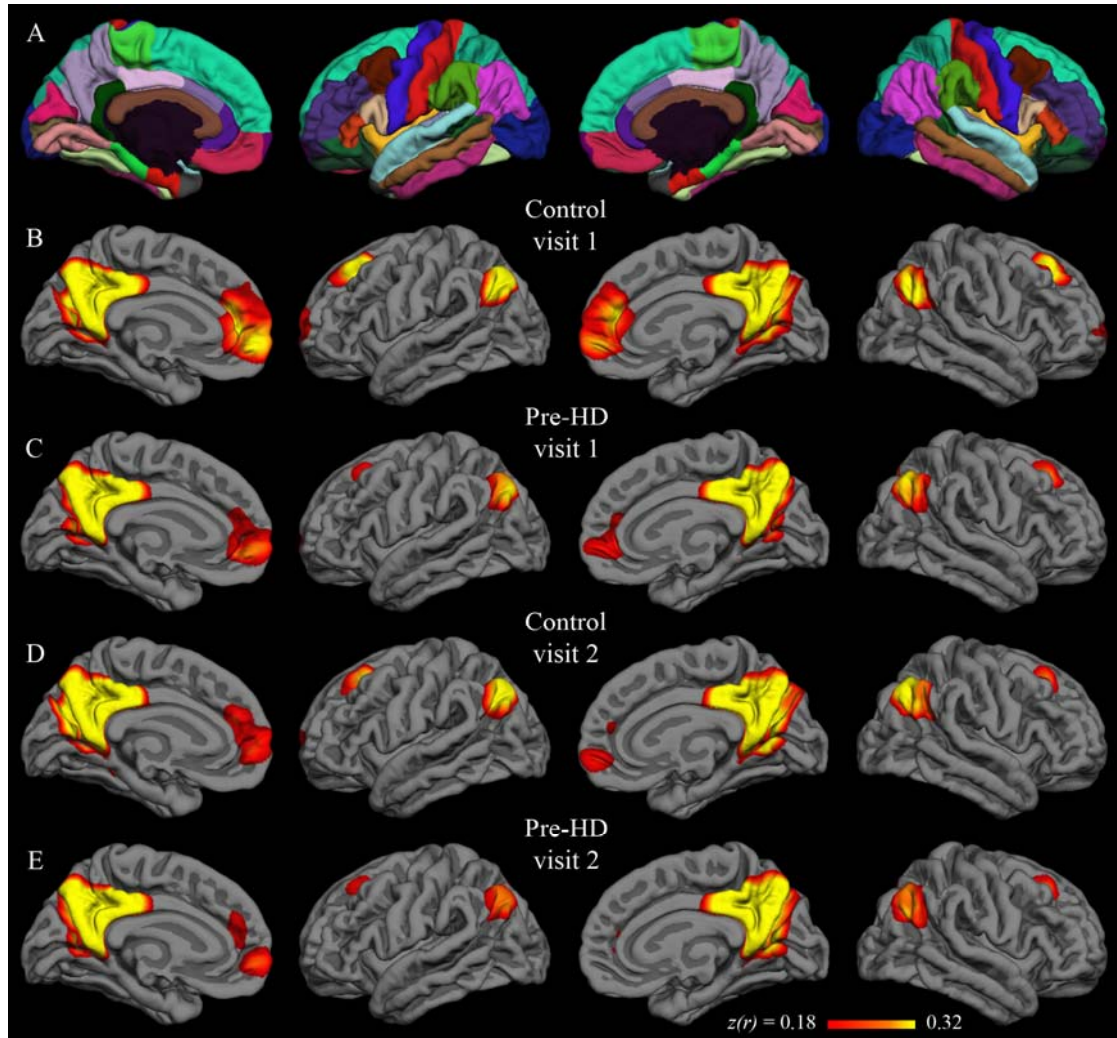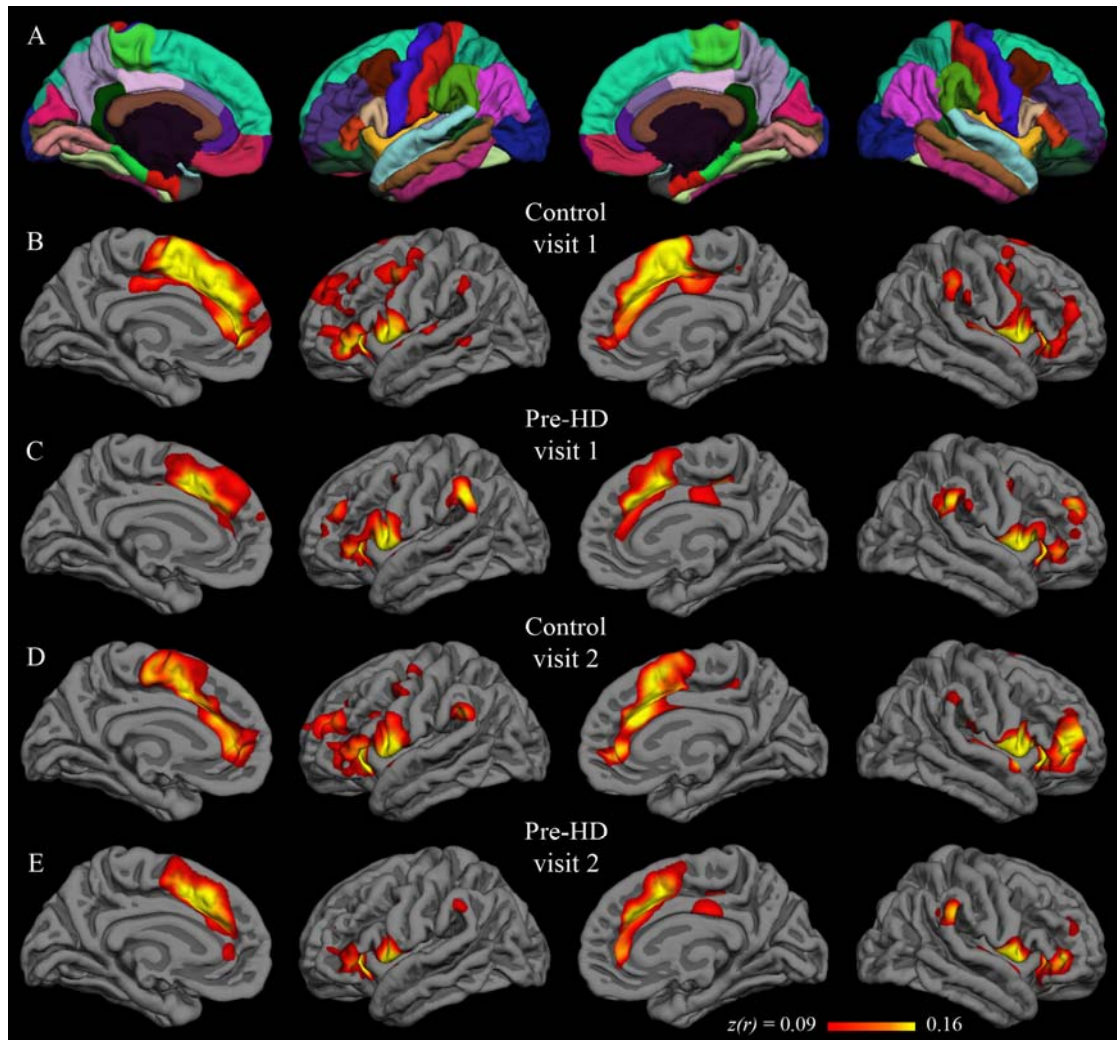
**Figure 4.2:** Group correlation maps with putamen seed. Fisher's *z*-transformed correlation coefficients for the correlation of each vertex on the surface with the average time series of the putamen seed. The minimum and maximum thresholds for the functional overlay represent one and two standard deviations, respectively, above the mean coefficient from the first-visit group map for control subjects (i.e., Figure 4.2B). The top row (A) shows the Desikan-Killiany cortical parcellation atlas.

### 4.3.3  Stability of fMRI interregional correlations

Qualitative similarity of group-level results between visit 1 and visit 2 are confirmed by quantitative comparison. In the control group, the correlation between visit 1 and visit 2 isthmus cingulate results (correlation coefficient across all native-

surface regions) was 0.93 in the left hemisphere and 0.90 in the right hemisphere. Pre-HD inter-visit correlations for the isthmus cingulate seed were also high, with coefficients of 0.96 in the left hemisphere and 0.94 in the right hemisphere. For the putamen seed, the control group visit 1 and visit 2 results had a correlation coefficient of 0.95 and 0.96 for the left and right hemispheres, respectively; the pre-HD group had values of 0.96 and 0.97 for the left and right hemispheres, respectively. Thus, group-level results for the native-surface parcellation regions were highly consistent for scans spaced a year apart.

Paired $t$-tests were applied to detect significant differences from visit 1 to visit 2. In the control group, with the isthmus cingulate seed, only the left rostral anterior cingulate region was significantly different after controlling for false discovery rate. The left rostral anterior cingulate had a group-mean $z$-transformed correlation coefficient of 0.46 at visit 1 and 0.24 at visit 2 ($t(21) = 4.11$; uncorrected $p < 0.001$). This rostral anterior cingulate finding was not replicated in the pre-HD group, though there was a trend in the same direction (0.36 at visit 1; 0.22 at visit 2; $t(33) = 2.75$; uncorrected $p < 0.01$). No region was significantly different from visit 1 to visit 2 in the pre-HD group for isthmus cingulate correlations. Likewise, no region showed a significant inter-visit difference in either group with the putamen seed. Vertex-wise paired $t$-test maps in Figure 4.3 (isthmus cingulate) and Figure 4.4 (putamen) also show very few significant inter-visit differences.

Power analyses were performed for each region to estimate the sample size necessary for 80% power to detect a difference of 0.2 in the group mean correlation coefficient when alpha is set at 0.05. With the isthmus cingulate seed, the median

calculated sample size (and interquartile range) across all regions was 21 (17-28) subjects for the control group and 25 (20-29) subjects for the pre-HD group. With the putamen seed, the median sample size was 21 (15-28) subjects for the control group and 22 (18-27) subjects for the pre-HD group. These estimates are comparable to the actual sample sizes of the present study.

While the correlation between visit 1 and visit 2 results was quite high at the group level, inter-visit correlation across native-surface regions was considerably lower for individual subjects. For control subjects, the median correlation coefficient between visit 1 and visit 2 with the isthmus cingulate seed was 0.59, with an interquartile range of 0.39-0.69. For pre-HD subjects, the median with the isthmus cingulate seed was 0.45, with an interquartile range of 0.21-0.59. With the putamen seed, the median (and interquartile range) for controls was 0.38 (0.17-0.60), and for pre-HD subjects was 0.51 (0.27-0.63).

Intraclass correlation coefficient analysis also suggested notable within-subjects variance from visit 1 to visit 2. ICC values for the regions from Tables 4.2 and 4.3 are shown in Tables 4.4 and 4.5, along with associated $p$-values. The greatest ICC with either seed was found in the right medial orbitofrontal region in the control group (ICC = 0.66, $p < 0.001$). ICC values significantly greater than zero ($p < 0.05$, uncorrected) with the isthmus cingulate seed were also found in the following regions in the control group: left cuneus, right rostral anterior cingulate, right frontal pole, and right superior frontal. In the pre-HD group, regions with ICC values significantly greater than zero with the isthmus cingulate seed included the left frontal pole, right medial orbitofrontal, and right inferior parietal. With the putamen seed, significant

ICC values for the control group were found in right superior frontal and right caudal anterior cingulate regions. In the pre-HD group, the putamen seed gave significant ICC values in the left amygdala, right caudate, and right precentral regions. An ICC value greater than 0.5 indicates that between-subjects variance is greater than within-subjects variance. With the isthmus putamen seed, only the right medial orbitofrontal region had an ICC of at least 0.50 in both control and pre-HD groups. With the putamen seed, no region had an ICC of at least 0.50 in either group.

**Figure 4.3:** Group *t*-test maps with isthmus cingulate seed. Functional overlays show *t*-values for each vertex for the relevant comparison. The threshold for each row was set independently to indicate *t*-values corresponding to a false discovery rate less than 0.05 (minimum) and 0.01 (maximum). A-B: Hot colors indicate significantly greater correlation in visit 2; cool colors indicate significantly greater correlation in visit 1. C-D: Hot colors indicate greater correlation in the pre-HD group than in the control group; cool colors indicate greater correlation in the control group. Thresholds are as follows (min, max): (A) *t* = 3.6, 4.3; (B) *t* = 3.4, 4.0; (C-D) *t* = 3.3, 3.9.
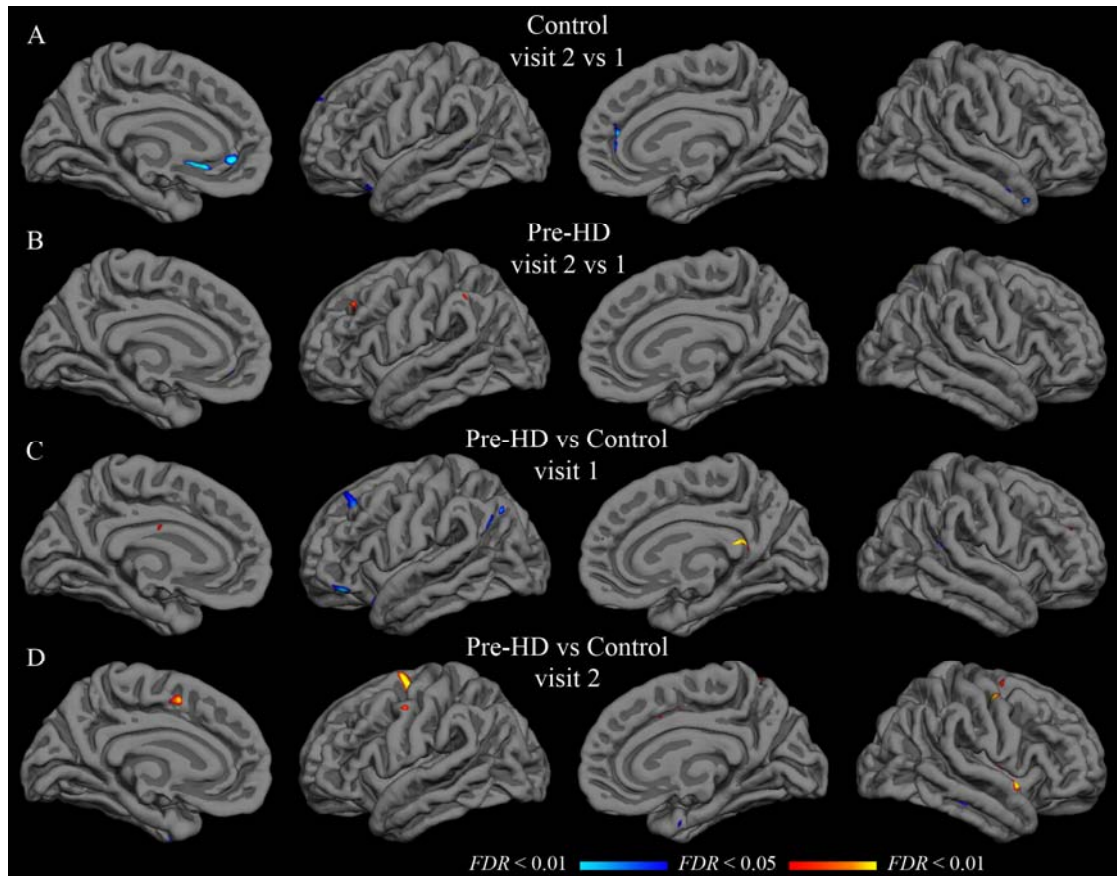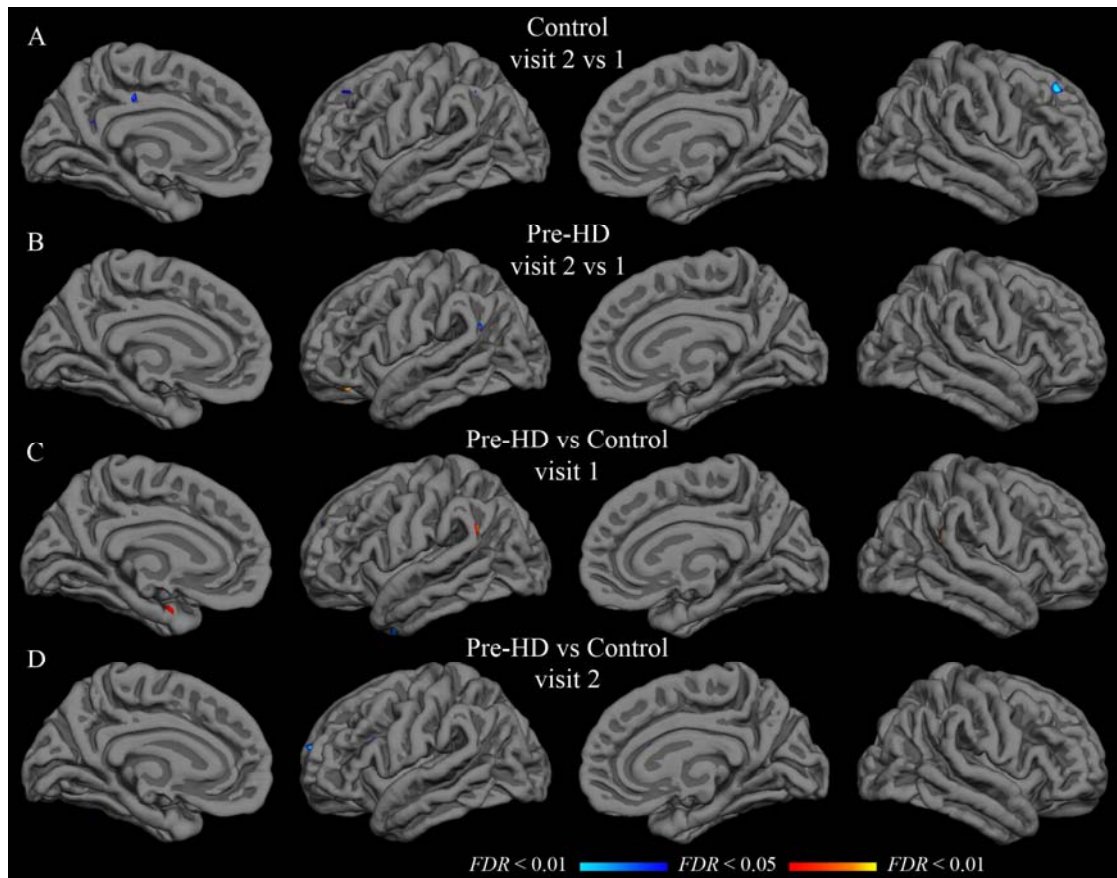
**Figure 4.4:** Group *t*-test maps with putamen seed. Functional overlays show *t*-values for each vertex for the relevant comparison. The threshold for each row was set independently to indicate *t*-values corresponding to a false discovery rate less than 0.05 (minimum) and 0.01 (maximum). A-B: Hot colors indicate significantly greater correlation in visit 2; cool colors indicate significantly greater correlation in visit 1. C-D: Hot colors indicate greater correlation in the pre-HD group than in the control group; cool colors indicate greater correlation in the control group. Thresholds are as follows (min, max): (A) *t* = 3.6, 4.3; (B) *t* = 3.4, 4.0; (C-D) *t* = 3.3, 3.9.

**Table 4.4:** Intraclass correlation coefficients with isthmus cingulate seed. For easy comparison, regions are ordered according to the strength of correlation in the left hemisphere of the control group (see Table 4.2) for the other sub-tables. Intraclass correlation coefficients were calculated from visit 1 and visit 2 data from all subjects within each group. Significance is indicated by associated $p$-values (null hypothesis: ICC = 0).

| CONTROL | | | | | |
|---|---|---|---|---|---|
| **LEFT HEMISPHERE** | | | **RIGHT HEMISPHERE** | | |
| Region name | ICC | $p$ | Region name | ICC | $p$ |
| Medial Orbitofrontal | 0.25 | 0.28 | Medial Orbitofrontal | 0.66 | < 0.001 |
| Rostral Anterior Cingulate | 0.36 | 0.10 | Rostral Anterior Cingulate | 0.50 | 0.02 |
| Frontal Pole | 0.32 | 0.16 | Frontal Pole | 0.45 | 0.03 |
| Inferior Parietal | 0.12 | 0.61 | Inferior Parietal | 0.28 | 0.22 |
| Superior Frontal | 0.27 | 0.24 | Superior Frontal | 0.52 | 0.01 |
| Cuneus | 0.43 | 0.04 | Cuneus | 0.01 | 0.89 |
| Hippocampus | 0.24 | 0.29 | Hippocampus | 0.19 | 0.42 |

| PRE-HD | | | | | |
|---|---|---|---|---|---|
| **LEFT HEMISPHERE** | | | **RIGHT HEMISPHERE** | | |
| Region name | ICC | $p$ | Region name | ICC | $p$ |
| Medial Orbitofrontal | 0.17 | 0.49 | Medial Orbitofrontal | 0.50 | < 0.01 |
| Rostral Anterior Cingulate | 0.26 | 0.21 | Rostral Anterior Cingulate | 0.27 | 0.18 |
| Frontal Pole | 0.52 | < 0.01 | Frontal Pole | 0.35 | 0.07 |
| Inferior Parietal | 0.23 | 0.28 | Inferior Parietal | 0.37 | 0.04 |
| Superior Frontal | 0.01 | > 0.99 | Superior Frontal | 0.12 | 0.70 |
| Cuneus | 0.23 | 0.30 | Cuneus | 0.26 | 0.20 |
| Hippocampus | 0.07 | 0.91 | Hippocampus | 0.12 | 0.72 |

**Table 4.5:** Intraclass correlation coefficients with putamen seed. For easy comparison, regions are ordered according to the strength of correlation in the left hemisphere of the control group (see Table 4.3) for the other sub-tables. Intraclass correlation coefficients were calculated from visit 1 and visit 2 data from all subjects within each group. Significance is indicated by associated $p$-values (null hypothesis: ICC = 0).

| CONTROL | | | | | |
|---|---|---|---|---|---|
| **LEFT HEMISPHERE** | | | **RIGHT HEMISPHERE** | | |
| Region name | ICC | $p$ | Region name | ICC | $p$ |
| Caudate | 0.11 | 0.63 | Caudate | 0.30 | 0.18 |
| Superior Frontal | 0.00 | 0.90 | Superior Frontal | 0.47 | 0.02 |
| Pars Triangularis | < 0.01 | 0.90 | Pars Triangularis | 0.16 | 0.49 |
| Pars Opercularis | < 0.01 | 0.90 | Pars Opercularis | 0.01 | 0.88 |
| Precentral | 0.10 | 0.67 | Precentral | 0.30 | 0.18 |
| Amygdala | 0.04 | 0.83 | Amygdala | 0.20 | 0.40 |
| Caudal Anterior Cingulate | 0.23 | 0.32 | Caudal Anterior Cingulate | 0.52 | 0.01 |

| PRE-HD | | | | | |
|---|---|---|---|---|---|
| **LEFT HEMISPHERE** | | | **RIGHT HEMISPHERE** | | |
| Region name | ICC | $p$ | Region name | ICC | $p$ |
| Caudate | 0.32 | 0.10 | Caudate | 0.49 | < 0.01 |
| Superior Frontal | < 0.01 | > 0.99 | Superior Frontal | < 0.01 | > 0.99 |
| Pars Triangularis | 0.20 | 0.37 | Pars Triangularis | 0.16 | 0.55 |
| Pars Opercularis | 0.01 | > 0.99 | Pars Opercularis | < 0.01 | > 0.99 |
| Precentral | 0.28 | 0.16 | Precentral | 0.42 | 0.02 |
| Amygdala | 0.38 | 0.04 | Amygdala | 0.15 | 0.59 |
| Caudal Anterior Cingulate | 0.22 | 0.33 | Caudal Anterior Cingulate | 0.25 | 0.23 |

### 4.3.4 Effect of pre-HD on interregional correlations

Population mean correlations with the isthmus cingulate seed for pre-HD and control groups did not differ significantly in any of the native-surface regions in either hemisphere at visit 1 (two-sample *t*-tests, FDR controlled at less than 0.05). This remained true approximately one year later at visit 2. Likewise, no statistically significant difference was found for correlation with the putamen seed in any of the parcellation regions at either visit. Vertex-wise *t*-tests on the group surface also yielded only sparse spots showing significant effects of pre-HD with either seed (Figures 4.3 and 4.4).

Though the change from visit 1 to visit 2 was unimpressive at the group level for either population, the size of the longitudinal change in pre-HD might still differ from controls in some region(s). However, two-sample *t*-tests comparing the visit 2 - visit 1 difference in pre-HD subjects to that of control subjects did not yield any native-surface parcellation regions with a statistically significant effect. This was true with both the isthmus cingulate and putamen seeds. Vertex-wise *t*-tests on the group surface were consistent with the native-surface region results (Figure 4.5 in Supplementary Materials).

Comparison of interregional correlations with indicators of disease severity in the pre-HD group did not reveal any associations for the isthmus cingulate seed correlations (results not shown), but potential associations were identified for the putamen seed correlations (Table 4.6). Subjects with weaker putamen-caudate functional correlation at visit 1 were also closer to disease onset using the Langbehn

method. This was true in each hemisphere. Similarly, subjects with weaker putamen-caudate functional correlation at visit 1 also had smaller caudate and putamen volumes (Table 4.6). These findings were less consistent at visit 2, though trends in the same direction remained.

**Table 4.6:** Association of putamen functional correlations with disease severity. Regions most strongly correlated with the putamen seed in the control group are included in the table. YTO: years to onset; r: Pearson's correlation coefficient.

| | Putamen–Region Correlation *vs.* Years to Onset | | | | | | | |
| | Visit 1 | | | | Visit 2 | | | |
| | Langbehn YTO | | Aylward YTO | | Langbehn YTO | | Aylward YTO | |
| Region name | r | p | r | p | r | p | r | p |
| --- | --- | --- | --- | --- | --- | --- | --- | --- |
| Left Caudate | 0.54** | <0.01 | 0.16 | 0.37 | 0.30† | 0.08 | 0.28 | 0.11 |
| Left Pars Opercularis | 0.07 | 0.71 | -0.08 | 0.67 | 0.06 | 0.72 | -0.13 | 0.46 |
| Left Superior Frontal | -0.17 | 0.35 | -0.34† | 0.05 | -0.09 | 0.62 | 0.03 | 0.87 |
| Right Caudate | 0.41* | 0.02 | 0.17 | 0.34 | 0.24 | 0.17 | 0.32† | 0.07 |
| Right Pars Opercularis | 0.21 | 0.24 | -0.06 | 0.76 | 0.09 | 0.62 | -0.01 | 0.96 |
| Right Superior Frontal | 0.04 | 0.81 | -0.23 | 0.19 | 0.15 | 0.40 | 0.09 | 0.62 |

| | Putamen–Region Correlation *vs.* Striatal Volume | | | | | | | |
| | Visit 1 | | | | Visit 2 | | | |
| | Caudate Volume | | Putamen Volume | | Caudate Volume | | Putamen Volume | |
| Region name | r | p | r | p | r | p | r | p |
| --- | --- | --- | --- | --- | --- | --- | --- | --- |
| Left Caudate | 0.36** | <0.01 | 0.31* | 0.02 | 0.37* | 0.03 | 0.29† | 0.09 |
| Left Pars Opercularis | -0.09 | 0.50 | -0.05 | 0.71 | -0.08 | 0.67 | -0.13 | 0.47 |
| Left Superior Frontal | <0.01 | 0.99 | 0.09 | 0.50 | -0.10 | 0.56 | -0.13 | 0.47 |
| Right Caudate | 0.27* | 0.04 | 0.23† | 0.09 | 0.24 | 0.18 | 0.22 | 0.22 |
| Right Pars Opercularis | -0.02 | 0.89 | 0.03 | 0.85 | 0.11 | 0.55 | 0.05 | 0.77 |
| Right Superior Frontal | 0.06 | 0.65 | 0.16 | 0.25 | -0.08 | 0.68 | -0.03 | 0.86 |

** $p < 0.01$
* $p < 0.05$
† $p < 0.10$

**4.4  Discussion**

In assessing the potential of resting correlations as a biomarker, the primary objectives of the present study were to evaluate the long-term stability of measures obtained in native space and to apply the technique to the premanifest HD population. Group correlation results obtained using the native-surface method highlighted corticostriatal and default patterns that were stable over one year in both the control and pre-HD populations. On the other hand, results from visit 1 and visit 2 were less stable at the individual-subject level. No significant group-level differences were demonstrated between the pre-HD and control groups, but weakening of resting correlation between the caudate and putamen in the pre-HD group may be related to disease severity as estimated by subcortical volumes or estimated years to symptom onset.

4.4.1   Isthmus cingulate and putamen seeds yield expected networks

Regions with strongest correlation with the isthmus and putamen seeds were consistent with previously published group-level resting fMRI results. Specifically, the isthmus cingulate seed highlighted default network areas such as dorsolateral prefrontal, medial prefrontal, inferior parietal, and medial temporal cortex bilaterally in both the control group and the pre-HD group (Table 4.2, Figure 4.1). The putamen seed, on the other hand, was most strongly correlated with motor-related areas (Table 4.3, Figure 4.2) in both populations. Distinguishable patterns with these two seeds converges with prior studies demonstrating dissociable "networks" of brain regions at rest (Beckmann et al., 2005; Seeley et al., 2009; Vincent et al., 2007) and, along with

supplementary analyses using the caudate seed, are further evidence that seeds defined by automated parcellation on the native surface yield meaningful and reproducible results. Consistent with known structural connectivity (Alexander et al., 1986; Lawrence et al., 1998; Leh et al., 2007), the caudate maps differ from those using the putamen seed, highlighting dorsolateral prefrontal and anterior cingulate cortex, whereas the putamen maps highlight ventrolateral prefrontal cortex and supplementary motor area (Figure 4.6 in Supplementary Materials). Also of note, the magnitudes of the isthmus cingulate correlations are generally greater than that of the putamen (or caudate) correlations. While this confirms multiple previous findings that the default network is particularly active at rest (Buckner et al., 2008; Greicius et al., 2003; Raichle et al., 2001), it also suggests a resting condition may not be optimal for studies specifically focused on corticostriatal networks. Resting correlations in this study did, however, highlight both corticostriatal and default networks in four data sets (two populations at two time points).

### 4.4.2   Resting interregional correlations stable over one year at group level

Group-level results with both putamen and isthmus cingulate seeds were longitudinally stable, yielding similar patterns in scans collected a year apart. Qualitatively similar group maps (Figures 4.1 and 4.2) and native-surface results (Tables 4.2 and 4.3) are corroborated by strong inter-visit correlations at the group level (greater than 0.9 in each hemisphere in all four data sets). Additionally, only a single region, in a single group, showed a statistical difference between visit 1 and visit 2. The congruency of group results from data collected a year apart is

encouraging for application of this technique to longitudinal studies such as clinical trials. That this relatively high long-term stability held in both control and pre-HD populations is also encouraging, as it suggests population differences could also be consistently measured over a year-long study.

Subject-level results were considerably less stable than group-level results from visit 1 to visit 2. Inter-visit correlations at the subject level had medians of 0.59 and 0.45 for the isthmus cingulate seed (left and right hemispheres), and 0.38 and 0.51 for the putamen seed. While there is still reasonable inter-visit agreement for many subjects (approximately 25% of subjects in each group had inter-visit correlations greater than 0.60), the within-subjects variance is approximately as great, or greater, than the between-subjects variance in nearly every case. In other words, for a given single region, on average, measurements taken from the same individual a year apart were at least as different as measurements taken from two different individuals from within the same group.

Strong group-level stability with high within-subjects variance is suggestive of a noisy marker that can be reliable at the group level because of improved signal-to-noise ratio with averaging. The sources of this noise may be varied. Technical imaging issues may contribute, including fluctuations in scanner properties, thermal noise, physiological noise (e.g., due to changes in respiration), and static field distortions. Additionally, different scan sessions might have involved different levels of anxiety, alertness, mood, fatigue, or mental activities. It is also unknown to what extent the physiological phenomenon underlying interregional BOLD correlations is stable in the absence of all measurement noise. The strength of these resting BOLD correlations

may naturally fluctuate over time; in fact, coherence analysis has provided evidence for such fluctuation even within a single scan (Chang and Glover, 2010). Despite the apparently high noise, the stable group results indicate that efforts to minimize measurement noise and account for biological variation might improve the reproducibility of resting fMRI results in individual subjects.

### 4.4.3 Resting interregional correlations only modestly affected in premanifest stage

Premanifest Huntington's disease did not greatly disrupt interregional BOLD correlations in the present study. Functional correlations for the pre-HD group were compared to age-matched controls with two different seeds and at two different time points. The lack of difference in fMRI correlations was found despite reliable genetic diagnosis and measured structural differences on MRI in the same subjects (Majid et al., 2011). It is possible there is an underlying effect of pre-HD, but the present results suggest it would be relatively small. Power analyses estimate the present sample sizes are sufficient for fairly high power to detect an effect size of 0.2 in most regions, a conservative value selected to detect an effect even in studies including healthy subjects at high-risk of other neurodegenerative diseases (Fleisher et al., 2009; Hedden et al., 2009; Koch et al., 2010). Power in the present study to detect a population difference was even higher because the initial comparison was repeated in a second set of measurements (visit 2). If there are subtle effects of pre-HD on interregional BOLD correlations, these might be detected with improved signal to noise or larger sample sizes. However, in light of the present results, other potential biomarkers might be

more sensitive to premanifest Huntington's pathology than resting fMRI correlations (Aylward et al., 1996; Majid et al., 2011; Tabrizi et al., 2011).

The paucity of significant differences in resting correlations between pre-HD and control groups may be unsurprising given that cognition is relatively intact and motor symptoms have not yet manifested at this early stage of the disease. While structural changes in these subjects' brains suggest disease progression, these changes may still be insufficient to overcome subjects' functional reserve. As gene-positive individuals begin to experience cognitive impairment, resting BOLD correlations may also become disrupted. Indeed, the within-group associations with disease severity shown in Table 4.6 suggest that disease progression might affect functional correlations between the caudate and putamen, even in the premanifest stage.

Efforts could be made in future studies to attempt to address limitations suggested in the present study. The most important limitation is probably the signal-to-noise ratio of the resting BOLD correlations. As intimated above, improvements in scanner reliability and technical aspects of functional imaging might lead to increases in signal to noise. Additionally, physiological noise arising from fluctuations in heart rate or respiration might be somewhat better controlled if these metrics were measured and their effects modeled (Glover et al., 2000). Rigorous investigation might also be directed toward achieving an optimal scanning environment to produce more homogeneity in the "resting" condition of the subjects; this could include instructions regarding the mental activities subjects should engage in or avoid, the illumination of the room, subject comfort in the scanner, whether visual fixation is encouraged, and many other considerations. Correlation measures have been shown to be fairly

consistent with four-minute resting scans (Van Dijk et al., 2009), and the six-minute scans used here are within the typical range for resting fMRI; however, increased scan duration might still improve signal-to-noise ratio and possibly improve individual-subject reliability.

## 4.5 Acknowledgements

Chapter 4, in full, has been submitted for publication of the material as it may appear in NeuroImage. Seibert, Tyler M.; Majid, Dewan-Syed A.; Aron, Adam R.; Corey-Bloom, Jody; Brewer, James B., Elsevier, Inc. The dissertation author was the primary investigator and author of this paper.
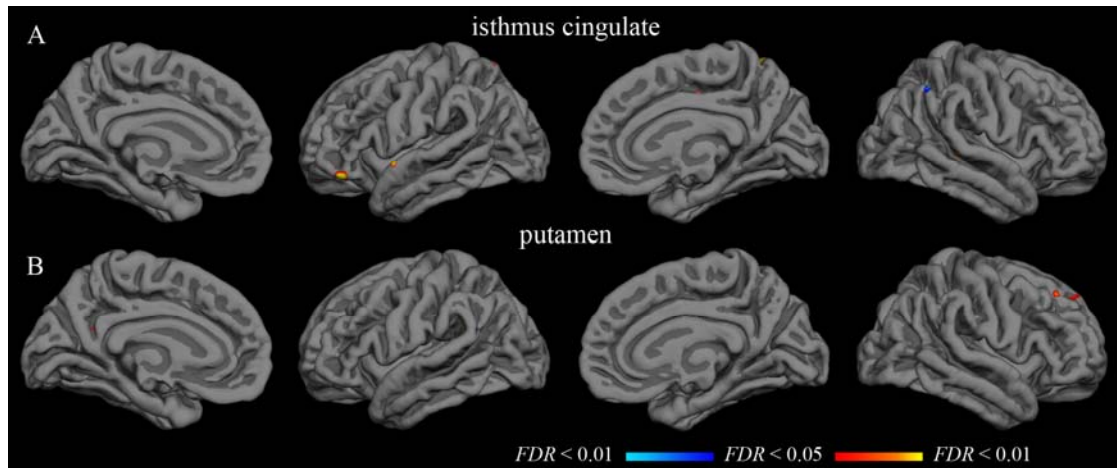
## 4.6 Supplementary Materials



**Figure 4.5:** Supplementary Figure – Longitudinal group *t*-test maps. Functional overlays show *t*-values for each vertex for the relevant comparison. The thresholds were set to indicate *t*-values corresponding to a false discovery rate less than 0.05 (minimum) and 0.01 (maximum). A-B: Hot colors indicate significantly greater longitudinal change in pre-HD subjects than in control subjects; cool colors indicate greater longitudinal change in control subjects. Thresholds are (min, max): $t = 3.3, 3.9$.
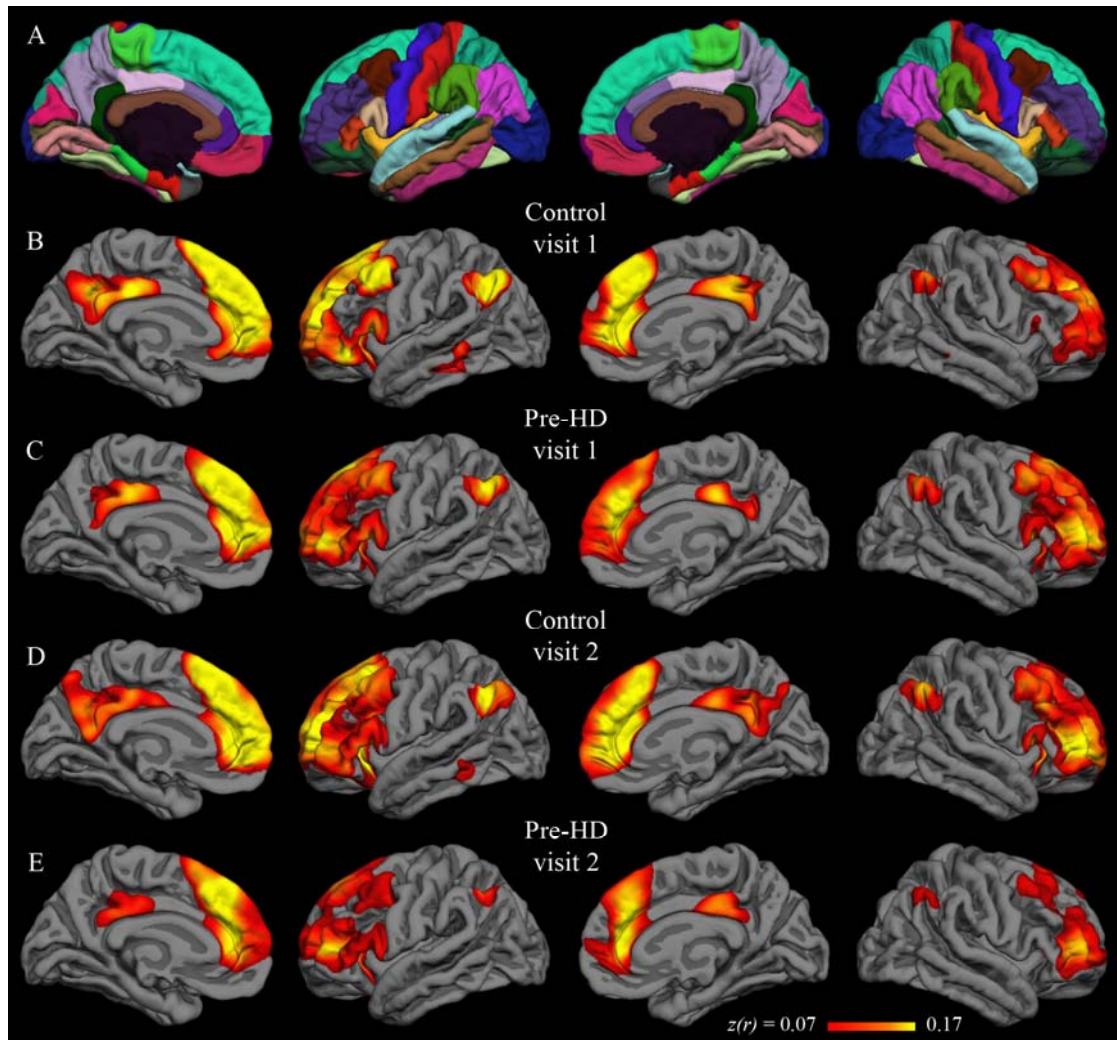
**Figure 4.6:** Supplementary Figure – Group correlation maps with caudate seed. Fisher's *z*-transformed correlation coefficients for the correlation of each vertex on the surface with the average time series of the caudate seed. The minimum and maximum thresholds for the functional overlay represent one and two standard deviations, respectively, above the mean coefficient from the first-visit group map for control subjects (i.e., Figure 4.2B). The top row (A) shows the Desikan-Killiany cortical parcellation atlas.

## 4.7 References

Alexander, GE, DeLong, MR, Strick, PL (1986): Parallel organization of functionally segregated circuits linking basal ganglia and cortex. Annu. Rev. Neurosci, 9, 357-381.

Auer, DP (2008): Spontaneous low-frequency blood oxygenation level-dependent fluctuations and functional connectivity analysis of the "resting" brain. Magn Reson Imaging, 26(7), 1055-1064.

Aylward, EH, Sparks, BF, Field, KM, Yallapragada, V, Shpritz, BD, Rosenblatt, A, et al. (2004): Onset and rate of striatal atrophy in preclinical Huntington disease. Neurology, 63(1), 66-72.

Aylward, EH, Codori, AM, Barta, PE, Pearlson, GD, Harris, GJ, Brandt, J (1996): Basal ganglia volume and proximity to onset in presymptomatic Huntington disease. Arch. Neurol, 53(12), 1293-1296.

Aylward, EH, Nopoulos, PC, Ross, CA, Langbehn, DR, Pierson, RK, Mills, JA, et al. (2011): Longitudinal change in regional brain volumes in prodromal Huntington disease. J. Neurol. Neurosurg. Psychiatr, 82(4), 405-410.

Bai, F, Watson, DR, Yu, H, Shi, Y, Yuan, Y, Zhang, Z (2009): Abnormal resting-state functional connectivity of posterior cingulate cortex in amnestic type mild cognitive impairment. Brain Res, 1302, 167-174.

Beckmann, CF, DeLuca, M, Devlin, JT, Smith, SM (2005): Investigations into resting-state connectivity using independent component analysis. Philos. Trans. R. Soc. Lond., B, Biol. Sci, 360(1457), 1001-1013.

Bohanna, I, Georgiou-Karistianis, N, Hannan, AJ, Egan, GF (2008): Magnetic resonance imaging as an approach towards identifying neuropathological biomarkers for Huntington's disease. Brain Res Rev, 58(1), 209-225.

Buckner, RL, Andrews-Hanna, JR, Schacter, DL (2008): The Brain's Default Network: Anatomy, Function, and Relevance to Disease. Annals of the New York Academy of Sciences, 1124(1), 1-38.

Chang, C, Glover, GH (2010): Time-frequency dynamics of resting-state brain connectivity measured with fMRI. Neuroimage, 50(1), 81-98.

Chen, S, Ross, TJ, Zhan, W, Myers, CS, Chuang, K-S, Heishman, SJ, Stein, EA, Yang, Y (2008): Group independent component analysis reveals consistent resting-state networks across multiple sessions. Brain Res, 1239, 141-151.

Cohen, J (1988): Statistical power analysis for the behavioral sciences (Second.). Psychology Press.

Cox, RW, Jesmanowicz, A (1999): Real-time 3D image registration for functional MRI. Magn Reson Med, 42(6), 1014-1018.

Dale, AM, Fischl, B, Sereno, MI (1999): Cortical surface-based analysis. I. Segmentation and surface reconstruction. Neuroimage, 9(2), 179-194.

Damoiseaux, JS, Rombouts, SARB, Barkhof, F, Scheltens, P, Stam, CJ, Smith, SM, Beckmann, CF (2006): Consistent resting-state networks across healthy subjects. Proc. Natl. Acad. Sci. U.S.A, 103(37), 13848-13853.

Dawson, B, Trapp, RG (2004): Basic & clinical biostatistics (Fourth.). Lange Medical Books/McGraw-Hill.

Desikan, RS, Ségonne, F, Fischl, B, Quinn, BT, Dickerson, BC, Blacker, D, et al. (2006): An automated labeling system for subdividing the human cerebral cortex on MRI scans into gyral based regions of interest. Neuroimage, 31(3), 968-980.

Eidelberg, D, Surmeier, DJ (2011): Brain networks in Huntington disease. J. Clin. Invest, 121(2), 484-492.

Fischl, B, van der Kouwe, A, Destrieux, C, Halgren, E, Segonne, F, Salat, DH, et al. (2004): Automatically Parcellating the Human Cerebral Cortex. Cereb. Cortex, 14(1), 11-22.

Fischl, B, Salat, DH, Busa, E, Albert, M, Dieterich, M, Haselgrove, C, et al. (2002): Whole brain segmentation: automated labeling of neuroanatomical structures in the human brain. Neuron, 33(3), 341-355.

Fischl, B, Sereno, MI, Dale, AM (1999a): Cortical surface-based analysis. II: Inflation, flattening, and a surface-based coordinate system. Neuroimage, 9(2), 195-207.

Fischl, B, Sereno, MI, Tootell, RB, Dale, AM (1999b): High-resolution intersubject averaging and a coordinate system for the cortical surface. Hum Brain Mapp, 8(4), 272-284.

Fleisher, AS, Sherzai, A, Taylor, C, Langbaum, JBS, Chen, K, Buxton, RB (2009): Resting-state BOLD networks versus task-associated functional MRI for distinguishing Alzheimer's disease risk groups. Neuroimage, 47(4), 1678-1690.

Folstein, MF, Folstein, SE, McHugh, PR (1975): "Mini-mental state". A practical method for grading the cognitive state of patients for the clinician. J Psychiatr Res, 12(3), 189-198.

Fox, MD, Raichle, ME (2007): Spontaneous fluctuations in brain activity observed with functional magnetic resonance imaging. Nat Rev Neurosci, 8(9), 700-11.

Genovese, CR, Lazar, NA, Nichols, T (2002): Thresholding of Statistical Maps in Functional Neuroimaging Using the False Discovery Rate. NeuroImage, 15(4), 870-878.

Glover, GH, Li, TQ, Ress, D (2000): Image-based method for retrospective correction of physiological motion effects in fMRI: RETROICOR. Magn Reson Med, 44(1), 162-167.

Greicius, MD, Krasnow, B, Reiss, AL, Menon, V (2003): Functional connectivity in the resting brain: a network analysis of the default mode hypothesis. Proc. Natl. Acad. Sci. U.S.A, 100(1), 253-258.

Greicius, MD (2008): Resting-state functional connectivity in neuropsychiatric disorders. Curr. Opin. Neurol, 21(4), 424-430.

Greicius, MD, Srivastava, G, Reiss, AL, Menon, V (2004): Default-mode network activity distinguishes Alzheimer's disease from healthy aging: evidence from functional MRI. Proc. Natl. Acad. Sci. U.S.A, 101(13), 4637-4642.

Harris, GJ, Pearlson, GD, Peyser, CE, Aylward, EH, Roberts, J, Barta, PE, Chase, GA, Folstein, SE (1992): Putamen volume reduction on magnetic resonance imaging exceeds caudate changes in mild Huntington's disease. Ann. Neurol, 31(1), 69-75.

Hedden, T, Van Dijk, KRA, Becker, JA, Mehta, A, Sperling, RA, Johnson, KA, Buckner, RL (2009): Disruption of functional connectivity in clinically normal older adults harboring amyloid burden. J. Neurosci, 29(40), 12686-12694.

Helmich, RC, Derikx, LC, Bakker, M, Scheeringa, R, Bloem, BR, Toni, I (2010): Spatial remapping of cortico-striatal connectivity in Parkinson's disease. Cereb. Cortex, 20(5), 1175-1186.

van den Heuvel, MP, Hulshoff Pol, HE (2010): Exploring the brain network: A review on resting-state fMRI functional connectivity. European Neuropsychopharmacology, 20(8), 519-534.

Huntington Study Group (1996): Unified Huntington's Disease Rating Scale: reliability and consistency. Huntington Study Group. Mov. Disord, 11(2), 136-142.

Jafri, MJ, Pearlson, GD, Stevens, M, Calhoun, VD (2008): A method for functional network connectivity among spatially independent resting-state components in schizophrenia. Neuroimage, 39(4), 1666-1681.

Klöppel, S, Henley, SM, Hobbs, NZ, Wolf, RC, Kassubek, J, Tabrizi, SJ, Frackowiak, RSJ (2009): Magnetic resonance imaging of Huntington's disease: preparing for clinical trials. Neuroscience, 164(1), 205-219.

Koch, W, Teipel, S, Mueller, S, Benninghoff, J, Wagner, M, Bokde, ALW, et al. (2010): Diagnostic power of default mode network resting state fMRI in the detection of Alzheimer's disease. Neurobiol Aging.

Langbehn, DR, Brinkman, RR, Falush, D, Paulsen, JS, Hayden, MR (2004): A new model for prediction of the age of onset and penetrance for Huntington's disease based on CAG length. Clin. Genet, 65(4), 267-277.

Lawrence, AD, Sahakian, BJ, Robbins, TW (1998): Cognitive functions and corticostriatal circuits: insights from Huntington's disease. Trends Cogn. Sci. (Regul. Ed.), 2(10), 379-388.

Leh, SE, Ptito, A, Chakravarty, MM, Strafella, AP (2007): Fronto-striatal connections in the human brain: a probabilistic diffusion tractography study. Neurosci. Lett, 419(2), 113-118.

Majid, DSA, Stoffers, D, Sheldon, S, Hamza, S, Thompson, WK, Goldstein, J, Corey-Bloom, J, Aron, AR (2011): Automated structural imaging analysis detects premanifest Huntington's disease neurodegeneration within 1 year. Mov Disord.

Meindl, T, Teipel, S, Elmouden, R, Mueller, S, Koch, W, Dietrich, O, Coates, U, Reiser, M, Glaser, C (2010): Test-retest reproducibility of the default-mode network in healthy individuals. Hum Brain Mapp, 31(2), 237-246.

Mohammadi, B, Kollewe, K, Samii, A, Beckmann, CF, Dengler, R, Münte, TF (2011a): Changes in resting-state brain networks in writer's cramp. Hum Brain Mapp.

Mohammadi, B, Kollewe, K, Samii, A, Dengler, R, Münte, TF (2011b): Functional neuroimaging at different disease stages reveals distinct phases of neuroplastic changes in amyotrophic lateral sclerosis. Hum Brain Mapp, 32(5), 750-758.

Paulsen, JS, Nopoulos, PC, Aylward, E, Ross, CA, Johnson, H, Magnotta, VA, et al. (2010): Striatal and white matter predictors of estimated diagnosis for Huntington disease. Brain Res. Bull, 82(3-4), 201-207.

Paulsen, JS, Zimbelman, JL, Hinton, SC, Langbehn, DR, Leveroni, CL, Benjamin, ML, Reynolds, NC, Rao, SM (2004): fMRI biomarker of early neuronal dysfunction in presymptomatic Huntington's Disease. AJNR Am J Neuroradiol, 25(10), 1715-1721.

Pihlajamäki, M, Jauhiainen, AM, Soininen, H (2009): Structural and functional MRI in mild cognitive impairment. Curr Alzheimer Res, 6(2), 179-185.

Raichle, ME, MacLeod, AM, Snyder, AZ, Powers, WJ, Gusnard, DA, Shulman, GL (2001): A default mode of brain function. Proc. Natl. Acad. Sci. U.S.A, 98(2), 676-682.

Reading, SAJ, Dziorny, AC, Peroutka, LA, Schreiber, M, Gourley, LM, Yallapragada, V, et al. (2004): Functional brain changes in presymptomatic Huntington's disease. Ann. Neurol, 55(6), 879-883.

Repovs, G, Csernansky, JG, Barch, DM (2011): Brain network connectivity in individuals with schizophrenia and their siblings. Biol. Psychiatry, 69(10), 967-973.

Rogers, BP, Morgan, VL, Newton, AT, Gore, JC (2007): Assessing functional connectivity in the human brain by fMRI. Magn Reson Imaging, 25(10), 1347-1357.

Rosas, HD, Feigin, AS, Hersch, SM (2004): Using advances in neuroimaging to detect, understand, and monitor disease progression in Huntington's disease. NeuroRx, 1(2), 263-272.

Rosas, HD, Salat, DH, Lee, SY, Zaleta, AK, Hevelone, N, Hersch, SM (2008): Complexity and heterogeneity: what drives the ever-changing brain in Huntington's disease? Ann. N. Y. Acad. Sci, 1147, 196-205.

Seeley, WW, Crawford, RK, Zhou, J, Miller, BL, Greicius, MD (2009): Neurodegenerative diseases target large-scale human brain networks. Neuron, 62(1), 42-52.

Seibert, TM, Brewer, JB (2011): Default network correlations analyzed on native surfaces. J Neurosci Methods.

Shehzad, Z, Kelly, AMC, Reiss, PT, Gee, DG, Gotimer, K, Uddin, LQ, et al. (2009): The resting brain: unconstrained yet reliable. Cereb. Cortex, 19(10), 2209-2229.

Sheline, YI, Raichle, ME, Snyder, AZ, Morris, JC, Head, D, Wang, S, Mintun, MA (2010): Amyloid Plaques Disrupt Resting State Default Mode Network Connectivity in Cognitively Normal Elderly. Biological Psychiatry, 67(6), 584-587.

Shrout, PE, Fleiss, JL (1979): Intraclass correlations: uses in assessing rater reliability. Psychol Bull, 86(2), 420-428.

Smith, SM, Jenkinson, M, Woolrich, MW, Beckmann, CF, Behrens, TEJ, Johansen-Berg, H, et al. (2004): Advances in functional and structural MR image analysis and implementation as FSL. Neuroimage, 23 Suppl 1, S208-219.

Sorg, C, Riedl, V, Mühlau, M, Calhoun, VD, Eichele, T, Läer, L, et al. (2007): Selective changes of resting-state networks in individuals at risk for Alzheimer's disease. Proc. Natl. Acad. Sci. U.S.A, 104(47), 18760-18765.

Sorg, C, Valentin, R, Robert, P, Alexander, K, Afra, WM (2009): Impact of Alzheimer's Disease on the Functional Connectivity of Spontaneous Brain Activity. Curr Alzheimer Res. Retrieved September 21, 2009, from http://www.ncbi.nlm.nih.gov/pubmed/19747154.

Stoffers, D, Sheldon, S, Kuperman, JM, Goldstein, J, Corey-Bloom, J, Aron, AR (2010): Contrasting gray and white matter changes in preclinical Huntington disease: an MRI study. Neurology, 74(15), 1208-1216.

Tabrizi, SJ, Langbehn, DR, Leavitt, BR, Roos, RA, Durr, A, Craufurd, D, et al. (2009): Biological and clinical manifestations of Huntington's disease in the longitudinal TRACK-HD study: cross-sectional analysis of baseline data. Lancet Neurol, 8(9), 791-801.

Tabrizi, SJ, Scahill, RI, Durr, A, Roos, RA, Leavitt, BR, Jones, R, et al. (2011): Biological and clinical changes in premanifest and early stage Huntington's disease in the TRACK-HD study: the 12-month longitudinal analysis. Lancet Neurol, 10(1), 31-42.

Thomason, ME, Dennis, EL, Joshi, AA, Joshi, SH, Dinov, ID, Chang, C, et al. (2011): Resting-state fMRI can reliably map neural networks in children. Neuroimage, 55(1), 165-175.

Van Dijk, KRA, Hedden, T, Venkataraman, A, Evans, KC, Lazar, SW, Buckner, RL (2009): Intrinsic Functional Connectivity As a Tool For Human Connectomics: Theory, Properties, and Optimization. J. Neurophysiol.

Vincent, JL, Patel, GH, Fox, MD, Snyder, AZ, Baker, JT, Van Essen, DC, et al. (2007): Intrinsic functional architecture in the anaesthetized monkey brain. Nature, 447(7140), 83-86.

Wolf, RC, Sambataro, F, Vasic, N, Schönfeldt-Lecuona, C, Ecker, D, Landwehrmeyer, B (2008): Altered frontostriatal coupling in pre-manifest Huntington's disease: effects of increasing cognitive load. Eur. J. Neurol, 15(11), 1180-1190.

Wu, T, Wang, L, Chen, Y, Zhao, C, Li, K, Chan, P (2009): Changes of functional connectivity of the motor network in the resting state in Parkinson's disease. Neurosci. Lett, 460(1), 6-10.

Zimbelman, JL, Paulsen, JS, Mikos, A, Reynolds, NC, Hoffmann, RG, Rao, SM (2007): fMRI detection of early neural dysfunction in preclinical Huntington's disease. J Int Neuropsychol Soc, 13(5), 758-769.

Zuo, X-N, Kelly, C, Adelstein, JS, Klein, DF, Castellanos, FX, Milham, MP (2010): Reliable intrinsic connectivity networks: test-retest evaluation using ICA and dual regression approach. Neuroimage, 49(3), 2163-2177.

CHAPTER 5

**Resting fMRI interregional correlations in Parkinson's disease and Parkinson-related dementia**

**Abstract**

Parkinson-related dementia (PRD) is the second leading cause of dementia in the United States, but the varied clinical presentation and lack of definitive, non-invasive tests contribute to frequent misdiagnosis, presenting challenges for clinicians and investigators. A functional imaging biomarker could improve diagnosis, facilitate scientific inquiry, and provide a tool for evaluation of potential therapies in clinical trials. Resting interregional fMRI correlations have already shown potential in Alzheimer's and other diseases. Here we use a method of calculating such correlations in the native space of individual subjects to compare resting correlation patterns in PRD, cognitively unimpaired Parkinson's disease, and in age-matched elderly controls. Two seeds are used: a medial parietal region that contributes to the default network affected in Alzheimer's disease, and the caudate, which is affected by loss of dopaminergic inputs in Parkinson's disease. Only moderate effects of PRD were found in the default network, but PRD was associated with significantly decreased corticostriatal correlations.

## 5.1 Introduction

Parkinson-related dementia (PRD) is the second most common cause of neurodegenerative dementia in the United States, estimated to make up 15-35% of all demented patients (Geser et al., 2005). Patients with PRD may experience the motor symptoms of parkinsonism as well as cognitive impairment that is frequently confused with Alzheimer's disease (Geser et al., 2005; Lippa et al., 2007; McKeith, 2007). Subtypes of PRD include Parkinson's disease dementia (PDD) and dementia with Lewy bodies (DLB), but these share a common hallmark neuropathology finding (α-synuclein deposits called Lewy bodies) and are primarily distinguished in clinics by the order of symptom onset (Galvin et al., 2006; Geser et al., 2005; Lippa et al., 2007; McKeith, 2007). A non-invasive imaging biomarker is needed to advance basic scientific investigation of this disease *in vivo*, as well as to aid in diagnosis and evaluation of potential treatments in clinical trials.

Interregional correlations of the resting blood oxygenation level dependent (BOLD) fMRI signal constitute one area of active interest in the search for biomarkers in disease. Functional imaging biomarkers are particularly attractive in that they may be able to detect pathology prior to widespread atrophy and could reflect therapeutic effects on a shorter time scale than structural techniques. Resting fMRI has a strong clinical appeal because it affords the ability to study multiple networks of the entire brain at once and, relative to task-based fMRI, is less susceptible to confounding effects of cognitive ability to perform a given behavioral task (Auer, 2008; Fox and Raichle, 2007; Greicius, 2008; van den Heuvel and Hulshoff Pol, 2010; Rogers et al., 2007). Variations in resting functional correlations (often termed "functional

connectivity") have already been reported in several neurological disorders, including

Alzheimer's disease (Greicius et al., 2004; Sorg et al., 2009), mild cognitive

impairment (Bai et al., 2009; Pihlajamäki et al., 2009; Sorg et al., 2007), and

Parkinson's disease (Helmich et al., 2010; Wu et al., 2009). Early reports have even

suggested resting functional correlations may be sensitive to neurological changes

prior to onset of clinical symptoms in neurodegenerative disease (Hedden et al., 2009;

Sheline et al., 2010).

One important challenge for resting fMRI studies in neurodegenerative

conditions such as PRD is the potential confound of registration errors in subjects with

atrophy. Nearly all available reports on resting interregional fMRI correlations in

disease, including all those that have included PD (Helmich et al., 2010, 2011; Wu et

al., 2009) or PRD (Galvin et al., 2011), have used methods that depend on

transformation of functional data to a standard volume atlas (e.g., Talaraich or

MNI152) based on healthy brains. Even small inaccuracies in the warping of

individual brains to the standard volume could result in areas of cerebrospinal fluid or

white matter being mistakenly labeled as gray matter in the standard space. We have

recently shown that such errors can be quite common; that they are easily overlooked;

and that they can have large, widespread effects on resting fMRI correlations. To

account for this problem, we proposed a method of group-level analysis of resting

fMRI correlations measured within the native space of individual subjects (Seibert and

Brewer, 2011).

The present study applies the native-space (or native-surface) method to

resting fMRI data acquired in patients with PRD, cognitively unimpaired PD, and age-

matched controls. The network of regions with activity correlated with an isthmus cingulate seed (the "default network") was examined, as prior studies have suggested disease-related effects on their correlated activity in Alzheimer's disease (Greicius et al., 2004; Sorg et al., 2009) and DLB (Galvin et al., 2011). In addition, the corticostriatal network identified by a caudate nucleus seed was examined, as basal ganglia involvement in parkinsonism is well known, and disruption of corticostriatal resting fMRI correlations have also been described in PD (Helmich et al., 2010; Wu et al., 2009)..For each seed, we identified the five regions that had the strongest resting correlation in independent data sets from healthy, younger adults, and we then limited regional analysis to these "within-network" *a priori* regions of interest to avoid excessive multiple comparisons. We hypothesized that Parkinson-related dementia would be associated with altered interregional BOLD correlations within both default-network and corticostriatal regions.

## 5.2  Methods

### 5.2.1  Participant characteristics

Participant characteristics are provided in Table 5.1. Fifty-six participants underwent resting-state scans for this study (19 PD, 18 PRD, 19 age-matched controls). Consent was provided in accordance with an Institutional Review Board at the University of California, San Diego.  Movement disorder specialists from the University of California faculty evaluated the PD and PRD participants and made diagnoses based on criteria established by the Movement Disorders Society Task Force (Geser et al., 2005; McKeith, 2007); participants meeting criteria for DLB or

PDD were included in the PRD group. Elderly controls and PD patients with no

cognitive impairment had a mini-mental status exam (MMSE) score of at least 27

(Folstein et al., 1975).

**Table 5.1:** Participant characteristics

| Participant group | n (females) | Age (mean ± SD) | MMSE (mean ± SD) |
|---|---|---|---|
| Elderly control | 19 (11) | 76 ± 9 | * |
| Parkinson's disease | 19 (7) | 70 ± 8 | * |
| Parkinson-related dementia | 18 (2) | 72 ± 7 | 23.8 ± 4.9 |

\* All participants MMSE ≥ 27

5.2.2   MRI acquisition

Structural and functional imaging procedures were described previously

(Seibert and Brewer, 2011). Two $T_2$*-weighted sequences of approximately 7 min

each were acquired for each participant on a 1.5 T system (General Electric

Healthcare, Waukesha, WI) (TE: 45 ms; TR: 2624 ms; flip angle: 90°; matrix: 64 x

64; voxel size: 3.75 mm x 3.75 mm x 5 mm; 32 adjacent sagittal slices; 155 samples

per series). Immediately prior to each functional series, a spin-echo volume was

acquired with opposite phase-encoding polarity for field inhomogeneity (Holland et

al., 2010). Participants were asked to rest motionless with eyes open during the

functional sequences (Van Dijk et al., 2009; Yan et al., 2009). In addition to the

functional volumes, a high-resolution, three-dimensional, $T_1$-weighted volume was

acquired for each subject (TE: 3.8 ms; TR: 8.5 ms; TI: 500 ms; flip angle: 10°; matrix:

256 x 256 x 256; voxel size: 0.9375 mm x 0.9375 mm x 1.2000 mm). Respiratory

effort and heart rate were monitored and recorded with a pressure transducer and a pulse oximeter, respectively (BioPac Systems Inc., Goleta, CA).

### 5.2.3   Structural MRI processing

A model of each subject's cortical surface was reconstructed from the $T_1$-weighted MRI volume (Dale et al., 1999; Fischl et al., 1999a). The surface was then anatomically parcellated using the Desikan-Killiany atlas (Desikan et al., 2006; Fischl et al., 2004). Subcortical structures were similarly identified by volume segmentation (Fischl et al., 2002). Results from each of these automated steps were inspected for accuracy, and manual corrections were applied as necessary according to procedures described previously, ensuring accurate native surfaces and identification of tissue boundaries (Seibert and Brewer, 2011). Parcellation regions used in functional analysis were tested for group differences in cortical thickness (or subcortical volume, after adjusting for intracranial volume) with ANOVA.

### 5.2.4   fMRI data pre-analysis processing

All fMRI pre-analysis processing was performed as described previously (Seibert and Brewer, 2011) and was primarily performed using custom software written in MATLAB (Mathworks, Natick, MA). After interpolation for slice acquisition timing, rigid-body volume registration was performed using AFNI (Cox and Jesmanowicz, 1999), followed by voxel-wise regression of six head motion parameters and a cubic polynomial baseline. Functional data were next projected onto

the subject's cortical surface model, and a bandpass filter of 0.01-0.08 Hz was applied

to the time series from each vertex on the surface.

### 5.2.5   fMRI interregional correlation analysis

Procedures for fMRI correlation analysis on native surfaces are described in

detail elsewhere (Seibert and Brewer, 2011); these procedures take advantage of the

FreeSurfer surface generation and parcellation tools and avoid transforming functional

data to an atlas volume. Briefly, a single region from the automated parcellation of

each individual surface is used as the seed time series for each hemisphere. The

functional time series from the seed region is then correlated with the average time

series from other cortical surface parcellation and volume segmentation regions in the

Desikan-Killiany atlas. Fisher's $z$-transform was applied to these native-surface

correlation coefficients.

Vertex-wise correlation analysis (surface equivalent of voxel-wise analysis)

was also performed after spherical-based surface registration to the FreeSurfer

fsaverage surface (Fischl et al., 1999b; Seibert and Brewer, 2011). The minimum and

maximum thresholds were set based on the group map for control subjects; the

minimum threshold was one half standard deviation above the map mean, and the

maximum threshold was 1.5 standard deviations above the map mean. To account for

possible variation in functional anatomy, individual maps were subjected to a surface-

based smoothing process (approximately equivalent to a 6 mm Gaussian kernel in two

dimensions) prior to performing vertex-wise group statistics. All group summary maps

were similarly smoothed for display. Tissue mislabeling can frequently arise during

transformation to a volume atlas such as Talairach or MNI152, introducing large effects on functional correlations; surface-based registration reduces these errors (Fischl et al., 1999a, 1999b; Seibert and Brewer, 2011).

Analyses were performed with two seed regions. The isthmus cingulate region has been shown to be a reliable seed for study of the default network (Seibert and Brewer, 2011). As midbrain dopaminergic projections affected by Parkinson's pathology directly modulate the striatum, the caudate was also chosen as a seed to investigate corticostriatal correlations. Each of these regions has been evaluated as a seed in other data sets using healthy adults (Seibert and Brewer 2011; Seibert et al., submitted). To avoid unnecessary multiple comparisons, the five regions most strongly correlated with each seed in those independent data sets were selected *a priori* for regional analyses (Table 5.2). Vertex-wise analyses were performed for the entire cortical surface.

Subjects with PD and PRD were compared to elderly controls to test for potential population differences attributable to Parkinson-related pathology. Two-sample *t*-tests were applied to data from each native-surface parcellation region of interest, and results were assessed for statistical significance after controlling the false discovery rate at less than 0.05 to correct for multiple comparisons (Genovese et al., 2002). Vertex-wise comparisons were also made, using two-sample *t*-tests at each vertex on the group surface. Group vertex-wise *t*-test maps were smoothed (approximately equivalent to a 12 mm Gaussian kernel in two dimensions) for display. All *t*-test results made no assumption of equal variance between groups.

**5.3  Results**

Regions selected *a priori* for group comparison were also tested for a structural effect of disease state. Cortical thickness for surface regions and subcortical volumes (adjusted for intracranial volume) for basal ganglia structures were compared by ANOVA. After controlling FDR at 0.05 (or 0.10), only the right parahippocampal region was significantly different across groups ($F(2,52) = 7.905$).

Despite the relatively advanced age of the elderly control participants (mean age was over 76 years) resting correlation results for this group were generally consistent with previous reports in college-aged and middle-aged adults (Seibert and Brewer, 2011). Isthmus cingulate maps (Figure 1B) show characteristic features of the default network, including prominent involvement of medial and inferior lateral parietal areas, as well as medial and lateral prefrontal cotex. Caudate maps differ from isthmus cingulate maps—particularly in that the caudate is strongly correlated with areas such as the supplementary motor area, pre-supplementary motor area, and middle frontal gyrus (Figure 2B), in agreement with known structural connectivity (Alexander et al., 1986; Lawrence et al., 1998; Leh et al., 2007). Table 2 (first column in each hemisphere) lists the *z*-transformed correlation coefficients for the elderly control group; regions in the table were selected *a priori* for their strong correlation with the respective seeds in independent data sets. Many of these *a priori* regions remain strongly correlated with their respective seeds in the present cohort of resting elderly controls, further demonstrating the overall qualitative consistency of these data with published resting fMRI data.

Potential effects of Parkinson pathology on the strength of interregional correlations within the default network were investigated by comparing group-level results from elderly controls to PD and PRD groups. The upper section of Table 2 reports correlation coefficients for *a priori* default-network regions and the isthmus cingulate seed. While there are some regions where a pattern of decreased correlation strength with PRD is suggested (especially bilateral superior frontal, left medial orbitofrontal, and right hippocampus), no default region significantly differs between PRD and elderly controls, or between PD and controls, after correcting for multiple comparisons. Indeed, no region showed a significant difference even when relaxing the FDR correction to only 0.10 (i.e., to look for trends). Group maps in Figure 1B-D also show some hint at diminished prefrontal (medial and lateral) involvement with PD and PRD relative to controls, but the maps for the three groups are still qualitatively very similar. No area of the cortex was significantly different between groups after correcting for multiple comparisons in vertex-wise tests. For illustration of possible trends, however, Figure 3A shows population differences at a very liberal threshold without correction for multiple comparisons ($p < 0.01$, uncorrected). While there were some suggestions of small group differences in both region-based and vertex-wise results, in the end there was not a single *a priori* default-network region or cortical vertex with a significant difference between disease and control groups when the isthmus cingulate was used as a seed.

Corticostriatal resting correlations were also examined for differences across Parkinson-related disease state. Contrary to the isthmus cingulate results, the lower section of Table 2 shows that several regions were significantly different in the PRD

group relative to elderly controls. These included bilateral superior frontal, bilateral caudal middle frontal, and right putamen (left putamen showed a trend toward significance, identified when FDR was relaxed to 0.052 instead of 0.05). No *a priori* region was significantly different in the PD group relative to either the elderly control or PRD groups. This pattern is illustrated in Figure 2, where there is a qualitative decrease in both magnitude and extent of corticostriatal correlations in the PRD maps relative to the control maps, with PD showing an intermediate level of correlations. However, these vertex-wise results do not reach statistical significance after a standard correction for multiple comparisons, and Figure 3B again shows areas where PRD and control groups differ when thresholds uncorrected for multiple comparisons are presented. While these vertex-wise corticostriatal differences do not survive correction for multiple comparisons, they are more widespread than in the analogous default-network differences, and they overlap well with the regions that were significantly different in the native-surface parcellation analysis.
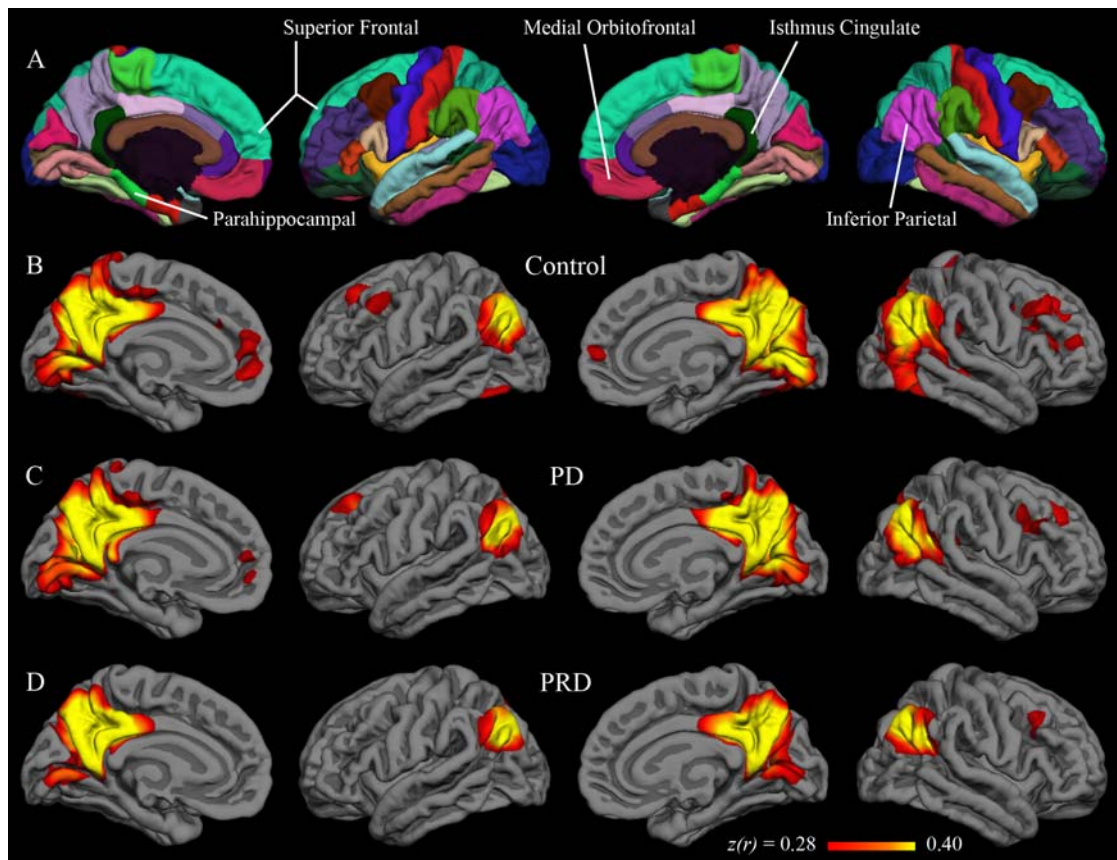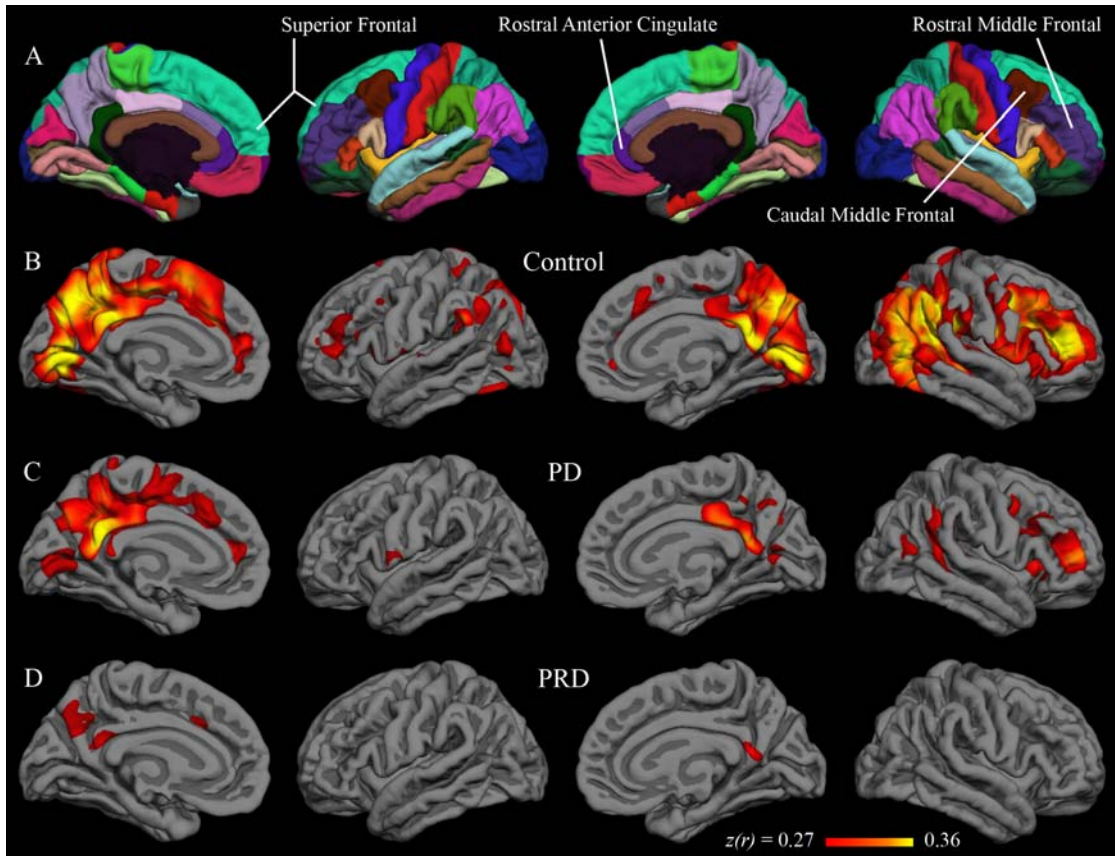
**Figure 5.1:** Group correlation maps with isthmus cingulate seed. Fisher's *z*-transformed correlation coefficients for the correlation of each vertex on the surface with the average time series of the isthmus cingulate seed. The minimum and maximum thresholds for the functional overlay represent 0.5 and 1.5 standard deviations, respectively, above the mean coefficient from the group map for control subjects (i.e., Figure 5.1B). The top row (A) shows the Desikan-Killiany cortical parcellation atlas.

**Figure 5.2:** Group correlation maps with caudate seed. Fisher's *z*-transformed correlation coefficients for the correlation of each vertex on the surface with the average time series of the caudate seed. The minimum and maximum thresholds for the functional overlay represent 0.5 and 1.5 standard deviations, respectively, above the mean coefficient from the group map for control subjects (i.e., Figure 5.2B). The top row (A) shows the Desikan-Killiany cortical parcellation atlas.

**Table 5.2:** Native-surface correlation analysis for default-network (isthmus cingulate seed) and corticostriatal correlations (caudate seed). Regions were selected *a priori* based on strength of correlation with the respective seed in independent data sets. Mean $z(r)$ and SE indicate the population mean $z$-transformed correlation coefficient and standard error.

### ISTHMUS CINGULATE

| | LEFT HEMISPHERE | | | RIGHT HEMISPHERE | | |
|---|---|---|---|---|---|---|
| | Control | PD | PRD | Control | PD | PRD |
| Region name | mean $z(r)$ (SE) | mean $z(r)$ (SE) | mean $z(r)$ (SE) | mean $z(r)$ (SE) | mean $z(r)$ (SE) | mean $z(r)$ (SE) |
| Superior Frontal | 0.90 (0.07) | 0.83 (0.07) | 0.70 (0.07) | 0.91 (0.06) | 0.77 (0.07) | 0.71 (0.06) |
| Inferior Parietal | 0.94 (0.07) | 0.90 (0.07) | 0.87 (0.06) | 0.90 (0.06) | 0.88 (0.06) | 0.82 (0.06) |
| Medial Orbitofrontal | 0.63 (0.06) | 0.62 (0.06) | 0.42 (0.06) | 0.55 (0.06) | 0.53 (0.07) | 0.42 (0.06) |
| Hippocampus | 0.65 (0.07) | 0.68 (0.09) | 0.58 (0.05) | 0.63 (0.05) | 0.58 (0.06) | 0.48 (0.05) |
| Parahippocampal | 0.50 (0.07) | 0.62 (0.09) | 0.56 (0.06) | 0.62 (0.05) | 0.51 (0.06) | 0.50 (0.05) |

### CAUDATE

| | LEFT HEMISPHERE | | | RIGHT HEMISPHERE | | |
|---|---|---|---|---|---|---|
| | Control | PD | PRD | Control | PD | PRD |
| Region name | mean $z(r)$ (SE) | mean $z(r)$ (SE) | mean $z(r)$ (SE) | mean $z(r)$ (SE) | mean $z(r)$ (SE) | mean $z(r)$ (SE) |
| Putamen | 0.83 (0.06) | 0.78 (0.07) | 0.63[†] (0.07) | 0.98 (0.08) | 0.83 (0.06) | 0.68* (0.07) |
| Superior Frontal | 0.98 (0.05) | 0.83 (0.08) | 0.69* (0.08) | 0.86 (0.07) | 0.70 (0.08) | 0.65* (0.06) |
| Caudal Middle Frontal | 0.70 (0.06) | 0.58 (0.07) | 0.47* (0.07) | 0.81 (0.06) | 0.61 (0.07) | 0.48* (0.07) |
| Rostral Anterior Cingulate | 0.46 (0.06) | 0.52 (0.07) | 0.52 (0.07) | 0.28 (0.06) | 0.35 (0.06) | 0.34 (0.07) |
| Rostral Middle Frontal | 0.81 (0.06) | 0.72 (0.08) | 0.66 (0.08) | 0.87 (0.05) | 0.69 (0.07) | 0.57* (0.07) |

\* significant (FDR < 0.05)

[†] trend (FDR = 0.052)

**5.4 Discussion**

When measurements were made in the native space of individual subjects, Parkinson-related dementia was associated with disruption of corticostriatal resting fMRI correlations relative to elderly controls. In default-network regions, interregional correlations also tended to be decreased in PRD relative to controls, but these effects were weak and did not reach significance after correcting for multiple comparisons. These results suggest that, as has been reported for fronto-temporal dementia and Alzheimer's disease (Seeley et al., 2009), disruption of resting fMRI correlations in PRD may differentially affect different resting networks.

While this is the first study to examine resting corticostriatal BOLD correlations in PRD, a very recent publication (Galvin et al., 2011) reported differences between DLB and controls in the default network. The suggestion in our data of decreased correlation between a medial parietal seed and prefrontal and medial temporal regions (Table 5.2) is consistent with their results, and the differences in both studies were found only when no correction was made for multiple comparisons.

Because (Galvin et al., 2011) is the only other comparison so far of resting interregional BOLD correlations in PRD, some consideration of methodological differences is appropriate. One primary difference is the previous study compared regions that were defined from group differences in same functional data, whereas we used anatomical regions that were defined *a priori* from independent data sets acquired in young, healthy adults. Additionally, our regions were defined from the native structural images of each subject, thus avoiding effects on the functional correlations that can be introduced during the warping of individual brains to a

common volume template (Seibert and Brewer, 2011). Participant selection also differed between the two studies; Galvin et al. included only the DLB subtype of PRD, and were able to exclude from their control group (but not the DLB group) individuals with a high amyloid burden. Similar numbers of PRD participants were included in the two studies (18 in the present study compared to 15 DLB in the previous study), but the Galvin et al. included a larger control group (38 compared to 19). Here we modeled and removed effects of respiratory fluctuations using RETROICOR (Glover et al., 2000); no method of controlling for physiological noise was mentioned by Galvin et al. Finally, negative interregional correlations ("anticorrelations") are frequently only present after regression of the mean global signal, a step we did not perform due to concerns about mathematical validity (Murphy et al., 2009) and associated controversy of interpretation (Chang and Glover, 2009; Fox et al., 2009; Glover et al., 2000; Murphy et al., 2009).

The primary limitation of this and other studies of PRD is the inherent diagnostic ambiguity of dementia. Without biopsy, we must rely on imperfect clinical diagnoses to classify the participants (Geser et al., 2005; Lippa et al., 2007; McKeith, 2007). Amyloid imaging (PiB) could be helpful in identifying participants with elevated fibrillar amyloid burden, though amyloid is known to accumulate in the absence of symptomatic Alzheimer's disease, and so the relative contribution of Parkinson- and Alzheimer-related pathologies to patients' symptoms (or altered resting fMRI correlations) would remain unknown (Rabinovici and Jagust, 2009). Ideally, PRD, PD, and control groups could all be screened for amyloid and comparisons could be made across only those subjects without any evidence of

Alzheimer-related pathology. This is made difficult, though, by the high comorbidity

of Lewy bodies and amyloid plaques (Geser et al., 2005).

Other limitations of the present study include the lack of a double dissociation. An

Alzheimer's disease group showing selective disruption of the default network, for

example, would support the selectivity of the present results. However, though

Alzheimer's patients were not included in this study, many studies have reported

effects on the default network in amyloid disease (Bai et al., 2009; Buckner et al.,

2009; Chen et al., 2011; Damoiseaux et al., n.d.; Greicius et al., 2004; Hedden et al.,

2009; Koch et al., 2010; Rombouts and Scheltens, 2005; Sheline et al., 2010; Sorg et

al., 2007, 2009; Sperling et al., 2009; Supekar et al., 2008). The number of *a priori*

regions for this study was intentionally limited to reduce multiple comparisons, though

larger sample sizes would make whole-brain analysis more feasible and might lead to

significant differences at the vertex level that would survive correction for multiple

comparisons. A limitation of native-space parcellation analysis is dependence on

anatomical regions of interest, but these also provide the advantages of avoiding

circularity (e.g., with functional region selection in the same data set), allowing ready

comparison across multiple studies, and increasing signal-to-noise over single voxels

or vertices.


## 5.5   Acknowledgements

Chapter 5, in part, is currently being prepared for submission for publication of the material. Seibert, Tyler M.; Murphy, Elizabeth A.; Brewer, James B. The dissertation author was the primary investigator and author of this material.

## 5.6 References

Alexander, GE, DeLong, MR, Strick, PL (1986): Parallel organization of functionally segregated circuits linking basal ganglia and cortex. Annu. Rev. Neurosci, 9, 357-381.

Auer, DP (2008): Spontaneous low-frequency blood oxygenation level-dependent fluctuations and functional connectivity analysis of the "resting" brain. Magn Reson Imaging, 26(7), 1055-1064.

Aylward, EH, Codori, AM, Barta, PE, Pearlson, GD, Harris, GJ, Brandt, J (1996): Basal ganglia volume and proximity to onset in presymptomatic Huntington disease. Arch. Neurol, 53(12), 1293-1296.

Bai, F, Watson, DR, Yu, H, Shi, Y, Yuan, Y, Zhang, Z (2009): Abnormal resting-state functional connectivity of posterior cingulate cortex in amnestic type mild cognitive impairment. Brain Res, 1302, 167-174.

Beckmann, CF, DeLuca, M, Devlin, JT, Smith, SM (2005): Investigations into resting-state connectivity using independent component analysis. Philos. Trans. R. Soc. Lond., B, Biol. Sci, 360(1457), 1001-1013.

Buckner, RL, Andrews-Hanna, JR, Schacter, DL (2008): The Brain's Default Network: Anatomy, Function, and Relevance to Disease. Annals of the New York Academy of Sciences, 1124(1), 1-38.

Buckner, RL, Sepulcre, J, Talukdar, T, Krienen, FM, Liu, H, Hedden, T, Andrews-Hanna, JR, Sperling, RA, Johnson, KA (2009): Cortical Hubs Revealed by Intrinsic Functional Connectivity: Mapping, Assessment of Stability, and Relation to Alzheimer's Disease. J. Neurosci., 29(6), 1860-1873.

Chang, C, Glover, GH (2009): Effects of model-based physiological noise correction on default mode network anti-correlations and correlations. Neuroimage, 47(4), 1448-1459.

Chang, C, Glover, GH (2010): Time-frequency dynamics of resting-state brain connectivity measured with fMRI. Neuroimage, 50(1), 81-98.

Chen, G, Ward, BD, Xie, C, Li, W, Wu, Z, L Jones, J, Franczak, M, Antuono, P, Li, S-J (2011): Classification of Alzheimer Disease, Mild Cognitive Impairment, and Normal Cognitive Status with Large-Scale Network Analysis Based on Resting-State Functional MR Imaging. Radiology.

Cox, RW, Jesmanowicz, A (1999): Real-time 3D image registration for functional MRI. Magn Reson Med, 42(6), 1014-1018.

Dale, AM, Fischl, B, Sereno, MI (1999): Cortical surface-based analysis. I. Segmentation and surface reconstruction. Neuroimage, 9(2), 179-194.

Damoiseaux, JS, Keller, KE, Menon, V, Greicius, MD (n.d.): Default Mode Network Connectivity Tracks Clinical Progression in Alzheimer's Disease.

Desikan, RS, Ségonne, F, Fischl, B, Quinn, BT, Dickerson, BC, Blacker, D, et al. (2006): An automated labeling system for subdividing the human cerebral cortex on MRI scans into gyral based regions of interest. Neuroimage, 31(3), 968-980.

Fischl, B, van der Kouwe, A, Destrieux, C, Halgren, E, Segonne, F, Salat, DH, et al. (2004): Automatically Parcellating the Human Cerebral Cortex. Cereb. Cortex, 14(1), 11-22.

Fischl, B, Salat, DH, Busa, E, Albert, M, Dieterich, M, Haselgrove, C, et al. (2002): Whole brain segmentation: automated labeling of neuroanatomical structures in the human brain. Neuron, 33(3), 341-355.

Fischl, B, Sereno, MI, Dale, AM (1999a): Cortical surface-based analysis. II: Inflation, flattening, and a surface-based coordinate system. Neuroimage, 9(2), 195-207.

Fischl, B, Sereno, MI, Tootell, RB, Dale, AM (1999b): High-resolution intersubject averaging and a coordinate system for the cortical surface. Hum Brain Mapp, 8(4), 272-284.

Fleisher, AS, Sherzai, A, Taylor, C, Langbaum, JBS, Chen, K, Buxton, RB (2009): Resting-state BOLD networks versus task-associated functional MRI for distinguishing Alzheimer's disease risk groups. Neuroimage, 47(4), 1678-1690.

Folstein, MF, Folstein, SE, McHugh, PR (1975): "Mini-mental state". A practical method for grading the cognitive state of patients for the clinician. J Psychiatr Res, 12(3), 189-198.

Fox, MD, Raichle, ME (2007): Spontaneous fluctuations in brain activity observed with functional magnetic resonance imaging. Nat Rev Neurosci, 8(9), 700-11.

Fox, MD, Zhang, D, Snyder, AZ, Raichle, ME (2009): The global signal and observed anticorrelated resting state brain networks. J. Neurophysiol, 101(6), 3270-3283.

Galvin, JE, Price, JL, Yan, Z, Morris, JC, Sheline, YI (2011): Resting bold fMRI differentiates dementia with Lewy bodies vs Alzheimer disease. Neurology.

Galvin, JE, Pollack, J, Morris, JC (2006): Clinical phenotype of Parkinson disease dementia. Neurology, 67(9), 1605-1611.

Genovese, CR, Lazar, NA, Nichols, T (2002): Thresholding of Statistical Maps in Functional Neuroimaging Using the False Discovery Rate. NeuroImage, 15(4), 870-878.

Geser, F, Wenning, GK, Poewe, W, McKeith, IG (2005): How to diagnose dementia with Lewy bodies: state of the art. Mov. Disord, 20 Suppl 12, S11-20.

Glover, GH, Li, TQ, Ress, D (2000): Image-based method for retrospective correction of physiological motion effects in fMRI: RETROICOR. Magn Reson Med, 44(1), 162-167.

Greicius, MD, Krasnow, B, Reiss, AL, Menon, V (2003): Functional connectivity in the resting brain: a network analysis of the default mode hypothesis. Proc. Natl. Acad. Sci. U.S.A, 100(1), 253-258.

Greicius, MD (2008): Resting-state functional connectivity in neuropsychiatric disorders. Curr. Opin. Neurol, 21(4), 424-430.

Greicius, MD, Srivastava, G, Reiss, AL, Menon, V (2004): Default-mode network activity distinguishes Alzheimer's disease from healthy aging: evidence from functional MRI. Proc. Natl. Acad. Sci. U.S.A, 101(13), 4637-4642.

Hedden, T, Van Dijk, KRA, Becker, JA, Mehta, A, Sperling, RA, Johnson, KA, Buckner, RL (2009): Disruption of functional connectivity in clinically normal older adults harboring amyloid burden. J. Neurosci, 29(40), 12686-12694.

Helmich, RC, Derikx, LC, Bakker, M, Scheeringa, R, Bloem, BR, Toni, I (2010): Spatial remapping of cortico-striatal connectivity in Parkinson's disease. Cereb. Cortex, 20(5), 1175-1186.

Helmich, RC, Janssen, MJR, Oyen, WJG, Bloem, BR, Toni, I (2011): Pallidal dysfunction drives a cerebellothalamic circuit into Parkinson tremor. Ann. Neurol, 69(2), 269-281.

van den Heuvel, MP, Hulshoff Pol, HE (2010): Exploring the brain network: A review on resting-state fMRI functional connectivity. European Neuropsychopharmacology, 20(8), 519-534.

Holland, D, Kuperman, JM, Dale, AM (2010): Efficient correction of inhomogeneous static magnetic field-induced distortion in Echo Planar Imaging. NeuroImage, 50(1), 175-183.

Koch, W, Teipel, S, Mueller, S, Benninghoff, J, Wagner, M, Bokde, ALW, et al. (2010): Diagnostic power of default mode network resting state fMRI in the detection of Alzheimer's disease. Neurobiol Aging.

Lawrence, AD, Sahakian, BJ, Robbins, TW (1998): Cognitive functions and corticostriatal circuits: insights from Huntington's disease. Trends Cogn. Sci. (Regul. Ed.), 2(10), 379-388.

Leh, SE, Ptito, A, Chakravarty, MM, Strafella, AP (2007): Fronto-striatal connections in the human brain: a probabilistic diffusion tractography study. Neurosci. Lett, 419(2), 113-118.

Lippa, CF, Duda, JE, Grossman, M, Hurtig, HI, Aarsland, D, Boeve, BF, et al. (2007): DLB and PDD boundary issues: Diagnosis, treatment, molecular pathology, and biomarkers. Neurology, 68(11), 812-819.

Majid, DSA, Stoffers, D, Sheldon, S, Hamza, S, Thompson, WK, Goldstein, J, Corey-Bloom, J, Aron, AR (2011): Automated structural imaging analysis detects premanifest Huntington's disease neurodegeneration within 1 year. Mov Disord.

McKeith, IG (2007): Dementia with Lewy bodies and Parkinson's disease with dementia: where two worlds collide. Practical Neurology, 7(6), 374-382.

Murphy, K, Birn, RM, Handwerker, DA, Jones, TB, Bandettini, PA (2009): The impact of global signal regression on resting state correlations: are anti-correlated networks introduced? Neuroimage, 44(3), 893-905.

Pihlajamäki, M, Jauhiainen, AM, Soininen, H (2009): Structural and functional MRI in mild cognitive impairment. Curr Alzheimer Res, 6(2), 179-185.

Rabinovici, GD, Jagust, WJ (2009): Amyloid imaging in aging and dementia: testing the amyloid hypothesis in vivo. Behav Neurol, 21(1), 117-128.

Raichle, ME, MacLeod, AM, Snyder, AZ, Powers, WJ, Gusnard, DA, Shulman, GL (2001): A default mode of brain function. Proc. Natl. Acad. Sci. U.S.A, 98(2), 676-682.

Rogers, BP, Morgan, VL, Newton, AT, Gore, JC (2007): Assessing functional connectivity in the human brain by fMRI. Magn Reson Imaging, 25(10), 1347-1357.

Rombouts, S, Scheltens, P (2005): Functional connectivity in elderly controls and AD patients using resting state fMRI: a pilot study. Curr Alzheimer Res, 2(2), 115-116.

Seeley, WW, Crawford, RK, Zhou, J, Miller, BL, Greicius, MD (2009): Neurodegenerative diseases target large-scale human brain networks. Neuron, 62(1), 42-52.

Seibert, TM, Brewer, JB (2011): Default network correlations analyzed on native surfaces. J Neurosci Methods.

Sheline, YI, Raichle, ME, Snyder, AZ, Morris, JC, Head, D, Wang, S, Mintun, MA (2010): Amyloid Plaques Disrupt Resting State Default Mode Network Connectivity in Cognitively Normal Elderly. Biological Psychiatry, 67(6), 584-587.

Sorg, C, Riedl, V, Mühlau, M, Calhoun, VD, Eichele, T, Läer, L, et al. (2007): Selective changes of resting-state networks in individuals at risk for Alzheimer's disease. Proc. Natl. Acad. Sci. U.S.A, 104(47), 18760-18765.

Sorg, C, Valentin, R, Robert, P, Alexander, K, Afra, WM (2009): Impact of Alzheimer's Disease on the Functional Connectivity of Spontaneous Brain Activity. Curr Alzheimer Res. Retrieved September 21, 2009, from http://www.ncbi.nlm.nih.gov/pubmed/19747154.

Sperling, RA, Laviolette, PS, O'Keefe, K, O'Brien, J, Rentz, DM, Pihlajamaki, M, et al. (2009): Amyloid deposition is associated with impaired default network function in older persons without dementia. Neuron, 63(2), 178-188.

Supekar, K, Menon, V, Rubin, D, Musen, M, Greicius, MD (2008): Network analysis of intrinsic functional brain connectivity in Alzheimer's disease. PLoS Comput. Biol, 4(6), e1000100.

Tabrizi, SJ, Scahill, RI, Durr, A, Roos, RA, Leavitt, BR, Jones, R, et al. (2011): Biological and clinical changes in premanifest and early stage Huntington's disease in the TRACK-HD study: the 12-month longitudinal analysis. Lancet Neurol, 10(1), 31-42.

Van Dijk, KRA, Hedden, T, Venkataraman, A, Evans, KC, Lazar, SW, Buckner, RL (2009): Intrinsic Functional Connectivity As a Tool For Human Connectomics: Theory, Properties, and Optimization. J. Neurophysiol.

Vincent, JL, Patel, GH, Fox, MD, Snyder, AZ, Baker, JT, Van Essen, DC, et al. (2007): Intrinsic functional architecture in the anaesthetized monkey brain. Nature, 447(7140), 83-86.

Wu, T, Wang, L, Chen, Y, Zhao, C, Li, K, Chan, P (2009): Changes of functional connectivity of the motor network in the resting state in Parkinson's disease. Neurosci. Lett, 460(1), 6-10.

Yan, C, Liu, D, He, Y, Zou, Q, Zhu, C, Zuo, X, Long, X, Zang, Y (2009):
    Spontaneous brain activity in the default mode network is sensitive to different
    resting-state conditions with limited cognitive load. PLoS ONE, 4(5), e5743.